POLITECNICO DI MILANO

Facoltà di Ingegneria Industriale

Corso di Laurea in
Ingegneria Meccanica

DESIGN OF A DOUBLE-STAGE HYDRAULIC ACTUATOR WITH

HIGH PERFORMANCES ENERGY-SAVING SYSTEM

Relatore: Prof. Ferruccio RESTA

Co-relatore: Ing. Francesco RIPAMONTI

Co-relatore: Ing. Christian GHIELMETTI

Tesi di Laurea di:

Francesco RINALDI   Matr. 735629

Anno Accademico 2009 - 2010

Index

Appendix A - Nomenclature

Appendix B - Hydraulic accumulators

B.1 State of the art

B.2 Accumulator typologies

B.3 Working parameters and principles

Appendix C - **Components datasheets (Bosch Rexroth®)**

Bibliography

Index of figures

Index of tables

Abstract

Hydraulic cylinders are between the most used actuators in industrial applications. Often, their elevate power absorption rate represents a big problem, especially for those uses which last for very long periods of time like fatigue tests. The thesis proposes an innovative design of a double-stage hydraulic cylinder, carrying a particularly high performance energy-saving system which allows impressive reductions in energy consumption. The system has been initially analyzed in a circuit for fatigue tests on steel cables for bridges buildings. In the second part, its advantages in the domain of frequencies have been investigated in a non-linear application for control vibration. The simulations led to observe a significant increase in stability and bandwidth, besides an improved disturbance rejection ability and a reduced power absorption.

Keywords: hydraulic actuator, energy-saving, fatigue test, vibration control.

Sommario

I cilindri idraulici sono tra gli attuatori più utilizzati in campo industriale. Spesso però, il loro elevato assorbimento energetico può costituire un grosso problema, soprattutto per quelle applicazioni con durate temporali elevate, quali un test di fatica. La tesi propone un design innovativo di cilindro idraulico a doppio stadio, con un sistema a risparmio energetico particolarmente performante, che permette significative riduzioni in termini di consumo energetico. Il sistema è stato inizialmente analizzato in un circuito per prove di fatica su cavi d'acciaio per la costruzione di ponti. Nella seconda parte, sono stati studiati i suoi vantaggi nel dominio delle frequenze, su un'applicazione non lineare per controllo di vibrazioni. Le simulazioni hanno portato ad osservare un significativo aumento della stabilità e della banda passante, oltre che un incrementata capacità di reiezione del disturbo e un ridotto assorbimento di potenza.

Parole chiave: attuatore idraulico, risparmio energetico, test di fatica, controllo di vibrazioni.

Estratto in lingua italiana

Il presente lavoro di tesi, svolto in collaborazione con Bosch Rexroth®, si è occupato della progettazione di un attuatore idraulico a doppio stadio con sistema di risparmio energetico, e della verifica delle sue prestazioni mediante simulazioni numeriche.

La tesi si colloca in realtà all'interno di un progetto più ampio, in cui Bosch Rexroth® giungerà all'effettiva realizzazione dell'impianto idraulico. In questa prospettiva, una validazione numerica su quanto aspettarsi dal cilindro in questione è risultata fondamentale.

Il sistema idraulico è inizialmente nato per l'applicazione su un impianto per prove di fatica su cavi d'acciaio. La prova, in particolare, consiste nella sovrapposizione di un carico medio positivo, ed uno alternato di minore entità, con il quale sollecitare ciclicamente il materiale di prova.

Sono questi generalmente dei test in cui si sviluppano forze molto elevate, per periodi di tempo mediamente molto lunghi. Ciò è dovuto al fatto che i sistemi di attuazione sono spesso molto lenti, e le prove in questione richiedono comunque l'esecuzione di un numero di cicli pari a $2x10^6$. Per questo motivo è nata la necessità di ricercare una soluzione impiantistica la quale potesse permettere una limitazione al cospicuo consumo in termini energetici.

Il cilindro idraulico che la presente tesi si propone di presentare e di modellare, è il *"Tandem"*, un servo-attuatore a doppio stadio, altamente performante, e dotato di sistema a risparmio energetico. Il sistema sfrutta la sua architettura a doppio stadio per attuare il risparmio in questione: in particolare, la sua struttura impiantistica permette ai due stadi di lavorare separatamente. Il primo cilindro, di dimensioni maggiori, è dedicato a sviluppare la forza per il raggiungimento del carico medio. Una volta ottenuto, il circuito viene chiuso e messo sotto accumulatore il quale, comportandosi come una molla (a rigidezza non lineare), mantiene il carico medio senza più bisogno di essere alimentato

(con buona approssimazione). Dunque in questo modo, lo stadio di dimensioni più contenute, può occuparsi di sviluppare il carico alternato, come detto, di dimensioni molto ridotte rispetto a quello statico.

Ciò consente quindi al sistema di dover alimentare con portata effettiva soltanto le operazioni di inseguimento del carico alternato, con conseguente abbattimento dei consumi globali dell'impianto.

Con l'obiettivo di dimostrare quanto teoricamente detto, è stato realizzato un modello dinamico del "Tandem" in AMESim®. La modellazione ha potuto permettere non solo la scelta e il dimensionamento più adatto di componenti e parti del sistema, ma anche, in una seconda fase, l'osservazione della fisica del sistema, consentendo un'accurata comprensione dei fenomeni alla base del funzionamento del sistema stesso. Il fine dello studio è stato tuttavia quello di portare avanti un confronto tra l'attuatore idraulico proposto nella tesi, una soluzione classica a singolo stadio, con cilindro regolato da singola servo valvola, ed infine una configurazione a doppio stadio intermedia tra le due, ma priva di accumulatore. Le simulazioni hanno dimostrato che i vantaggi della soluzione "Tandem" andavano ben oltre le iniziali aspettative, lasciando registrare un abbattimento dei consumi significativo. Inoltre, considerando che i tre sistemi, avendo ricevuto tre dimensionamenti differenti, venissero confrontati nella maniera più coerente, è stato definito un parametro di energia utile, in cui si è calcolata l'effettiva energia elastica assorbita dai sistemi per la deformazione del cavo di prova. Con questo dato, la trattazione è giunta ad elaborare un parametro di efficienza energetica, che per il cilindro classico si è attestata al 32,0 %, per il doppio stadio "intermedio" al 25,7%, per il "Tandem" addirittura al 58,9%.

Il dimensionamento più contenuto del "Tandem" rispetto agli altri sistemi (dovuto al fatto che esso deve alimentare soltanto per il carico alternato) ha motivato una ricerca di definizione delle performance anche nel dominio delle frequenze. Sfortunatamente AMESim® non dispone di strumenti molto affidabili nell'analisi in frequenza dei sistemi. Per questo motivo le diverse configurazioni sono state analizzate in una sorta di test di sweep "pseudo - sperimentale". In pratica, ai cilindri (controllati in posizione) è stato fornito un ingresso di riferimento con contenuto armonico a frequenza linearmente

crescente nel tempo. La risposta dei cilindri è stata salvata come fosse stato un campionamento dati vero e proprio, e le "misurazioni" sono state poi analizzate nel dominio delle frequenze.

Una nota molto importante va fatta a questo proposito. Nella iniziale simulazione per la misurazione dell'efficienza energetica, i tre sistemi erano stati dimensionati in modo differente, ma tale che tutti e tre raggiungessero la performance richiesta dalle specifiche del test. In questo secondo test di analisi in frequenza però, si desidera studiare le risposte dei sistemi indipendentemente delle condizioni al contorno di alimentazione, portate massime, valvole disponibili, ecc. È per questo motivo che i circuiti sono stati dimensionati allo stesso modo, in modo che i risultati finali discendessero puramente dalle proprietà di un cilindro piuttosto che dall'altro.

I dati ricavati dalle simulazioni, come già anticipato, sono stati passati nel dominio delle frequenze con un algoritmo di FFT per una iniziale operazione di ripulitura da un segnale a bassa frequenza di scarso interesse. Successivamente questa parte di storia temporale è stata sottratta alla storia totale, ottenendo dunque soltanto la parte interessante ai fini dell'analisi.

I risultati hanno mostrato per il "Tandem" una funzione di trasferimento con banda passante lunga ben 2,5 volte quella del sistema a cilindro classico.

Pertanto questa prima analisi, su sistema per prove di fatica ha ampiamente dimostrato i vantaggi del nuovo attuatore proposto, nei confronti delle precedenti configurazioni disponibili.

La significatività dei risultati ottenuti, ha però lasciato pensare che anche altri campi d'applicazione avrebbero potuto beneficiare dell'innovativa concezione idraulica dell'attuatore "Tandem". In particolare la seconda parte della tesi è stata dedicata alla verifica dei vantaggi dell'applicazione del "Tandem" su un sistema non-lineare con l'obiettivo del controllo di vibrazioni.

Il sistema meccanico utilizzato per questa seconda analisi è un braccio rotante, incernierato a terra, sul quale dall'esterno vengono applicate delle forze/coppie di disturbo. Il sistema richiama chiaramente l'applicazione per controllo di vibrazioni su bracci per movimentazione di calcestruzzo, e tale esempio viene adottato per il dimensionamento del sistema. È questa tuttavia un'ipotesi di impostazione del problema, poiché l'analisi portata avanti nella presente tesi è in realtà semplice da un punto di vista modellistico.

Ad esempio l'osservazione corretta delle vibrazioni di tale sistema, e lo sviluppo di una logica di controllo adatta a tale fine, richiederebbero senza ombra di dubbio una modellazione più accurata e definita, come ad esempio una FEM oppure un'analisi su corpi continui.

Ricordiamo però che l'obiettivo prefissato dalla tesi non è tanto raggiungere questi scopi, quanto in realtà dimostrare effettivamente la bontà della soluzione impiantistica "Tandem" rispetto alle precedenti configurazioni. Pertanto si è ritenuto sufficiente condurre un'analisi su sistema non lineare ad un grado di libertà.

Il sistema è stato studiato nella sua dinamica non lineare ed in quella linearizzata, sia per il sistema attuato dal cilindro a doppio stadio, sia per la configurazione classica con singolo cilindro. L'integrazione delle equazioni di moto ha reso possibile l'instaurazione di un confronto tra le due soluzioni adottate.

Tale analisi è stata condotta su più fronti parallelamente. In primo luogo è stato effettuato uno studio delle matrici di stato e dei poli del sistema. Questo primo step ha permesso di determinare che la soluzione proposta dalla tesi, a doppio stadio, gode di una maggiore stabilità intrinseca, dovuta alle fondamentali differenze impiantistiche con una configurazione a cilindro semplice. Inoltre, per sistemi posti a pari condizioni al contorno (pompa, servo-valvole, controllore, ecc.) il cilindro "Tandem" può "permettersi" dei guadagni proporzionali e derivativi in media molto più elevati del cilindro semplice, senza rischiare di incorrere in instabilità.

Successivamente alla scelta dei guadagni di controllo, è stata portata avanti un'analisi nel dominio di Laplace. La rappresentazione del sistema in schemi a blocchi ha facilitato il calcolo delle funzioni di trasferimento tra gli ingressi del sistema e la sua uscita, ovvero la posizione angolare dello stesso. Tale tipo di confronto si è concluso con l'osservazione della banda passante dei sistemi, in cui quella dell'attuatore "Tandem" è risultata essere quasi di estensione doppia rispetto alla configurazione con cilindro classico a singolo stadio.

Infine l'integrazione nel tempo delle equazioni di moto ha permesso di ricavare la variazione temporale di posizione e pressioni, nonché dell'errore del sistema sollecitato da una coppia esterna di disturbo. Quest'ultima osservazione in

- 7 -

particolare ha denotato la bontà dell'attuatore proposto nella ridurre l'errore di circa l'80%.

Infine anche in questo caso il cilindro "Tandem" si è comportato apprezzabilmente dal punto di vista degli assorbimenti energetici, in quanto la potenza media consumata è risultata essere del 42% inferiore rispetto al cilindro classico.

Introduction

The present work of thesis deals with the design of a hydraulic actuator characterized by a high performances energy-saving system.

Because of their high ratio power/weight, hydraulic actuators are generally used for industrial applications in which significant forces are produced and, consequently, big quantities of energy are absorbed. This underlines the importance of researching and looking for innovative solutions which could decrease consumptions without affecting negatively the performances.

The thesis has been drawn up during a stage experience in Bosch Rexroth®, leader about industrial hydraulics, in which the work has represented a part of a wider project, that eventually aimed at the construction of the hydraulic cylinder. The starting idea which led the design to the final concept was the necessity to conceive an actuator with an energy-saving circuit, for fatigue tests in which a static load and an alternate one had to be produced.

Considering the long times of execution (millions of cycles at generally low frequencies) and the degree of order of the forces exerted during these tests, it is immediate to understand how rapidly the power consumed becomes huge. The energetic absorption is therefore a fundamental and critical aspect in the evaluation of the goodness of an actuator.

The "Tandem", the hydraulic actuator under investigation, is expected to carry significant reductions in energy consumption thanks to its architecture (Figure 1): the cylinder is in fact designed in a double-stage structure, with a big piston and a small one rigidly connected together by the same double-rod. In particular, while the big piston is meant to reach the static load and to keep it constant by means of an accumulator, only the small cylinder will actively work to chase the alternate reference.
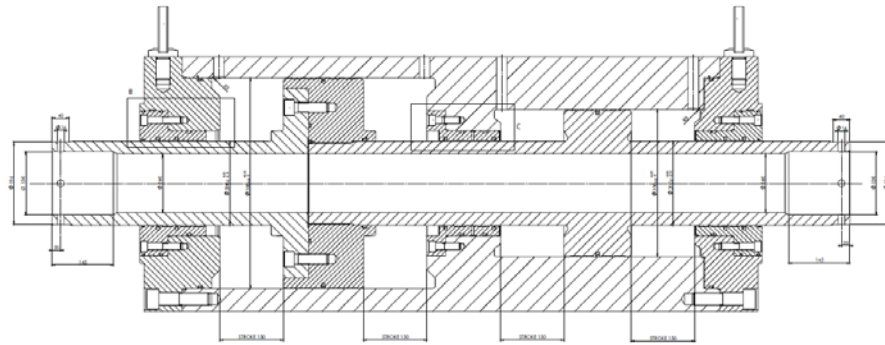
Figure 1: Section view of the "Tandem" cylinder.

The initial objective of the present thesis was hence to study a suitable control strategy for such a circuit. Afterwards a dynamic model of the whole system has been realized in AMESim®, in order to simulate the behavior of the circuit and to observe its advantages and disadvantages with respect to other cylinder configurations.

The great potentialities shown both in the time domain (reduced power consumption) and in the frequency domain (increased bandwidth), forced a re-orientation of the design process towards the possibility of other applications for this actuator architecture.

In particular, in the second part of the work, a non linear application for vibrations control has been investigated. The "Tandem" cylinder has been applied on a simple mechanical system representing a model of an arm for concrete-handling (Figure 2). In all the models of this type of machinery, the handling is achieved by means of hydraulic actuators, connected to the arms by suitable kinematic motion. Unfortunately, because of their light and slender sections, and considered their usage, booms for concrete-handling are unavoidably subject to deformation and vibration propagation. These ones are therefore critical applications in which large forces have to be developed and fast corrections of the error need to be applied to the boom in order to have a suitable control.

For this second application a numerical model has been developed in the Matlab® environment: the model created is a simple 1 D.o.F. mechanism, which actually does not embody the complexity of a real, deformable arm for concrete handling. The model is however sufficient to pursue the objective of

observing and demonstrating the benefits of the "Tandem" architecture of enhanced controllability of the overall system, of improved bandwidth in the response to reference signals, of better rejection of external disturbances and, in the end, of reduce power absorption.

Figure 2: Example of mobile application of booms for concrete-handling

The thesis is hence divided into two main parts, both of them articulated in three chapters.

Part 1 has been dedicated to the investigation of the application for the fatigue test.

In chapter 1 a description of the application has been carried out. The requirements of the load cycle are presented; in addition to this, an overview of the architecture of the "Tandem" and of its control strategy (with respect to other actuators configurations) is provided.

Chapter 2 is instead dedicated to the creation of a dynamic model for the system in AMESim®. The cylinder is suitably sized (structure, components, control parameters) in order to satisfy the required performance. Once set up, the system is then simulated and a comparison of the results between the "Tandem" and other two cylinder configurations is proposed.

In chapter 3 the "Tandem" system and the classical single-stage cylinder are studied in the domain of frequencies. Both the systems are stimulated with a sweep input with frequency linearly increasing over time. Output data are then subject to a Fourier Transform, in order to compute the transfer functions of the systems and evaluate their bandwidths.

- 11 -

In part 2 the non-linear application of the "Tandem" on the arm for concrete-handling has been investigated. The system has been compared to a classical solution with a single-stage hydraulic cylinder.

Chapter 1 gives a brief presentation of the non-linear mechanical system, with information about the sizing and its kinematic motion.

In chapter 2 the numerical model of the system is developed. The system is initially studied in non-linear terms, and then the non-linear equations of motion are computed through a Lagrange approach. Afterwards the energy forms are linearized around a desired angle position θ_0 and the linearized equations of motion are calculated. Both the operations are executed for the "Tandem" and the classical cylinder configurations.

Chapter 3 is in the end dedicated to the analysis of the results. Systems are compared in the state-space domain, in the Laplace domain and in the time domain. In the end power absorption of both the solutions are proposed.

Part 1

Hydraulic actuator for fatigue tests

The main actor of the first half of the present thesis is a servo-hydraulic actuator for fatigue tests. We refer, in particular, to those kinds of tests performed to sample the fatigue resistance of building materials used for civil structures, such as cables for bridges.

Let us think about the importance of verifying the appropriateness of the choice of a material, or a particular component for raising such a civil building. The consequences of any form of carelessness or procrastination in every single phase of the design process could be devastating, and an engineer has the onerous responsibility to consider the importance of each aspect, each eventuality, each combination of factors.

In fact, even if the bridge in question was perfectly designed to resist to a precise static load, nobody could ensure us about its intrinsic resistance to an alternate load. The physical phenomenon of *fatigue* is indeed well-known, and it refers to the progressive and localized mechanical harm which occurs in correspondence of the application of a cyclic load to the tested material [1].

There exists a nominal maximum stress value (usually much lower than ultimate tensile stress limit and yield stress limit) over which the material experiences the birth, and then the growth, of local micro-cracks. [2]

Figure I.1 depicts for instance the Whoeler curve, which explains the behavior of a metallic component subjected to a cyclic alternate load. The stress value σ_{FL} under which the component demonstrates an infinite service lifetime is called "fatigue limit stress".
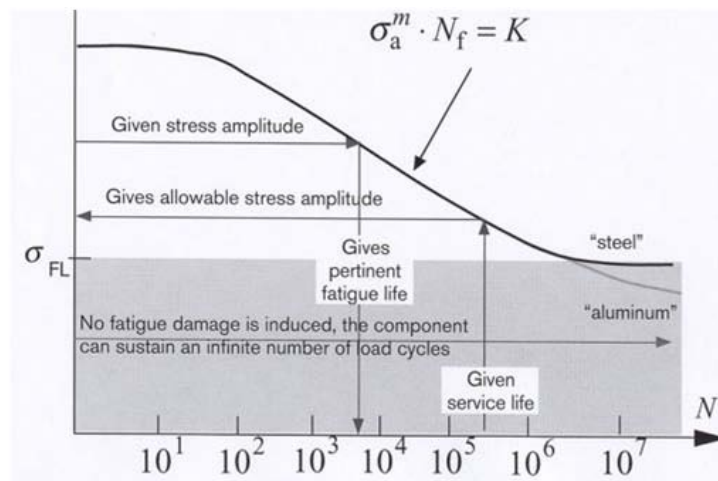
Figure I.1: Parametric Whoeler curve for metals.

Fatigue is indeed a stochastic process which (especially in metals and alloys) always starts with the dislocation movement of metallic grains within the crystal lattice, which eventually originates initially permanent slip bands and then small cracks. Notwithstanding the first studies on fatigue breaks are dated back to the first half of the 19th century, this phenomenon is still considered one of the principal dangers in many engineering sectors (automotive, railways, aeronautics, off-shore, civil buildings, etc.) for which the STAT-USA yearly counts a quantity of nearly 200 billion $ spent worldwide in repairs for fatigue failures.

This is why setting up an experimental procedure addressed to test the fatigue resistance, in our case of a building material, is not only advised but, in specific cases, compulsory in order to spare money and, not necessarily more rarely, human lives.

Considering the long times of execution, and the degree of order of the forces exerted during these tests, it is easy to understand how the real cost is not actually represented by not only the selling price of the actuator, but also by the power consumed. The energetic absorption becomes therefore a fundamental and critical aspect in the evaluation of the goodness of an actuator.

This first part of the thesis is in particular dedicated to development and the analysis of a new concept of hydraulic actuator called "Tandem", endowed with an innovative circuit which is expected to be able to spare great quantities of energy. The "Tandem", will carry these significant reductions in energy consumption thanks to its architecture: the cylinder is in fact designed in a double-stage structure, with a big piston and a small one rigidly connected together by the same double-rod. In particular, while the big piston is meant to reach the static load and to keep it constant by means of an accumulator, only the small cylinder will actively work to chase the alternate reference.

In this configuration, it is the accumulator which plays the true innovation. In particular, hydraulic accumulators have a good tradition in energy-saving systems, for which we defer to Appendix B, to the state of art of accumulators applications.

In the following sections, a model for the system at stake has been set up. Thanks to the simulations run in the AMESim® environment, a comparison between the classical single-stage cylinder and the new hydraulic architecture has been carried out. Results will show in the end how much the proposed solution is convenient.

Chapter 1

Description of the application

Despite in the last decades the industrial world has experienced an impressive growth in electric applications, justified by definitely higher velocities and very lower costs, there are still limits that cannot be physically overcome by electric motors and actuators, beyond which only hydraulic ones manage to achieve the required performances.

We are referring to the need of exerting incredibly high forces (or torques) and supplying huge powers, which is certainly the case of a fatigue test where the goal is to verify the resistance of an axially-loaded cable for bridges.

Literature and experience tell us that, in general, this kind of mechanical tests has usually been executed by means of hydraulic linear (or in some cases rotational) actuators, namely cylinders able to transform fluid power into mechanical one. In particular, in the case of the present thesis, we want to apply a static load and an alternate one on a cable used in building bridges. The forces at stake in this kind of application become dramatically high if we consider that the goal is to process a steel cable, with section diameter of nearly 60 millimeters, long more than 7 meters and with modulus of elasticity of nearly 200000 MPa.

More details about the cycle to be performed by the system are given in the following section. This analysis we are going through will certainly help the reader in understanding the reasons why this work aims to suggest a new concept of testing machine. In addition to this he will be involved in sensing more in depth the main dynamic issues faced during the design phase.

1.1 Desired load cycle and requirements of the hydraulic system

The component to be tested is, as already mentioned, a cable for bridges. Datasheets concerning the execution of the test say that it has a cylindrical geometry with the following characteristics:

- Diameter of 58,55 mm
- Nominal section area of about 2692 mm^2, including the external layer of Zinc (corrosion protection)
- Length of 7,5 m

It will be made of steel (including Cr and Zn) characterized by an ultimate tensile strength of nearly 1820 MPa, a 1% yield strength of 1630 MPa and a modulus of elasticity of 195000 MPa.

During the test, the cable will be assumed to be like a spring with constant stiffness, which can be determined according to the following expression:

$$k_{cable} = \frac{E \cdot A}{L} = \frac{195000 \, MPa \cdot 2692 \, mm^2}{7500 \, mm} \cong 70 \, \frac{kN}{mm} \qquad (1.1)$$

The cable will be processed axially by the "Tandem" hydraulic actuator. The fatigue test in particular consists in the repetition of 2x10^6 cycles of a static load overlapping on an alternate one (with frequency of 2 Hz) in such a way to produce a deformation of 27 ± 1 mm (which will be taken as reference signal in the feedback control of the system).

Given the mechanical properties of the material to be tested, this position reference signal corresponds to a stress behavior of 702 ± 26 MPa (Figure 1.1).
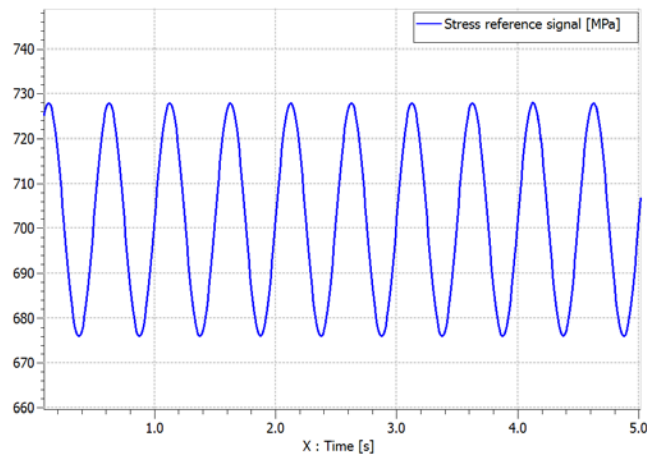
Figure 1.1: Stress reference signal for the cable.

Key target of the present thesis is hence to develop a new concept of energy-saving hydraulic actuator to reproduce such experimental test, with a significantly decreased power absorption.

1.2 "Tandem": a hydraulic cylinder for fatigue tests

In the following sub-sections some different types of hydraulic actuators and circuits to perform such a test will be presented.

As far as we know, the simplest configuration of hydraulic actuator to execute this kind of test is represented by a single-stage cylinder system, controlled by a big servo-valve and fed by a volumetric hydraulic pump.

The aim of this work is to start from this classical and simple setting, to reach in the end a final concept, possibly carrying a *decrease in complexity* and *burden*, besides a *marked improvement* (namely a lowering) *in the energetic consumption* of the plant, which is critical in this case.

The basic idea on which the "Tandem" cylinder has been conceived is the separation of the work, classically performed by a sole cylinder, in two distinct parts: the static stress on a side, the alternate one on the other. That is why its architecture has been called with such a name, in order to remind the idea of a tandem bicycle.

The only way to carry out these two different jobs, separately, is to come up with the solution of a two-stage double-acting cylinder, with two different pistons (mechanically coupled by the same double-type rod), the big one providing for the static load, the small one providing instead for the alternate one.

There will follow 3 sub-sections in which they will be investigated the fundamental steps that the design process has gone through before reaching the final concept:

1. The classical configuration with a single-stage cylinder and a big servo-valve controlling it.
2. A mid-span configuration with a double-stage cylinder and two servo-valves, each one controlling the job of one single piston.
3. The "Tandem", the final set up with a double-stage cylinder, one single servo valve and an accumulator.

1.2.1 Single-stage cylinder with one servo-valve

As already mentioned, the first step of the design process towards the final solution is represented by the classical configuration of a single cylinder acting on the cable, and being controlled by a big servo-valve. For a better understanding of the system, look at Figure 1.2.
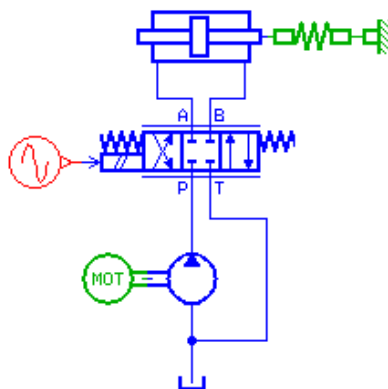
Figure 1.2: Sketch of the classical solution circuit, with one single-stage cylinder driven by a servo-valve.

As shown in the figure, the entire system is fed by a hydraulic pump (in this case a fixed-displacement one) which, driven by a motor, sucks the fluid from

the tank and pushes it into the circuit, by providing it with a certain quantity of energy. The servo-valve is then placed in the middle: its internal spool moves depending on the signal supplied to the solenoid, and in this way it allows the fluid power to be alternatively led to the chambers of the actuator. The actuator, namely the cylinder, is in particular a double-rod and double-acting type, and it is mechanically connected to the tested cable, whose stiffness is represented by a simple spring.

The aim of the fatigue test is to try the cable resistance by submitting it to a cyclically alternate load overlapping on a static one, and observing the evolution in behavior of the material after usually several thousands of cycles. In this fashion, what is of real interest in this experimentation is to monitor continuously stresses applied on the sample cable and, consequently, the strains occurred on it.

This can be practically and easily done by placing a load cell or a position transducer between the actuator and the sample cable. The measured signal is fed back to a controller which compares it with the reference signal proposed as requirement, by elaborating (according to a specific control logic) and delivering a command to the valve, such to reduce the tracking error.

Anyways, this kind of solution carries with itself a series of intrinsic disadvantages which always makes the execution of these tests onerous and undesirable. We can list, for example:

- The generally big dimensions of the actuator which has to generate the entire stress on its own.
- The elevate values of flow rate needing to be delivered to the cylinder in order to foster the process.
- The very high powers and energies which are absorbed during the operation of the system (as a consequence of the very high flow rates, besides pressures).
- The "slowness" that the system generally takes to answer to the inputs (whose consequence is the very long time of execution of such a test), given the large dimensions of the cylinder and the valve.

We will see further on how a simulation of such a process can be set up, in order to understand the quantities at stake in the system, and how much they can be reduced by the introduction of the innovation of a "Tandem" cylinder.

1.2.2 Double-stage cylinder with two servo-valves

The idea that the separation of the two loads (the static and the alternate one) in two different stages of the machine could lead to an improvement in the performances of the whole system stays at the base of the current thesis. In particular, what this work proposes is a new interpretation of the design, wishing to solve, or at least mitigate, the problems encountered by the classical actuator solutions listed in the previous paragraph.

In this mid-span configuration, the new actuator hence rises from the connection of two cylinders (where the piston rod of the first one pushes through the piston area of the second one). For a major clearness and understanding of the issue, a draft of this possible mechanical concept is depicted in Figure 1.3.
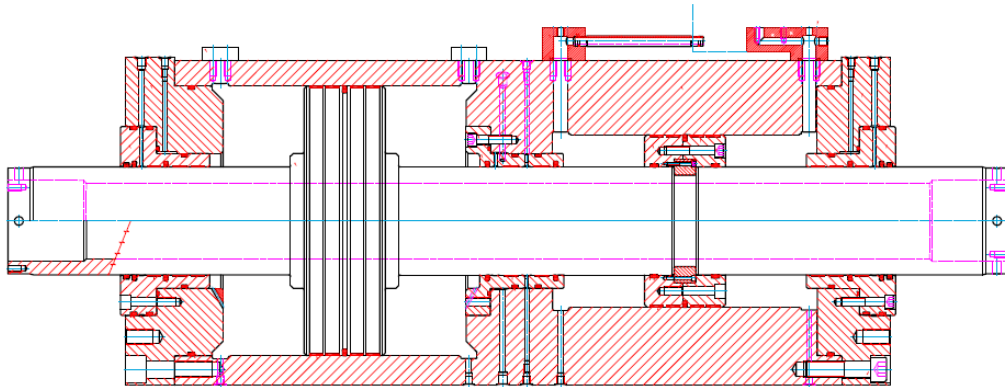
Figure 1.3: Section view of an example of double-stage hydraulic actuator.

While the big piston (on the left) will devote to generate and hold the large pre-charge load, corresponding to the static stress, the small one (on the right) will deal with the alternate load which, as we have seen in section 1.1, represents only a small part of the work that the cylinder will have to develop during the fatigue test.

As depicted in Figure 1.4, the actuator is schematizable by two separate cylinders, mechanically bound one to each other thanks to an infinitely-stiff spring (assuming that axial deformation during operation is negligible).
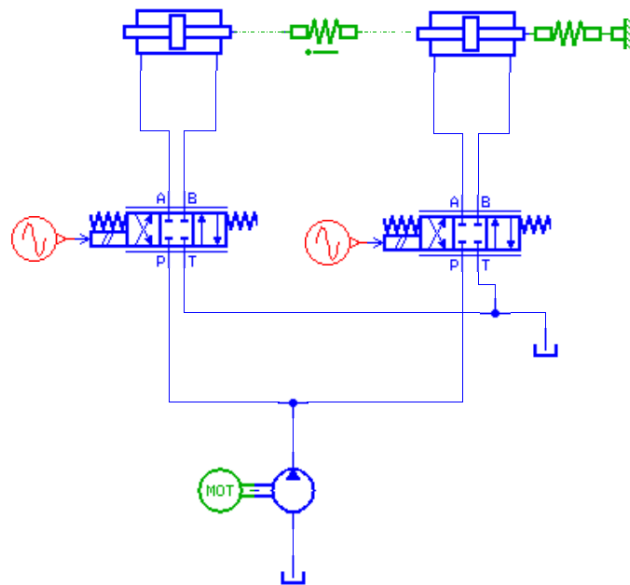
Figure 1.4: Sketch for the circuit solution of the double-stage actuator, driven by two servo-valves.

In this intermediate phase of the design process however, the actuator is still conceived in such a way that each piston (and then each couple of chambers) needs its own servo-valve to be controlled and be put into motion. Here comes from one side the contradiction of keeping on feeding the system with very large flow rates which actually clash the initial requirement of decreasing the energy absorption (we will demonstrate it in chapter 2); from the other side the difficulty of regulating the two valves in a synchronous way, whose possible drawbacks are examined hereinafter.

In fact the target of the fatigue test is still to follow the force reference signal, and to correct the behavior of the machine in order to eliminate the tracking error. As already seen before, this goal is achieved again by feeding an appropriate signal to the servo-valves. Unfortunately, in this case the two pistons are mechanically bound one to the other through the rod, thus the system will need a particularly well-designed controller if we wish to avoid cases of dysregulations in which, for example, the two sides of the cylinder could be loaded in opposite directions.

It is easy to understand that this eventuality will have a twofold non-positive consequence on the machine, because:

- obviously the presence of forces applied on the same object (the cylinder), but in opposite directions, will <u>not</u> produce useful work (hence part of the fluid power will be dissipated meaninglessly)
- this kind of configuration affects negatively the service lifetime of the same machine, because this energy will be entirely released in the deformation of the mechanism, which is unpredictable and, first of all, undesired.

Ideally, in a simulation phase, the software will allow to reach a stable configuration avoiding all these problems and this will be investigated more in detail further on in chapter 2. Anyways this outcome is not expected to be entirely possible in reality, hence this mid-span design concept will eventually lead the work to the birth of the "Tandem" cylinder.

1.2.3 Double-stage "Tandem" cylinder

Having examined both the previous configurations, we can now fully understand why and how such a new hydraulic design can be conceived and put into operation.

Apparently, so far the idea of dividing the work into two stages has represented a great potential but not really exploited, at least according to the previous sub-section, in which we have seen that the configuration with two different servo-valves is still not efficient.

The real breakthrough, which definitely makes this cylinder successful with respect to the previous setups, is the suggestion of placing a hydraulic accumulator on the line of the bigger stage (accumulators have been deepened in chapter 2, in order to let the reader acquire a better understanding of the advantages of such a solution).
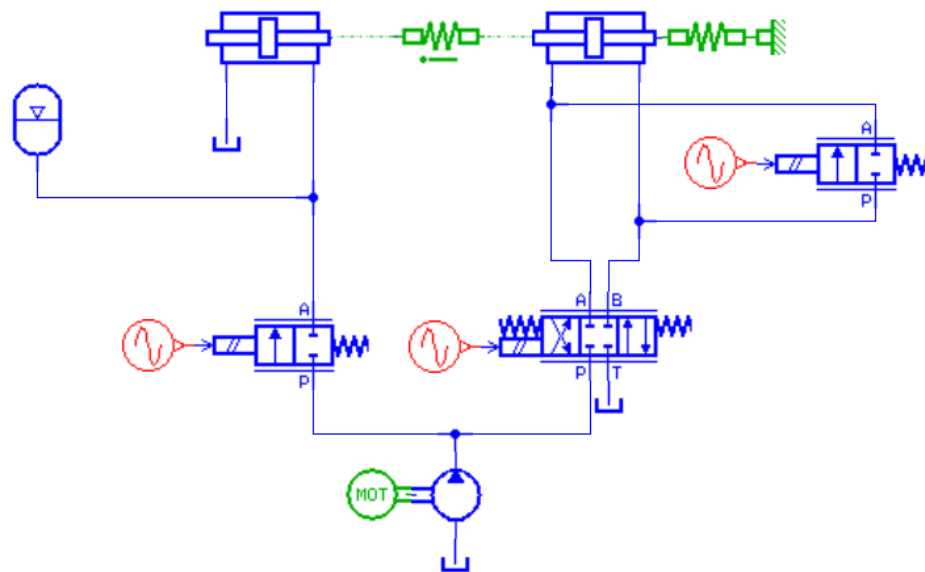
Figure 1.5: Sketch of the circuit of the "Tandem" hydraulic actuator.

Let us now give a look to Figure 1.5. The working principle at the base of this final circuit is exactly the one proposed since the beginning, namely to separate the static load from the alternate one.

In fact, this circuit configuration (where the bigger cylinder is the one on the left) carries a series of modifications which result absolutely determinant: first of all, as already mentioned, the introduction of an accumulator; secondly the disappearance of one of the two servo-valves; in the end, the insertion of two new 2-way proportional valves.

The system, and its precise setup, will be developed and analyzed at a later time in chapter 2, in before running the time simulations. Anyways, performances will in principle be achieved according to the following steps:

- At the beginning the left 2-way valve will be open, in such a way to let the flow pass towards the big cylinder. At the same time the right 2-way valve will be open as well, in order to bypass the small cylinder from being interested from the flow of fluid supplied by the pump. With this combination the big cylinder will start moving leftward, pulling the spring (the cable stiffness), while in both chambers of the second cylinder the same pressure will be ideally kept.

- After the system having reached the static (mean) load configuration, both the 2-way valves will be closed so that the big cylinder will keep on holding the static force, and at the same time the small cylinder will be adequately regulated by the servo-valve in a cyclic way (by following a reference force signal, as already seen before), such that the alternate stress will be produced.
- Due to the leakages (internal and external), we expect the average pressure in the big cylinder to decrease in time. In order to restore the static level of force, the left 2-way valve will be periodically re-opened and closed as soon as the pressure reaches a set point.

As already said, the main aspects of this system configurations have been presented here briefly and in a pretty "rough" way, which was principally aimed to let the reader understand the basic working principles. However, the system will be studied more in depth and sized in chapter 2; explanations given so far are anyway sufficient to make some remarks on how and why this new configuration results better than the previous ones. As a matter of fact, the accumulator fulfils in this case a twofold function:

1. It is used as a storage of energy which allows the system to not continuously foster a servo-valve (by loading and downloading entirely the system, each cycle). Apart from periodical small restorations of pressure, in fact the big cylinder is fully charged only the first time, then its 2-way valve gets closed, and the system holds the mean stress pretty much "for free".
2. After having reached the mean stress, the servo-valve of the small cylinder only needs to work on the alternate part of the load cycle. Considering that the left part of the system is steady, the small cylinder is actually supposed to work against a double resistance: from one side the stiffness of the cable, from the other the compressibility of the fluid in the left line, which would tend to keep the system swinging around the mean position. This second "stiffness" would be dramatically high if we had a second servo-valve instead of the accumulator. Fortunately the accumulator can count of the high compressibility of the gas inside its structure then this resistance results absolutely lowered, with the

additional intrinsic advantage of being adjustable by acting on the dimension of the same component and on the pre-charge pressure of the gas.

This is at last the final configuration of the "Tandem" cylinder. This solution is innovative and winning, and in next chapters a demonstration for it will be provided. For the moment it is possible to list all the advantages that this plant design owns:

- Given that, apart from the initial charging phase, only the small part of the plant is supposed to work continuously (to apply only a small variation of stress with respect to the average level) the system is expected to be actuated with an impressive reduction in fluid absorption, and consequently a huge reduction in the energy consumption.
- The absence of a continuously-controlled servo-valve on the big line of the system, makes the whole regulation easier and, for sure, more efficient. No problems of synchronization will be noticed inside the circuit, and then it will never occurs a dissipation of energy due to opposite forces on the cylinders as mentioned in the previous paragraph.
- The successful apportionment of the load cycle in two different cylinders allows to design the actuator in reduced dimensions: this represents a favorable aspect first of all from an economic point of view, because a smaller machine will certainly cost less than a bigger one.
- A second positive consequence of the contained dimensions of the system could be the increased bandwidth of the whole system. Actually, if the systems were sized to satisfy the requirement of a certain stress reference with a certain frequency, then both the systems would reach nearly the same bandwidth. Using smaller cylinders and servo-valves will however imply theoretical quicker responses to the external inputs.

Chapter 2

Time domain analysis

This second chapter is hence dedicated to the core part of the thesis, namely the design of the hydraulic circuit and to its simulation by using the LMS Imagine.Lab AMESim®.

The chapter will be structured according to the following path: at the beginning a deepened description of the "Tandem" plant will be given, with details about the control strategy and choice of components, with the objective of setting up and running a correct simulation. In the end a discussion of the results and a comparison between the three possible configurations (see section 1.2.1 and 1.2.2) will be carried out.

2.1 Simulation of the hydraulic actuator "Tandem"

The simulation of the "Tandem" is so far the most important part of the current work. In order to provide the reader with a better understanding of the system, the principal points of the following analysis are listed: at the beginning the description of a preliminary scheme of the hydraulic circuit has been carried out. Afterwards an opportune control strategy and adequate components will be chosen for the plant, to close eventually the paragraph with the analysis of the results.

2.1.1 Plant description

As it can be seen from Figure 2.1, the sketch (taken from AMESim® in *sketch mode*) represents exactly those working principles briefly explained in section 1.2.3, when talking about the application in general and its goals.
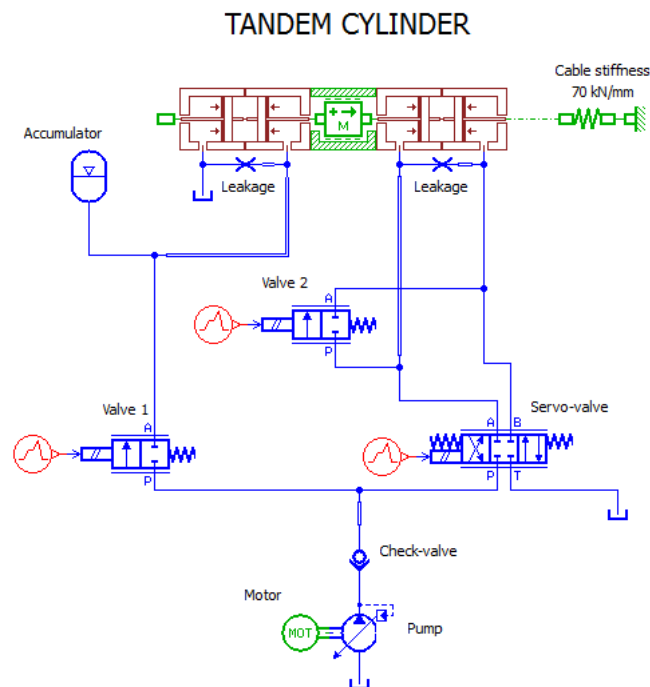
Figure 2.1: Basic skect of circuit of the "Tandem" actuator.

The system is again based on a double stage double-rod type cylinder which actuates the cable, by applying a tensile stress on it, against the opposition of

its stiffness. The whole system is fed by a pump, which is protected by a check valve preventing from the fluid flowing back to the tank side.

The fluid leaving the pump divides then into two different flows: the first of them runs (through Valve 1) directly towards the first stage of the cylinder, making the cable reach the mean stress of its load cycle. Once this value has been reached, Valve 1 gets closed and it is reopened only occasionally to restore potential losses of pressure due to leakages. The second flow feeds instead the second stage where the servo-valve controls the direction of the flow, achieving in this way the tracking of the reference.

Despite everything so far looks the same of what presented in section 1.2.3, some substantial differences have been carried out, in order to optimize the functioning of the system, and to make it as much as possible similar to reality.

First of all the cylinder, which is the fulcrum of the "Tandem" design. As Figure 2.1 clearly depicts, the configuration adopted in this design is totally different from Figure 1.5. AMESim® has to its disposal a series of pre-made hydraulic cylinders inside the hydraulic library, like presented in Figure 2.2: single and double acting, single and double rod type, spring loaded, etc.
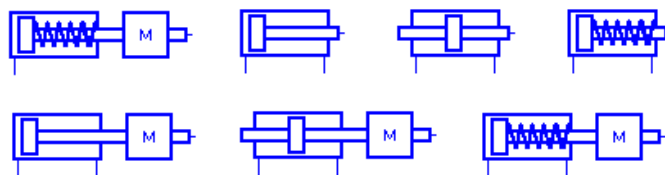
Figure 2.2: Examples of pre-made cylinders block in AMESim®.

Despite this method could look quicker and easier, literature about AMESim® modeling has demonstrated that, often, the direct design of hydraulic components by using the "Hydraulic Component Design" library gives results much more plausible and close to reality. It is desirable, for example, the possibility to express with greater precision leakages, frictions and so on.

A series of documents and scientific papers have been taken as a guide, besides a source of inspiration, in the modeling of the cylinder. For example, S. Yang, S. Kwon and S. Jin already confirmed the advantages of the hydraulic design library in their paper about the optimization of a remote control system of a

field robot [3]. Since hydraulic excavators generally operate in hazardous circumstances, they need a complex and efficient automation and remote control system to prevent workers from getting injured. This means that valves, cylinders and other components are usually characterized by special structures or configurations which AMESim® does not include in its libraries. That is why the "Hydraulic Component Library" becomes fundamental in such applications. In fig. 10.5 it is shown the modeling of the boom valve used in their circuit: it is a 6 ports 3 positions type, including bypass circuits. The component is built through the concatenation of several small blocks, each one representing one single piece of the valve (the piston, the rod, the spring, the mass, etc.).
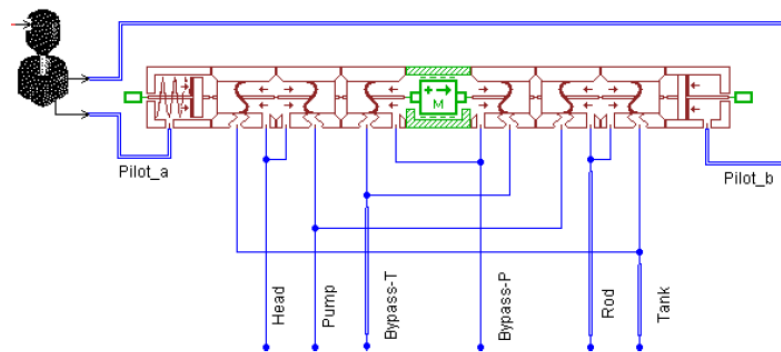
Figure 2.3: 6 ports 3 positions with internal by-pass boom valve of a field robot [3].

Our cylinder is definitely simpler than this valve, but this example has certainly been useful in the understanding of the potentials of AMESim®'s library.

The proposed solution for the "Tandem" is depicted below in Figure 2.4. The double-stage cylinder is built up through the pairing of two pistons by the connection of the mass element. Each piston, in particular, is composed of two specific elements each representing the single chamber of the cylinder.
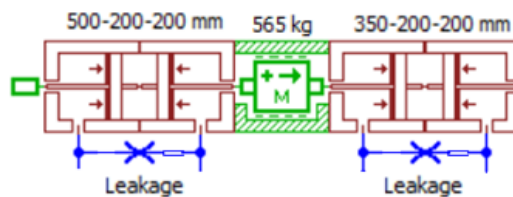
Figure 2.4: Sketch representation of the "Tandem" cylinder double-stage structure.

For the current design it has been chosen to size the two pistons according to the working principle: the big cylinder (symmetrical), which will be devoted to hold the big mean static stress, will be characterized by a piston diameter of 500 mm, and a rod diameter of 200 mm. The small piston (symmetrical as well), instead dedicated to produce the alternate part of the load, can be reasonably undersized to a piston diameter of 350 mm and rod diameter kept at 200 mm. The total stroke of the two cylinders (the same for both of them) is in the end 300 mm, with an initial position of the piston at half of the stroke. Figure 2.5 shows the typical AMESim® dialog box in which it is possible to configure all these parameters.
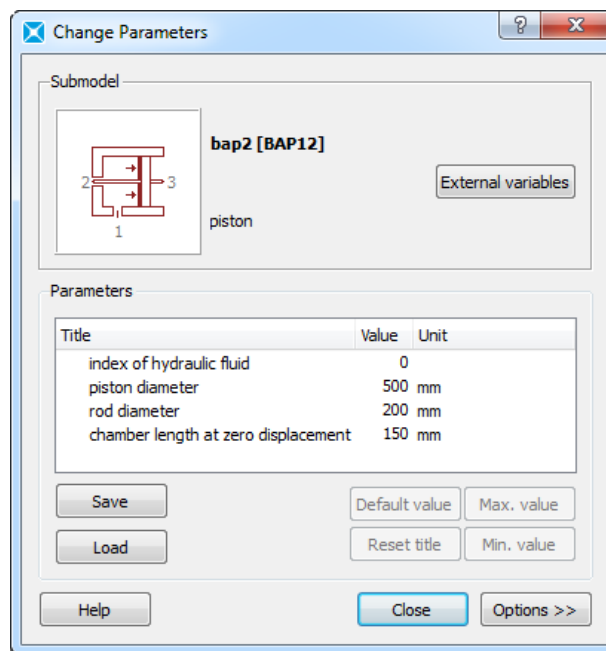
Figure 2.5: AMESim® dialog box for changing the cylinder's dimensions parameters.

The mass element, which rigidly connects the two cylinders making them as one single, represents in fact the total mass of the moving part of the structure, evaluated to be around 565 kg. A cad representation (Figure 2.6) of the cylinder has helped in the computation of such value.
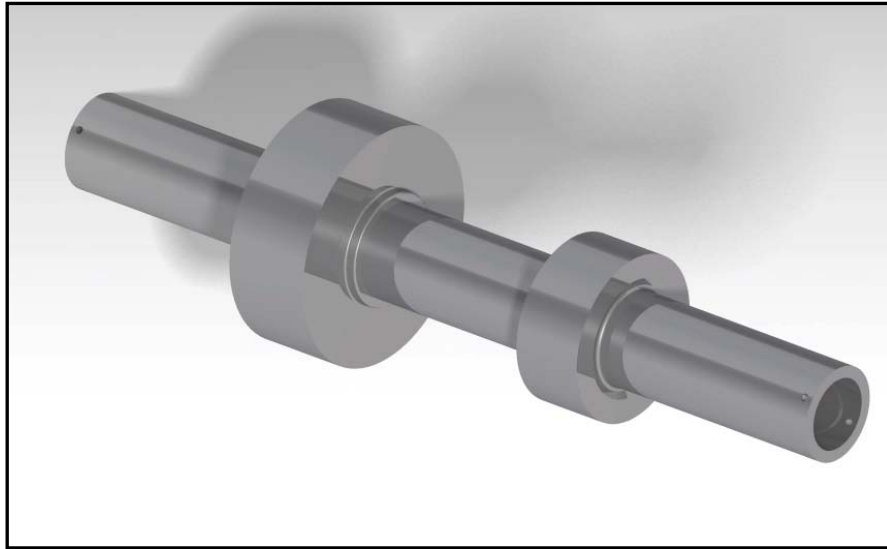
Figure 2.6: CAD representation of the "Tandem" cylinder.

In the dialog box of the mass element, as depicted in Figure 2.7, it is also possible to define all the friction parameters which describe the behavior of the cylinder.
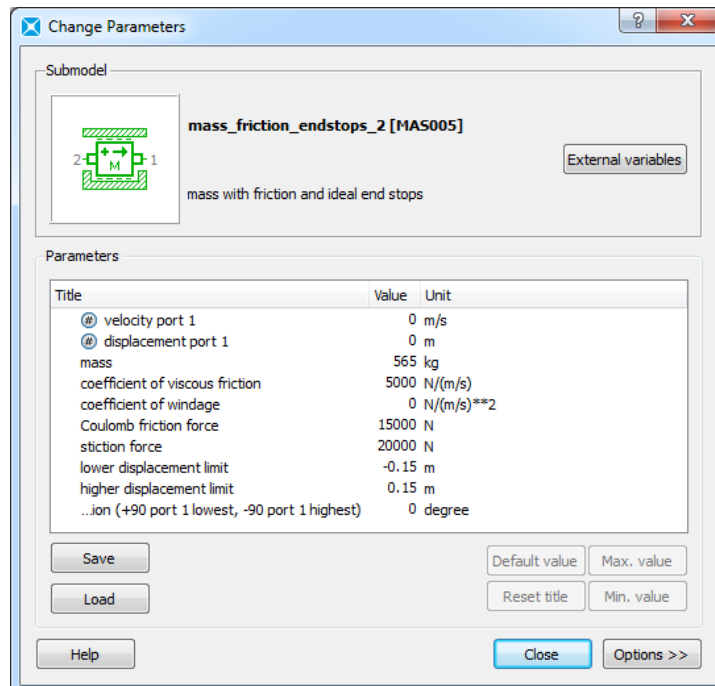
Figure 2.7: AMESim® dialog box for changing piston mass and friction parameters.

Literature is wide with regard to this theme: in general, hydraulic servo-systems are modeled as constant friction systems to which a velocity-dependent term is added [4]. Several papers have, however, investigated the various combinations between linear viscous damping, Coulomb friction and stiction. A. Bonchis, P. I. Corke and D. C. Rye demonstrated that even different friction regimes can be revealed in correspondence of "low" and "high" velocities [5], as shown in Figure 2.8.
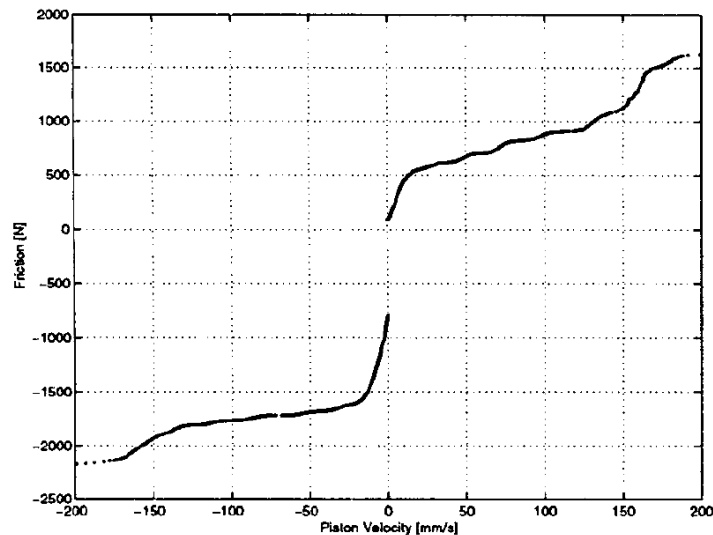
Figure 2.8: Experimental relationship between friction forces and piston velocity in a hydraulic cylinder, measure in [5].

In particular, our cylinder is expected to have peak velocities in the second range, in which viscous friction is, as filled-in in the dialog box, about 5000 N/(mm/s).

Leakages have instead been modeled with the interposition of flow control valves between the two chambers. The physical principle at the base of this scheme is actually the same of an internal leakage: the two sides of the valve are subdued to a pressure differential which leads the fluid to flow through the orifice. These flow control valves are however characterized by very small equivalent orifice areas (and diameters). The reason why this is true is that the "Tandem" cylinder is expected to be endowed with special scraper seals so that external leakages could be even neglected. For what concerns the internal ones, the motion of the head of the piston always causes small quantities of

fluid moving from one chamber to the other: this leakage is hence, according to technical tables filled out by hydraulic manufacturers, modeled as a very small orifice area, with equivalent diameter of 1 mm (Figure 2.9).
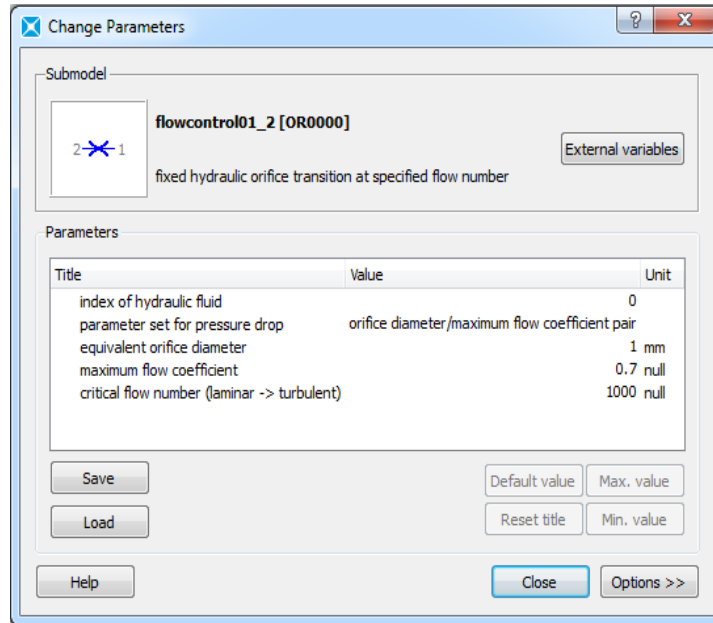
Figure 2.9: AMESim® dialog box for changing leakage parameters.

The last important plant differentiation from what shown in section 1.2.3 concerns the pump. In order, in fact, to design a proper hydraulic circuit with special care towards the energy consumption, it is necessary to install a kind of pump with the possibility of regulation, able hence to reduce or increase its characteristics according to the needs.

Regulation in pumps is achieved thanks to *variable displacement* in different ways, and generally results in an improvement in energy consumption. In industrial hydraulics it is possible to perform different typologies of regulations:

- Pressure regulation (DR)
- Flow rate regulation (LS/FR/S)
- Power regulation (DFLR, LR, etc.)

The pump of the "Tandem" (in practice a pumped storage station) is in particular endowed with a pressure regulation device, like depicted in Figure

2.1. This means that the machine is able to vary its displacement in such a way to ensure a certain constant pressure, with even blocking the entire flow rate.

According, in fact, to the scheme presented below in Figure 2.10, pressure-regulated pumps are endowed with a max pressure valve which sends the "pressure signal" to a device able to change the displacement. The spring inside the max pressure valve is calibrated on a pressure P*: till the line pressure is under this value, the flow rate is constant and equal to Q_{max}. When, instead, the line pressure goes beyond this limit, the hydraulic force equals the elastic one and the poppet can rise up. When this happens, part of the fluid can flow towards a regulating piston whose spring, being very "soft", lets the rod move directly to the stop limit. The pump, being linked to the cylinder, undergoes a substantially immediate reduction of displacement. The flow rate is then blocked, and because of this the pressure is forced to decrease: the poppet elastic force thus prevails again on the hydraulic one, and the line flow rate is "pushed" back to its maximum value.
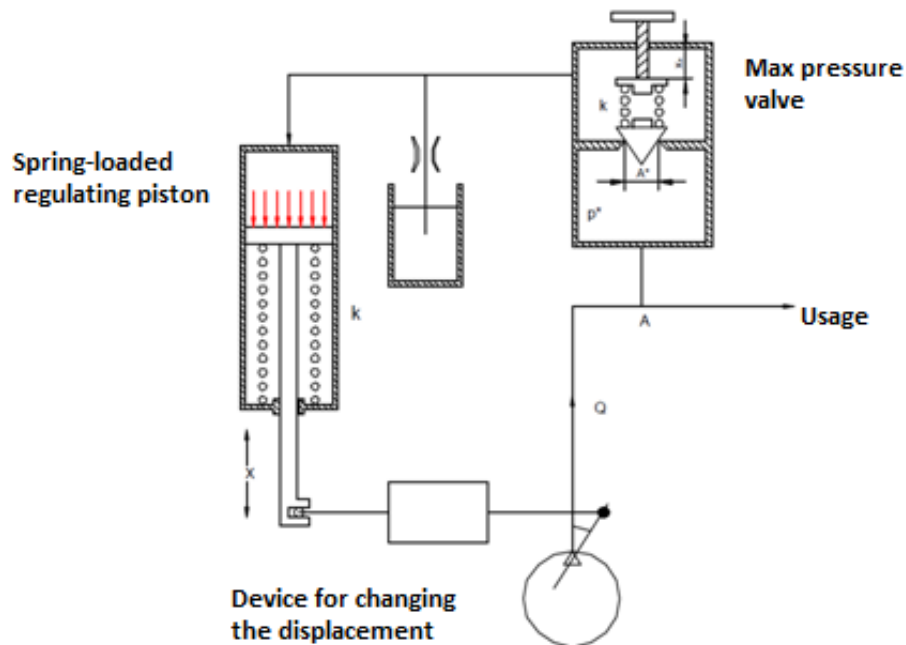
Figure 2.10: Schematic representation of the pressure regulated pump principles.

Figure 2.11 shows therefore the theoretical advantage (in terms of reduction of dissipated power) achieved when using such pressure regulation in pumps.
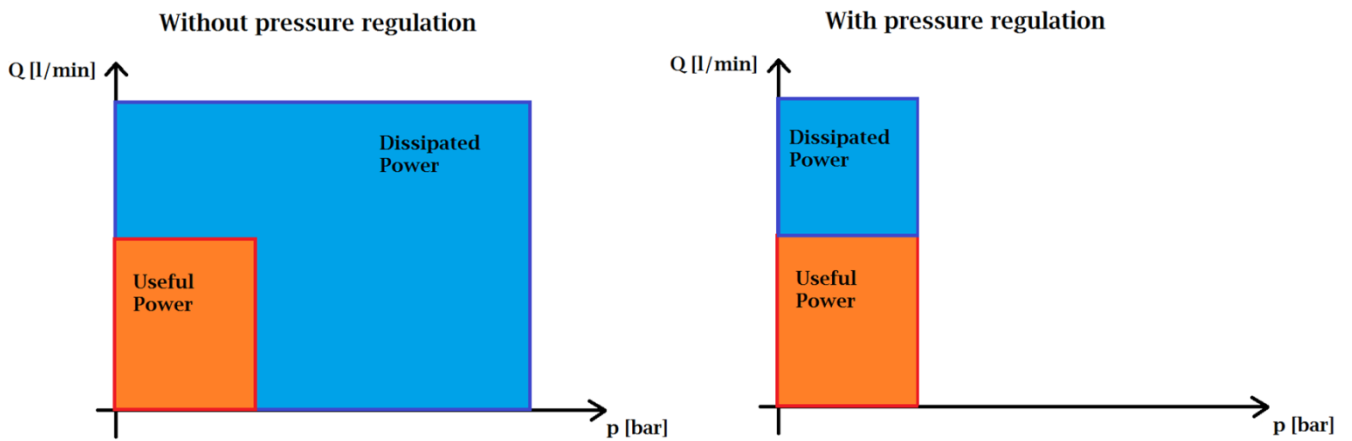
Figure 2.11: Power spare when using a pump regulated in pressure.

The typical characteristic curve of such a pump is shown hereinafter in Figure 2.12.
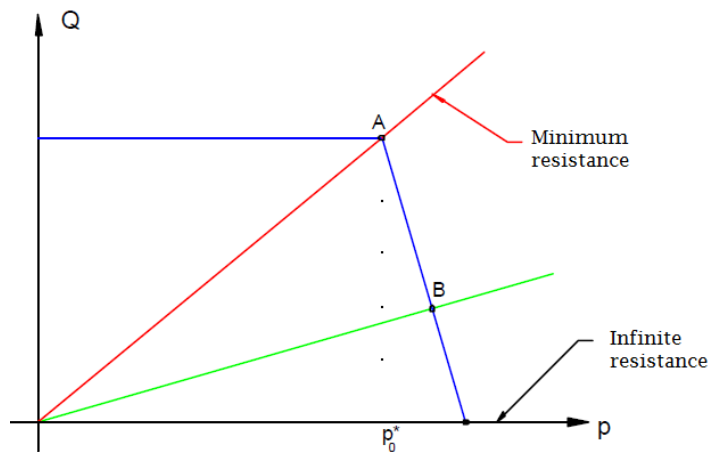
Figure 2.12: Characteristic curve of a pressure regulated pump.

In the case of the "Tandem", this kind of design takes shape in a pump with max displacement of 100 cc/rev which, with a nominal shaft velocity of 1450 rev/min, corresponds to nearly 145 l/min. The chosen configuration (that will ensure a good functioning of the whole system) is depicted in Figure 2.13.
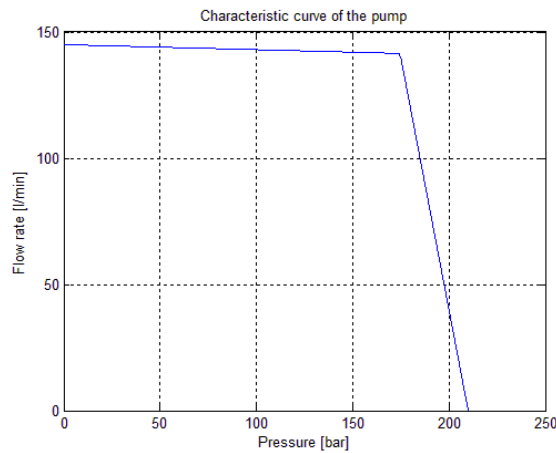
Figure 2.13: Characteristic curve of the pump of the "Tandem".

The circuit is in the end completed by the three valves and the accumulator, whose choice will be treated further on in paragraph 2.1.2 aiming to fulfill all the initial requirements of the machine.

2.1.2 Development of an energy-efficient control strategy.

Is this probably the most important part of the design process: even if the best and most innovative components were chosen for the system and the most advanced technology was applied in the realization of the cylinder, this would be totally useless without an appropriate control strategy, able to manage and coordinate each part of the circuit, according to (and achieving) the target in question.

As already mentioned in the previous chapters, the "Tandem" machine is conceived to be a linear actuator for fatigue tests, with energy-saving principles. In particular its design was requested for a specific test on a steel cable for the construction of a bridge.

The system will work as briefly explained in section 1.2.3:

- Initially the 2-way valve controlling the accumulator side will be open, in such a way to let the flow pass towards the big cylinder. At the same time the 2-way valve on the right side will be open too, bypassing the

- small cylinder from the flow of fluid supplied by the pump. In addition to this, aiming to spare as much fluid as possible (energetic improvement), in this phase also the servo-valve will be closed.
- After the system having reached the static (mean) load configuration, both the 2-way valves will be closed so that the big cylinder will keep on holding the static force, and the small cylinder will be adequately regulated by the servo-valve producing the alternate stress.
- Due to the leakages (internal and external), we expect the average pressure in the big cylinder to decrease in time. In order to restore the static level of force, the left 2-way valves will be periodically re-opened and closed as soon as the pressure reaches a set point.

Specifications say that the cable to be tested shows a linear elastic behavior, with stiffness of around 70 kN/mm. In addition to this, the requested displacement to be performed is 27 ± 1 mm.

Considering that, at least in the first phase, only the big cylinder will produce force to pull the cable (and the left chamber of the cylinder is constantly at 0 relative bar), the pressure in the right chamber will be proportional to the force, namely to the same displacement. In few words:

$$p_1 = \frac{F}{A_{an}} = \frac{k \cdot x}{\pi \cdot \frac{d_{ext}^2 - d_{int}^2}{4}} = 114,59 \pm 4,24 \; bar$$

(2.1)

This means that, during the load cycle, if only the big cylinder was devoted to the develop the entire stress (static + alternate), the right head of the big piston would be periodically loaded with a pressure between about 110 and 119 bar.

However, regulating separately (but coordinately) all the valves is everything but an easy task. The control scheme, applied on the system, is now completely depicted in Figure 2.14.
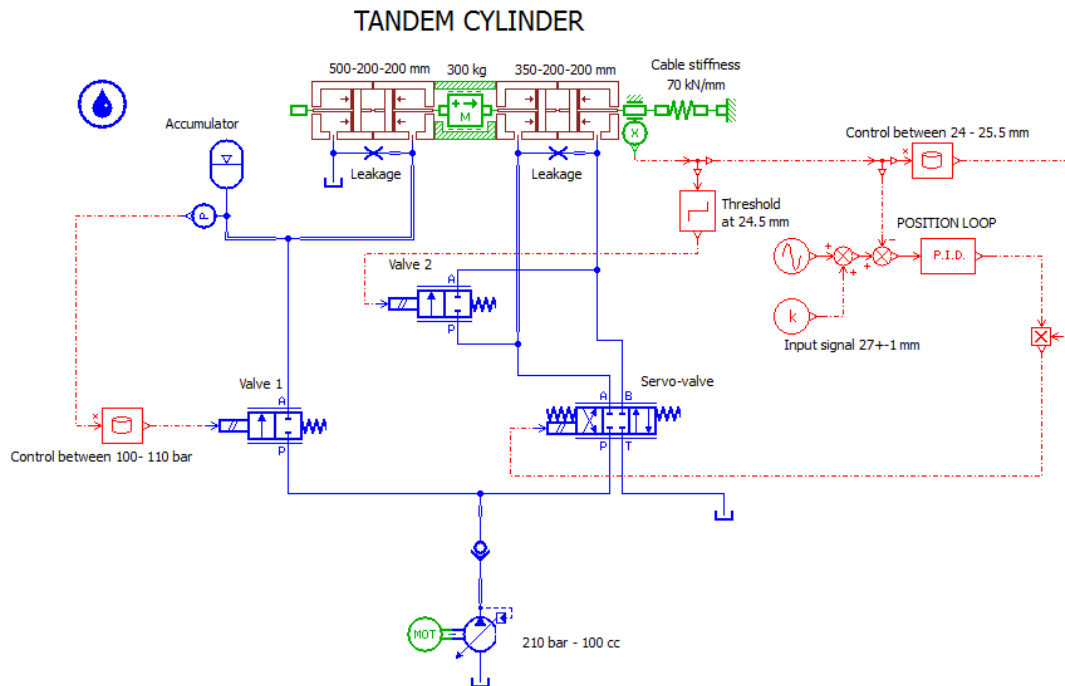
Figure 2.14: Complete sketch of the circuit controlling the "Tandme" actuator.

As it can be seen from the figure, two transducers, one of pressure, one of position, will be used in the control of the circuit. The pressure transducer, in particular, measures the pressure next to the accumulator, which (apart from small load losses along the pipe) is the same of the right chamber of the cylinder. The operating pressure will be between about 110 and 119 bar (with a static stress of 114,59 bar), but we want the two parts of the system (accumulator side, servo-valve side) operate separately, without overlapping with each other, to avoid any sort of malfunctioning.

In this sense, the best solution is to make the accumulator side load the cable until reaching the lower limit of the load cycle (around 110 bar), and let the servo-valve do all the rest. This choice would be advised especially for the optimization of the working conditions of the small cylinder: in fact it is common practice to make hydraulic actuators work always under a positive pressure, never around a discharge condition. This is advised to preserve the cylinder from premature damages. If the big cylinder loaded the system until

the mean stress, the small cylinder would work around a discharge point, which is hence to be avoided.

For what concerns Valve 1, the red control block ("Control between 100 – 110 bar) takes the pressure signal from the transducer and compares it with a table, containing the data in Figure 2.15, giving out to the valve an input between 0 and 1. When 1 (namely $p_1 \leq 100\ bar$), Valve 1 will be wide-open; when 0 ($p_1 \geq 110\ bar$) it will be closed. In particular, with such decreasing ramp, it is possible to handle gradually the big cylinder with smoother movements of the valve.
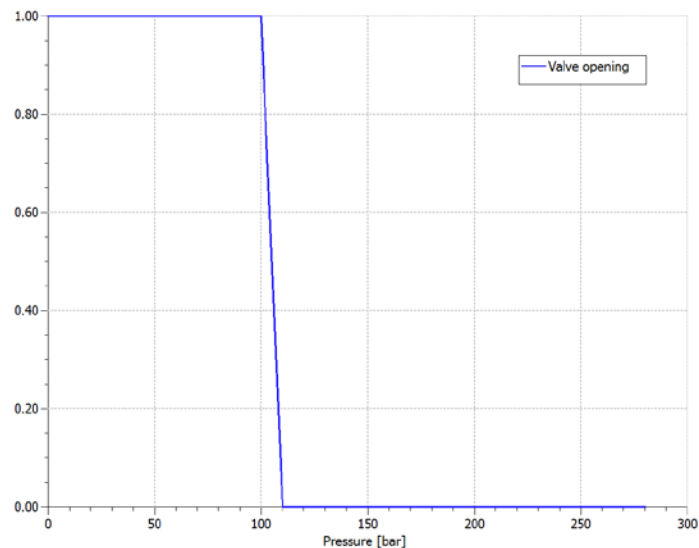
Figure 2.15: Regulating function for Valve 1.

As already said, at the beginning the pump pushes fluid only towards the big cylinder. In this first phase the right side of the circuit remains totally excluded. When however the pressure is between 100 and 110 bar, Valve 1 closes gradually. This means that, within this range, it is necessary to open Valve 2 and the servo-valve before having the system completely stuck.

The small cylinder, as clearly depicted in fig. 10.13, is controlled by using the position signal coming out from the transducer. In particular, Valve 2 is designed to be only a bypass, which means that also a "On/Off" valve (non proportional) could be used. The threshold at which the valve gets closed (putting in communication the cylinder with the servo-valve) is set at 24.5 mm, which corresponds to a pressure (on the big cylinder) of nearly 103.98 bar.

In the meanwhile, the servo-valve needs to be controlled in order to cut out the tracking error. In the application of the bridge cable, the reference signal derives from the sum between a constant value (27 mm) and an alternate one of 1 mm with frequency of 2 Hz ($\sin(2\pi f \cdot t)$). The error signal is hence fed back to the servo-valve through a PID controller.

In general, in industrial hydraulics, the type of controller is chosen by referring to specific tables which, depending on the cylinder and the chosen valve, say which is the best configuration [6]. For the case at stake, a P controller (proportional) is more than enough, and we will see further on how to select an appropriate proportional gain K_p. The application of an integral controller would result in a delay on the system response (and possibly in wind-up problems); the derivative one, instead, is generally chosen to speed up the response of a too slow valve, which is hence useless if the valve is selected correctly.

The servo-valve is started with a gradual control, as well as Valve 1 gets closed. In fact, in order to soften the impact of the fluid filling the cylinder's chambers, its opening is regulated by the external loop containing the control block called "Control between 24 – 25.5 mm". This block gives out a signal which, according to fig. 10.15, for positions below 24 mm is always 0, for positions under 25.5 mm is always 1. This signal is hence multiplied with the PID output.
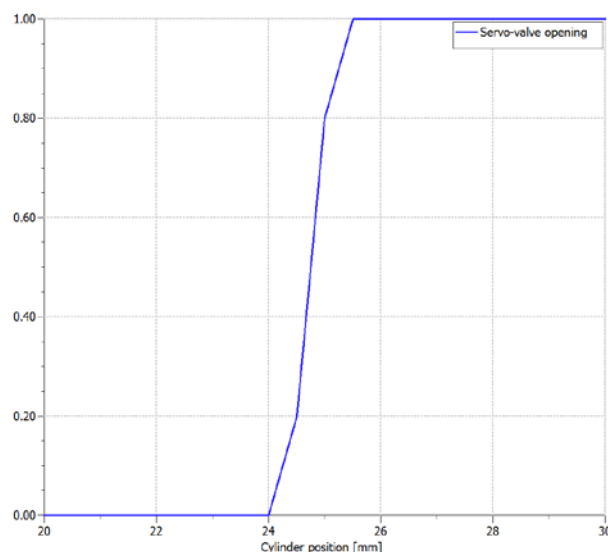
Figure 2.16: Regulating function for the Servo-valve.

This simple regulation makes the servo-valve being completely closed in the initial phase, while being totally relying on the PID controller in the second phase. For a better understanding of the working principles selected for the regulation of the whole system, a summarizing image has been proposed in Figure 2.17.
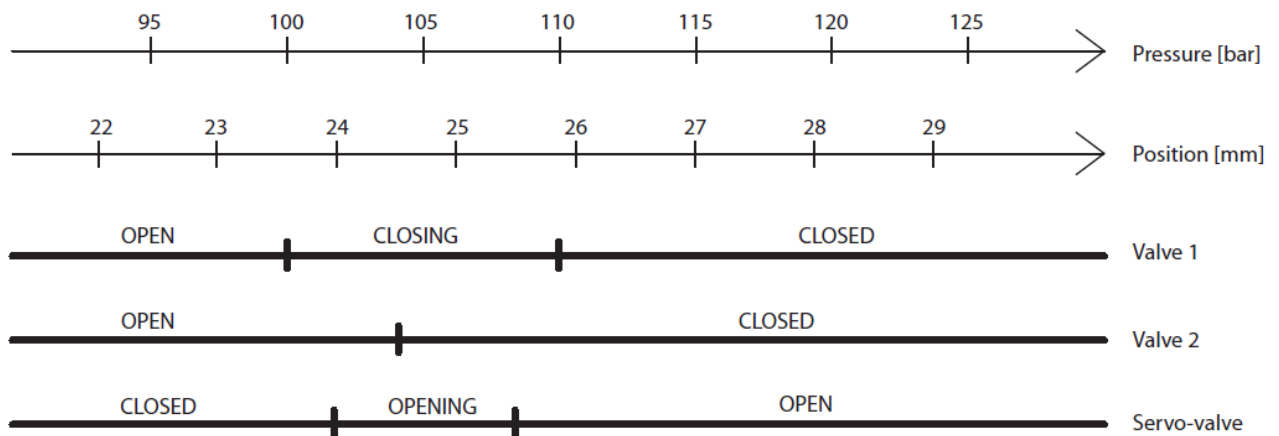
Figure 2.17: Summarizing representation for the valve management over time.

2.1.3 Choice of proper hydraulic components

The system presented so far has been defined and sized quite in detail, except for the valves and the accumulator.

Actually, in a normal hydraulic design process, these elements are usually taken from catalogues as pre-made components, only in very rare cases they are appositely realized for the application at stake. The "Tandem" is precisely considered a special cylinder, whose mechanical design and construction require specific techniques not typically adopted for a single-stage cylinder. On the other hand its reduced dimensions and energy absorption, descending directly from its particular working principle which asks much lower flow rates, just need ordinary valves (and, in this case, accumulators).

Accumulator

The most important component is for sure the accumulator. In Appendix B a pretty detailed explanation about how an accumulator works is give. Anyways in this application its function is to charge the left side of the circuit and to hold the mean stress, by "isolating" the big cylinder from the small one.

A first observation on the system is about the accumulator's *volume*: by introducing this component along the circuit, the designer will necessarily increase the time needed for charging the line, simply because more liquid will need to be pushed inside the system before reaching the pressure set. In Figure 2.18 it is shown the different behavior of three accumulators, respectively with V_0 of 40 l, 20 l and 5 l. The larger the accumulator is, the longer it takes to be filled.
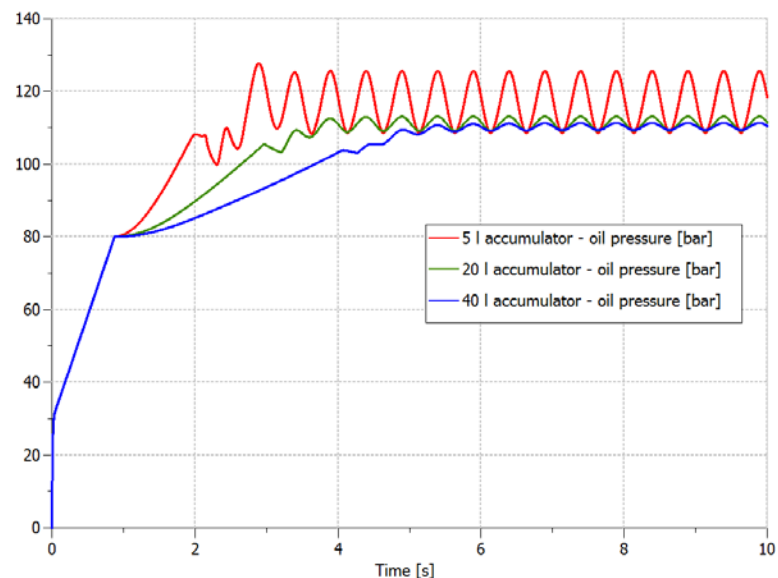
Figure 2.18: Time behavior of oil pressure within three different accumulators.

In the case depicted in the figure above, the system is initially fully discharged (initial pressure of 0 bar) while the three accumulators are both characterized by a pre-charge pressure of 80 bar. This means that once filled (line pressure = pre-charge pressure) the pressure curve changes inclination, becoming lower. This is a direct consequence of the fluid finding a new resistance in loading the

system, namely the gas stored in the accumulator with its compressibility. The phenomenon is more evident in the larger systems. The transient of sudden pressure oscillations just before reaching the pressure set is in this case due to the contemporaneous opening of the Servo-valve, but which is not really important with the purpose of our analysis (Figure 2.19).
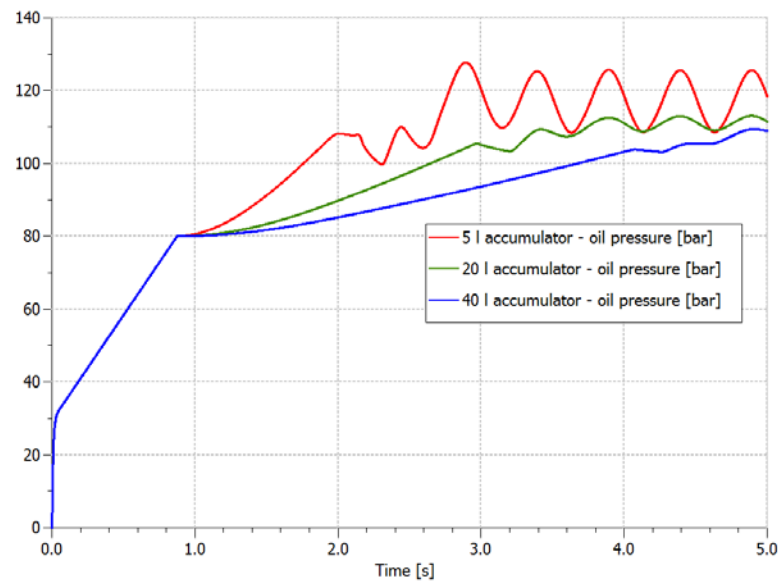
Figure 2.19: Zoomed view on the transient of the accumulators before reaching the set pressure.

A second physical phenomenon which is straight connected to the sizing of the component, is the variation in operating pressures. As explained in Appendix B, the choice of V_0 affects (through a $\frac{\gamma}{\gamma-1} > 1$ power) p_1 and p_2 of the load cycle imposed: in particular, by increasing the volume of the accumulator, the difference between max and min pressures on the piston will decrease, and vice versa (Figure 2.18).

This behavior is explained by the following formula:

$$V_0 = \frac{\Delta V}{\left(\frac{p_0}{p_1}\right)^{\frac{1}{\gamma}} + \left(\frac{p_0}{p_2}\right)^{\frac{1}{\gamma}}}$$

(2.2)

Anyways, the phenomenon is easy to understand without the help of mathematical expressions: once charged the left line, the servo-valve will work against the load of the cable (elastic spring) and, in the meanwhile, against the compressibility of the fluid in the big cylinder. If the left side was connected to a large accumulator, a big amount of gas (which is easier to be compressed) would decrease the resistance of the fluid (in terms of equivalent compressibility). A smaller accumulator, instead, would result in an increased resistance.

A clarification is necessary at this point: even if V_0 was large enough to reduce pressures, its benefit would be useless, or better "wasted", if the orifice of the accumulator was not large enough to let the flow pass. In this case the system would in fact behave as there was not accumulator, with an extremely rigid dynamics, lengthened transients and steep peaks of pressure in the cylinder (Figure 2.20).
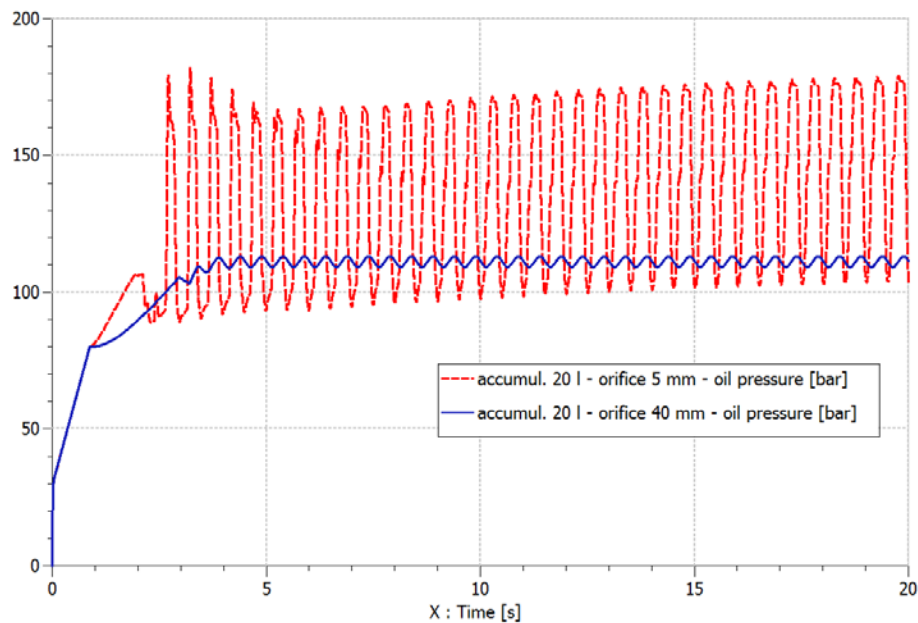
Figure 2.20: Behavior comparison for the oil pressure within two accumulators with different orifice diameter.

This not only cause the pressures to increase during the load cycle, but also worsen the tracking of the reference, because a too small orifice would require the servo-valve to push much more fluid to make the cylinder move according to the path (which is actually the reason why pressures rise up), risking then to saturate and to lose controllability of the system.

The choice of V_0 descends therefore from a compromise between a low value of pressures (high volume) and a fast system response (low volume), which is natural consequence of the quantity of fluid flowing back and forth to the accumulator every cycle. For the application of the "Tandem" it is selected a Bosch Rexroth S.p.A bladder accumulator:

- HAB 20-330-4X/2

which is a 20-liter accumulator, with pre-charge pressure of 80 bar, orifice diameter of 40 mm, designed to resist to a max pressure of 330 bar (configured in AMESim® according to the dialog box shown in Figure 2.21). Results of this choice will be exposed in the next paragraph.
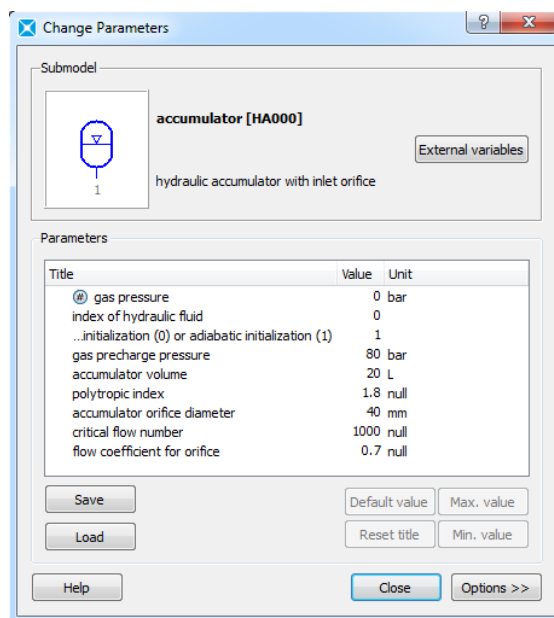
Figure 2.21: AMESim® dialog box for changing the parameters of the accumulator.

Before moving to conclusions and numbers, the system still needs to be completed by the definition of which valves will be used as Valve 1, Valve 2 and Servo-valve.

Valve 1

Valve 1 is, as already mentioned, a 2 positions 2 ways proportional directional valve whose task is to periodically open the passage to let some fluid flow towards the accumulator side of the circuit. The problem here is the same as before: a correct functioning of the system requires a sufficient nominal flow rate (and adequate pressure drop) in order to feed the cylinder and to make it reactive.

Referring again to the Bosch Rexroth S.p.A product catalogue, it is easy to find a solution to the system's requirements in the following valve:

- KKDSR1NB/HCG24N9K4V

It is a 2/2 proportional directional, direct operated, spool-type cartridge valve. As shown in Figure 2.22, it is normally closed, with a 65 ms step response, and its characteristic curves show a max flow rate of nearly 34 l/min, in correspondence of a pressure differential of 10 bar.
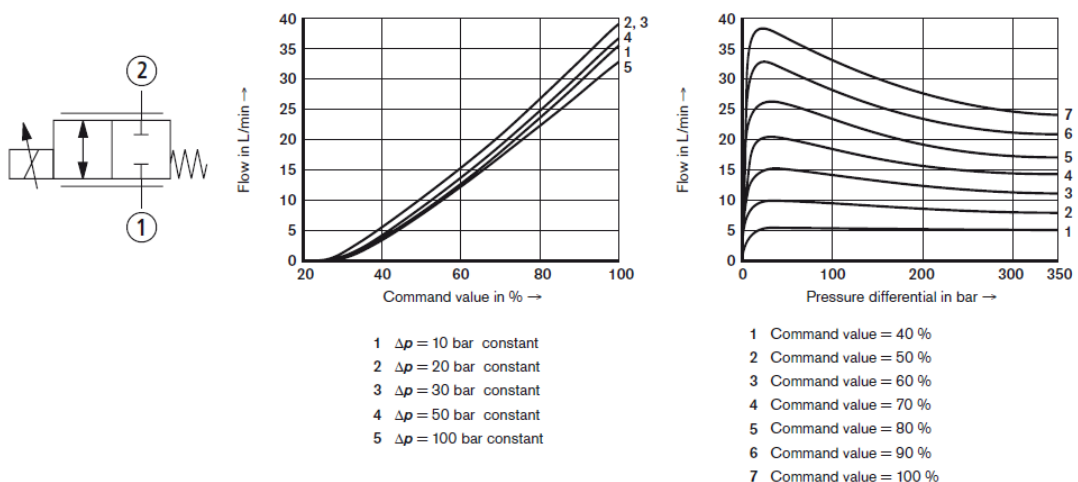
Figure 2.22: Valve 1 characteristics, from Bosch Rexroth's catalogue.

Below, in Figure 2.23, it is presented its configuration in AMEsim®'s dialog box:
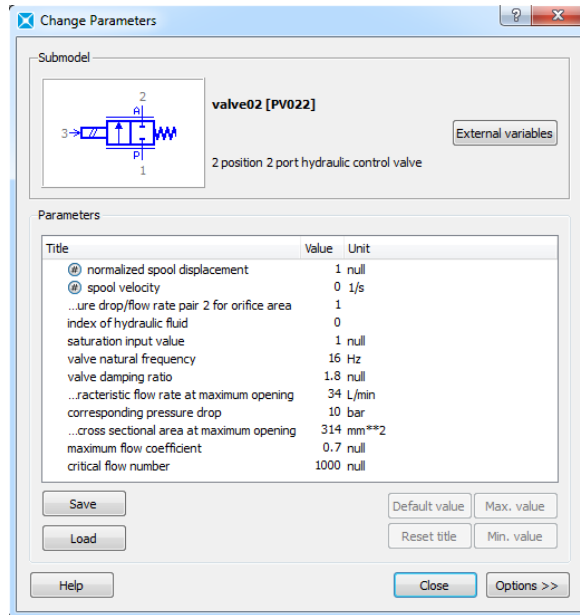
Figure 2.23: AMESim® dialog box for changing the parameters of Valve 1.

Valve 2

Valve 2 is instead a 2 ways 2 positions on-off control valve, whose task is simply to bypass the fluid on the small cylinder during the starting of the system: it will be open at the beginning and, once the bigger cylinder having reached the mean stress set, it will be closed e never re-opened. All this considered, using a proportional 2 ways valve (as for Valve 1) would definitely be a waste.

The valve chosen for this task is the following (Bosch Rexroth S.p.A):

- KSDER1NA/HN9V

It is a 2/2-way poppet, direct operated, pressure balanced, cartridge valve. As shown in Figure 2.24, it is normally closed, with max flow rate of 20 l/min, and switching step time of nearly 60 ms.
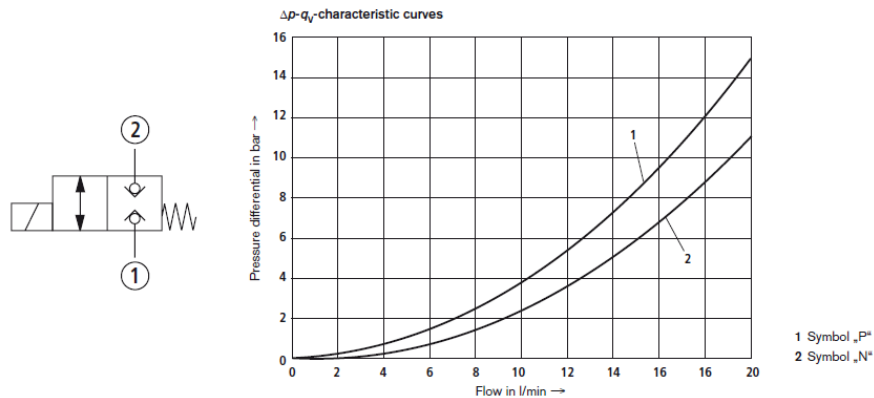
Figure 2.24: Valve 1 characteristics, from Bosch Rexroth's catalogue.

Below, in Figure 2.25, it is presented its configuration in AMEsim®'s dialog box:
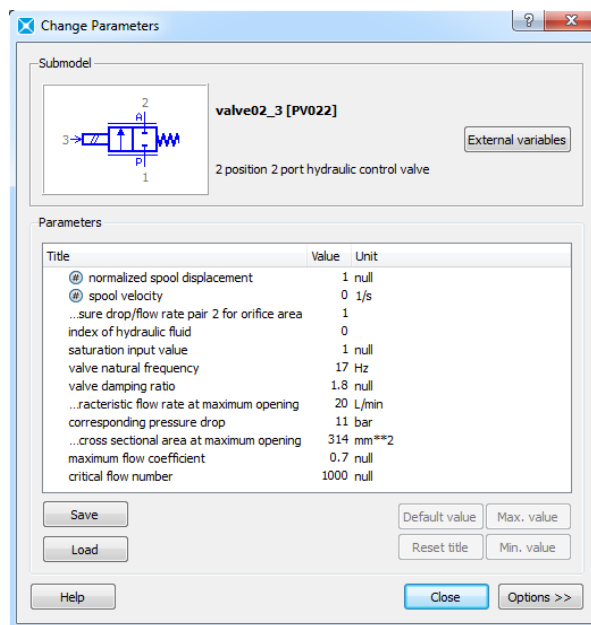
Figure 2.25: AMESim® dialog box for changing the parameters of Valve 2.

Servo-valve

The servo-valve is, in the end, the most delicate component which needs to be carefully chosen, because the entire tracking of the reference depends only on it. What the system really needs is a good equivalent section (and then an

adequate nominal flow rate) and a fast dynamic response to external inputs (even if the reference is in the case a signal with frequency of only 2 Hz).

While, however, in the big cylinder one of the chambers was directly connected to the tank (and then only one needed to be fed by the pump), the small cylinder has a different configuration, in which fluid will be alternatively fed to either the first or the second chamber, in order of course to follow the reference.

This intrinsic difference results in the need of a 4 ways valve, precisely of a 3 positions 4 ways proportional directional valve. By looking over Bosch Rexroth S.p.A's catalogues, a good solution can be found in the following valve:

- 4WS2EM10-5X/45B11XNET315K31EV

which is, indeed, a 2-stage 4/3-way servo directional control valve, with nominal flow rate of 45 l/min (with nominal pressure drop of 35 bar) and whose characteristic curves are presented hereinafter in Figure 2.26.
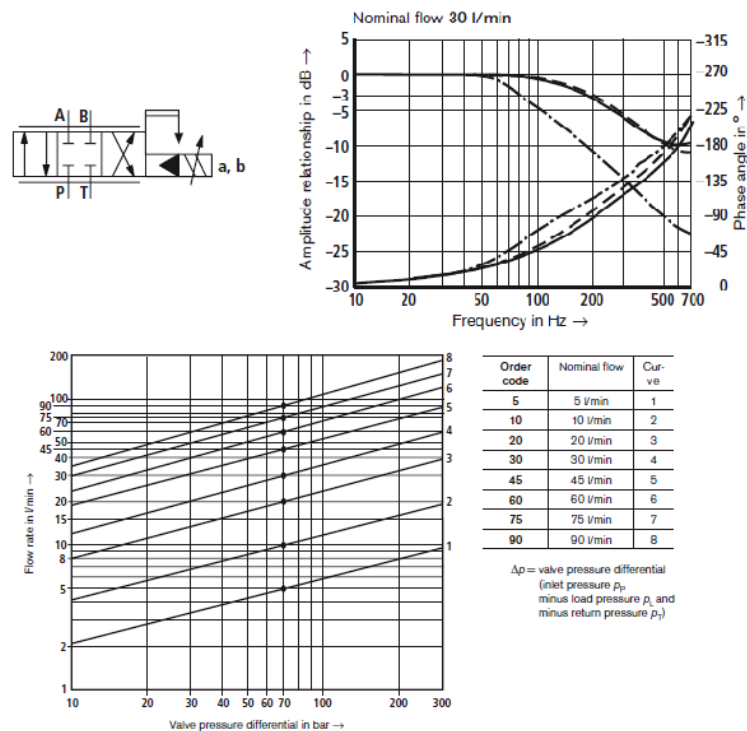
Figure 2.26: Servo-valve characteristics, from Bosch Rexroth's catalogue.

Its configuration in AMEsim® is shown below in Figure 2.27:
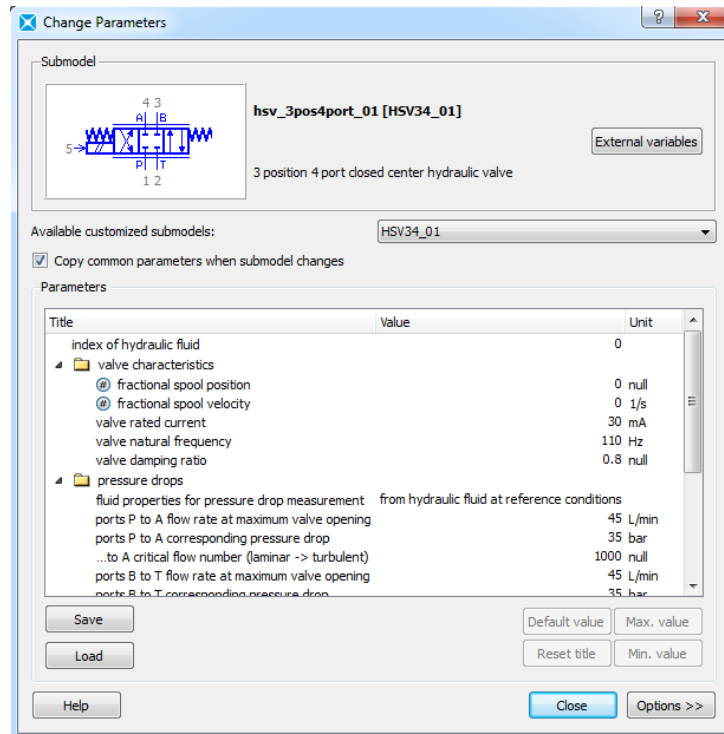
Figure 2.27: AMESim® dialog box for changing the parameters of the Servo-valve.

The system is now completed, and then ready to run the simulation. The following paragraph will be dedicated to the analysis of the results.

2.1.4 Results analysis

Before starting the discussion of results got from the simulations, it is presented the final circuit of the "Tandem" hydraulic actuator, including some modifications which will be explained and used further on in the section (Figure 2.28).
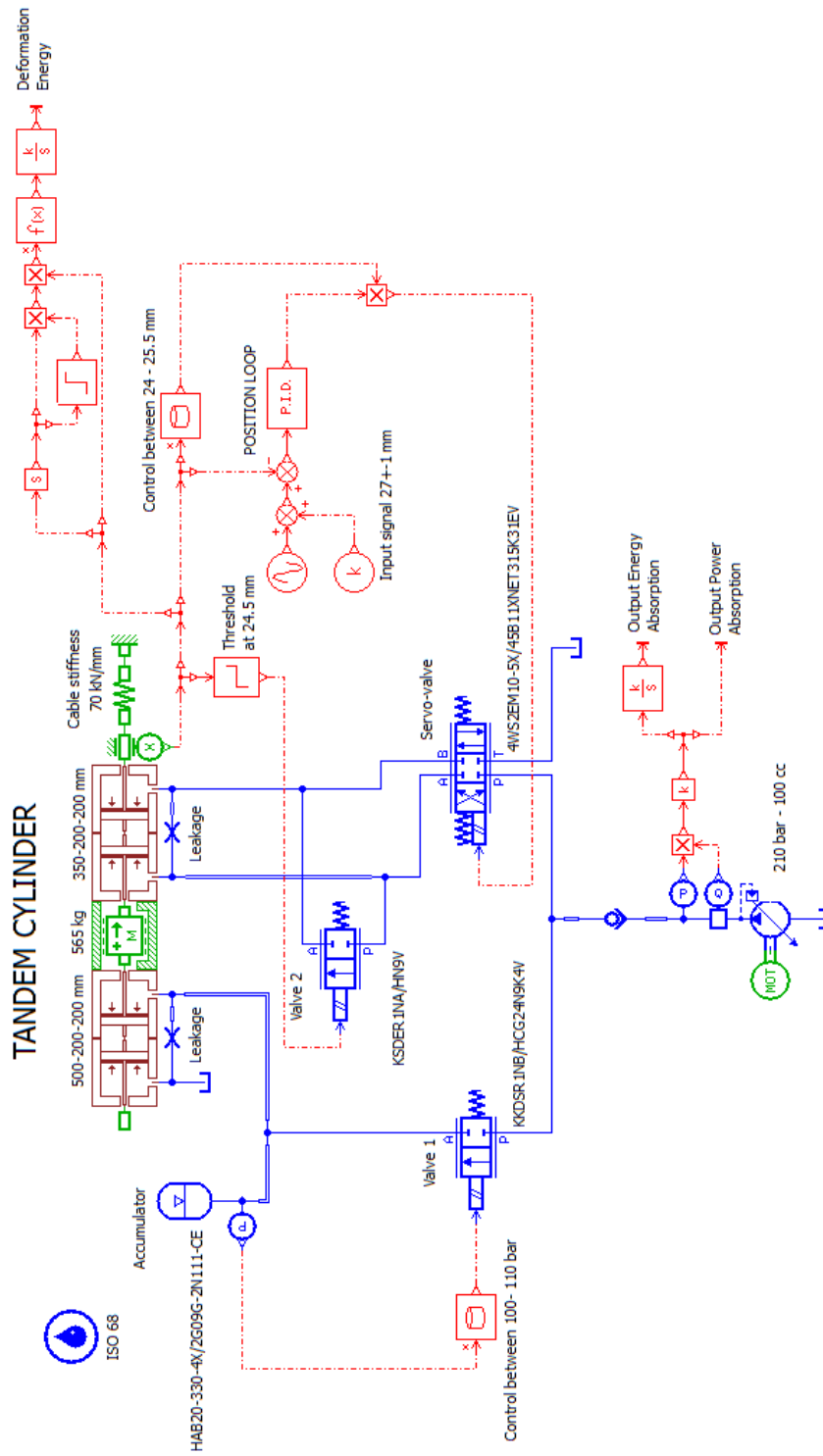
Figure 2.28: Final sketch of the circuit for the "Tandem" system actuator.

Actually, the system is now totally defined in every its component, but the definition of one parameter is still pending, namely the proportional gain K_p of the controller which will ensure the tracking of the reference. To do so, it is possible to execute a batch run of the system, by varying this constant between a well-defined range of values. The K_p corresponding to the best response could be taken as final effective gain.
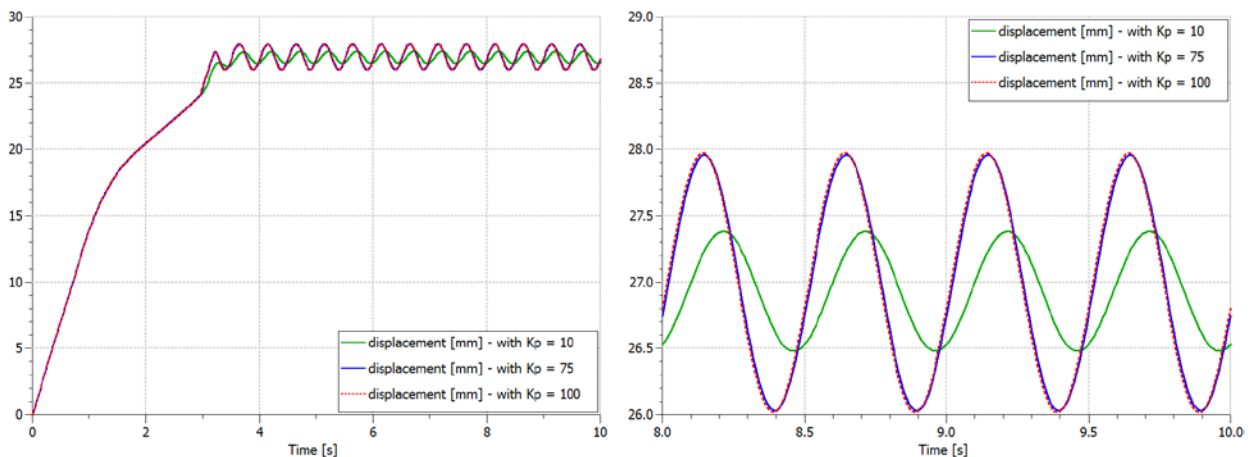
Figure 2.29: Displacement of the "Tandem" cylinder over time, with zoomed view (right), by varying the value of Kp.

As it is possible to see from Figure 2.29, at least in the reference tracking, K_p equal to 10 causes the worst behavior, while the best controller is the one with K_p equal to 100 (and the result would become even more precise if this value was increased). On the other hand, increasing the proportional gain always involve a growth in the effort (in terms of energy/flow rate), considering that the system strives much more to follow the reference in a quicker and more accurate way.

In this sense, the right choice of K_p needs to be made as a compromise between a good tracking (measured as a low tracking error) and a contained consumption (as a non excessive opening of the servo-valve).

According to the requirements of the application, the load cycle which the "Tandem" is designed for consists in a 2 Hz reference of 27 ± 1 mm, with max acceptable error of 1%. Here it comes the definition of error as:

$$error = \frac{abs(ref.\,signal - measured\;displ.)}{ref.\,signal} * 100\%$$

(2.3)

In Figure 2.30 the four error functions are depicted. As it can be noticed, only with K_p equal to 75 or to 100 the error dips down the threshold of 1%.
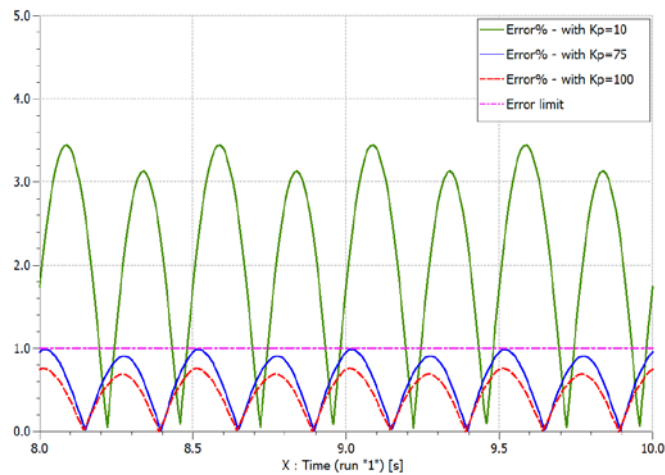
Figure 2.30: Error% over time for the three system configurations, by varying Kp.

The normalized opening of the Servo-valve is instead shown in Figure 2.31. It is clear that, according to what just mentioned, by increasing the K_p the valve will try to chase the reference more quickly, which implies greater openings. In these cases, however, the servo-valve never gets saturated, which is essential.

Considered, then, that requirements are satisfied either in the red (K_p= 75) or in the blue curve (K_p = 100), it is possible to address the final choice towards the minimum effort possible: this means that K_p = 75 will be the conclusive proportional gain. Hence the system is now ready to be simulated.
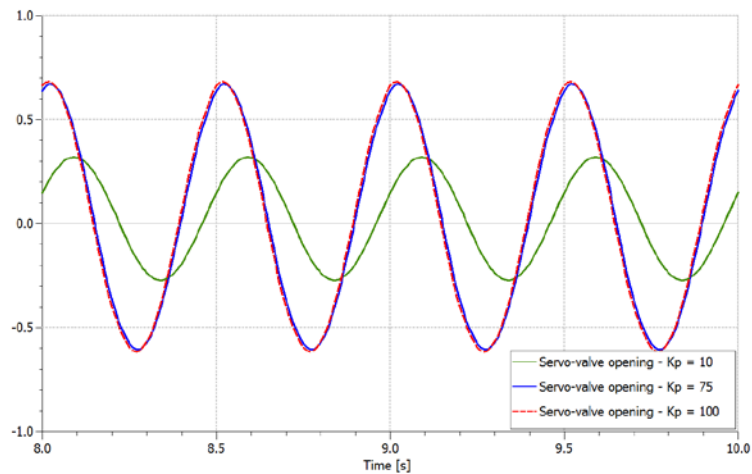
Figure 2.31: Servo-valve percentage opening, by varying Kp.

The simulation of the circuit is carried out on a time span of 10 seconds. The following part of the section in hence dedicated to a critical analysis of the results of such simulation.

First of all, the actual displacement of the cylinder, measured thanks to the transducer. Figure 2.32 shows how the system behaves over time with respect to the reference.
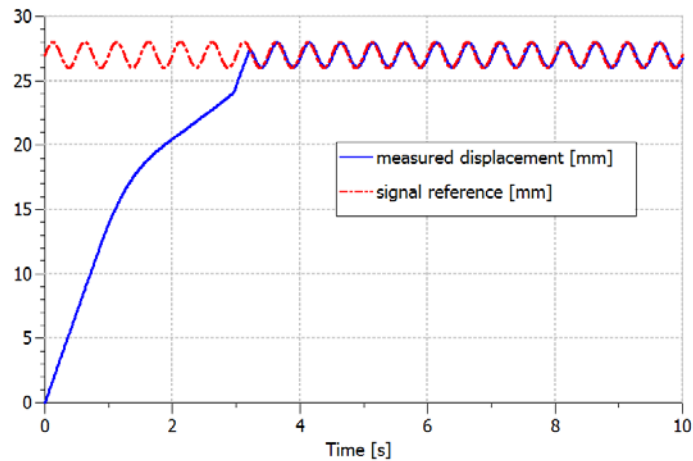
Figure 2.32: Cylinder displacement over time, with respect to the reference signal.

It is interesting also to try to understand more in detail what actually happens in the system, step by step. By zooming again on the position plot, but now on

the initial part (as shown in Figure 2.33), it is possible to notice a truly specific trend.
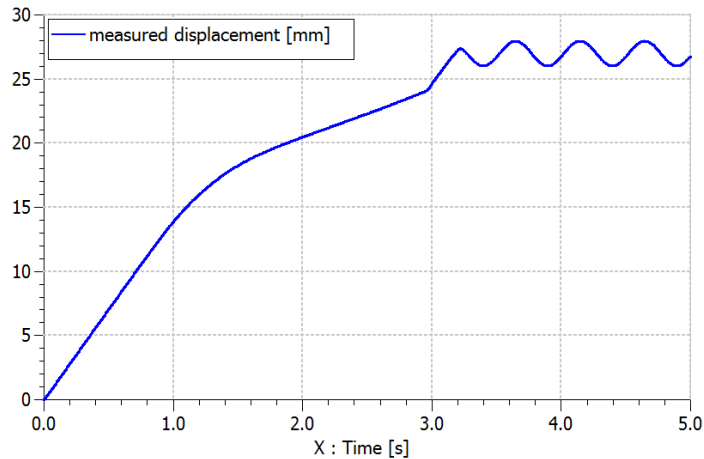
Figure 2.33: Zoomed view on the initial part of the displacement plot.

The cylinder, in fact, moves initially with a certain velocity and its position grows then linearly. Around 1.6 seconds, however, the inclination of the curve changes, becoming lower (thus lower velocity), even if the cylinder keeps on moving linearly. This modification occurs because the accumulator is completely filled with liquid and the pressure has reached the pre-charge level. From this moment onwards, the pump feeds the system finding a new resistance (apart from inertia of cylinder and friction), namely the compressibility of the gas, stored in the accumulator.

This trend is then kept until around 4 seconds. Here, in fact, the cylinder is about to reach the position set at which the right side of the hydraulic circuit is put into motion. As soon as 24 mm are achieved, the servo-valve is activated: the controller sees that position is still far from the reference, hence it sends a signal to the solenoid which moves the spool and opens the ports. In addition to this, when the cylinder is at 24.5 mm, the 2-way bypass valve is closed, letting the servo-valve control effectively the cylinder. Here, in fact, the curve changes again the slope, dragged up by the pushing power of the servo-valve, and the system is finally able to follow the reference signal.

This physical behavior is observable also from the pressures point of view. In fig. Figure 2.34 is depicted, for instance, the pressure curve over time, measured inside the big cylinder.
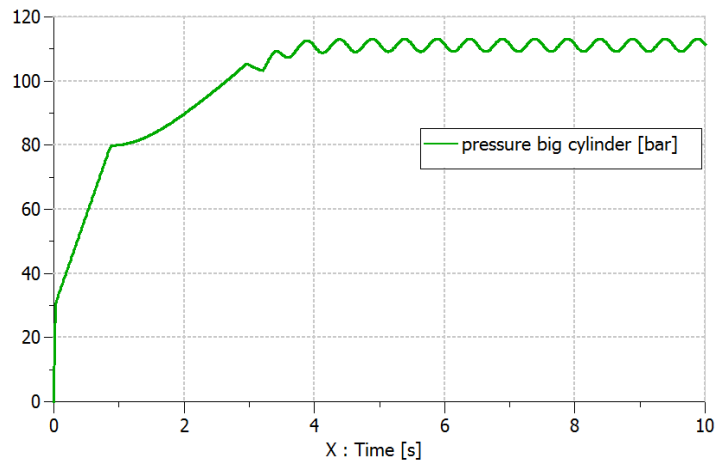
Figure 2.34: Pressure in the big cylinder over time.

Apart from a first peak, which happens at the beginning because of the starting of the pump, pressures follow exactly the same performance of the position: they increase linearly, then a sharpen change in inclination occurs and, in the end, the chasing of the reference signal is achieved.
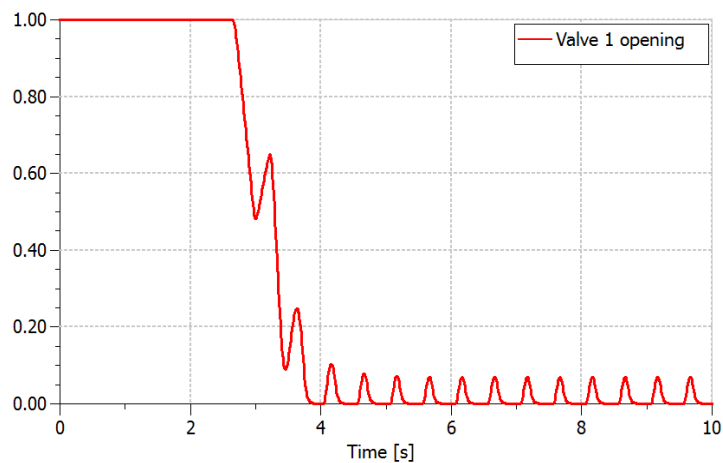
Figure 2.35: Valve 1 percentage opening over time.

Other confirmations to this interpretation of the functioning of the system can be obtained by looking at the normalized spool displacement of the valves. Let us look, for example, at Valve 1 (Figure 2.35).

The spool is initially wide open; when the pressure reaches 100 bar, it starts to get closed but also to oscillate, as the servo-valve begins working. Even when stabilized, the valve keeps on opening periodically because of the presence of leakages and because the pressure is forced to go down 110 bar each cycle by the servo-valve. Although the continuous opening and closure of the valve could seem to be a problem, the system does not risk a decrease in service-life because these valves are designed to work at least for 20 millions of cycles.

Valve 2, instead, has a much simpler normalized spool displacement than Valve 1. Its behavior, shown in Figure 2.36, ties exactly in with what explained so far: the small cylinder is initially bypassed (Valve 2 opened), but once reached 24.5 mm in position, the servo-valve can directly control the actuator (Valve 2 closed) without never needing Valve 2 to bypass the system. That is why a simple on/off valve is more than enough in this situation.
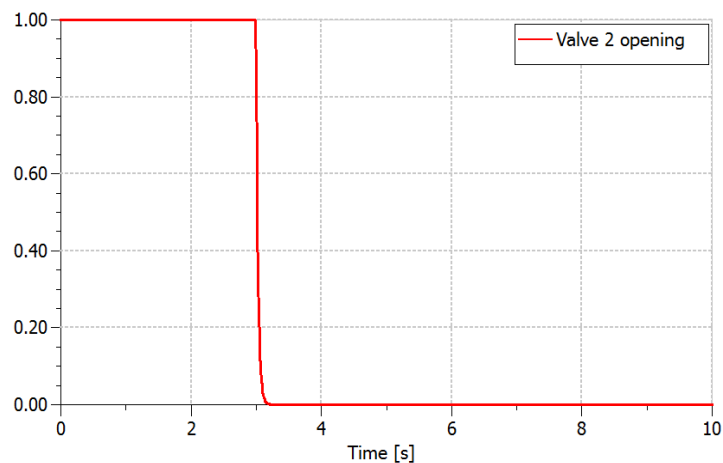
Figure 2.36: Valve 2 percentage opening over time.

In the end, the servo-valve normalized spool displacement is shown in Figure 2.37. First difference that shows up from the other two valves is the presence of negative values, which is obvious in a 3-position valve. The spool is blocked in the center at the beginning but, once the position having reached the 24

mm, it is activated and immediately gets saturated trying to compensate for the tracking error, too high. The mean position is however quickly achieved, and the regulation function can be performed, with openings of the spool never higher than the 70%.
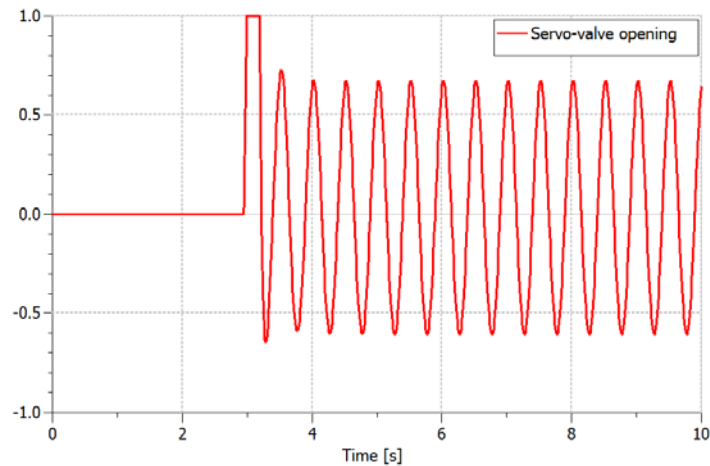
Figure 2.37: Servo-valve percentage opening over time.

A final remark is about the asymmetry existing between the higher peaks and the lower peaks: in fact, when in positive position, the valve feeds the right chamber of the small cylinder, contributing then to pull the cable against its elastic resistance. When, instead, the second half of the load cycle has to be performed, the valve opens a bit less than before, because part of the elastic energy is released and thus part of the job is "automatically" done by the same spring.

It is now the moment to look at the energy consumption of the system. For this second type of analysis of the system, about energy, we will run a second simulation of 100 seconds, in order to have numbers less affected by the initial transients. The computation of the energy absorbed can be done by placing two transducers, one of pressure, the other of flow rate, right after the pump. Their signals, if multiplied and opportunely integrated, return the effective *cumulative energy* consumed over the considered time horizon (Figure 2.38).
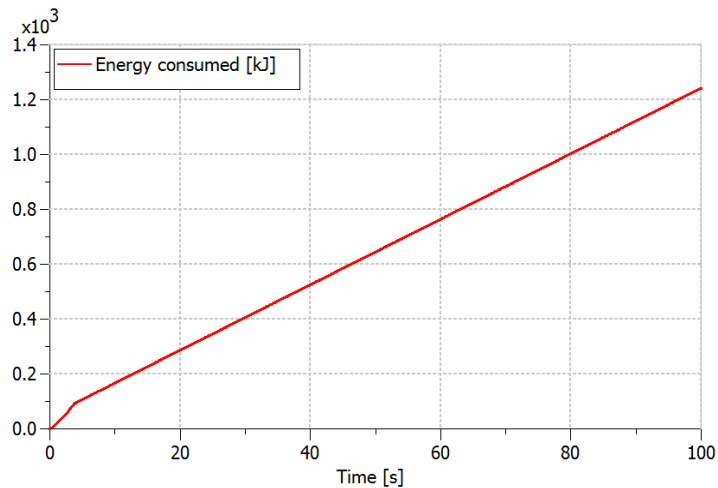
Figure 2.38: Cumulative energy consumed by the "Tandem" over time.

For the moment this graph is not that significant. We infer that, over a time span of 100 seconds, the system absorbs a quantity of around 1.294 MJ; his true meaning will be fully understood at a later time in the chapter, when a comparison between the behavior of traditional circuits and the "Tandem" will be carried out.

In parallel with this measurement, a second energy index is computed by the system, namely the effective cumulative "Deformation Energy". This one is calculated as follows:

$$E_{def} = \int kx\dot{x}\, dt \quad with \; \dot{x} > 0$$

(2.4)

In few words, this one can be considered as the "Useful Energy", namely the energy used in the effective traction of the, because the "downloading" part of the load cycle could theoretically be done for free, with the same cable just releasing the accumulated elastic energy. Its graphical trend is shown in Figure 2.39:
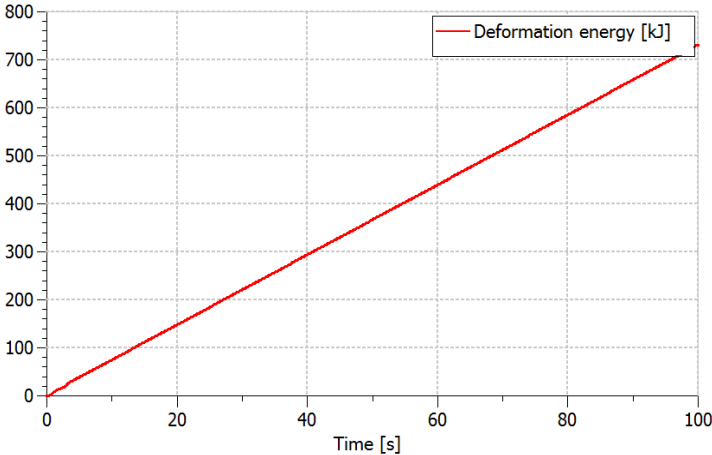
Figure 2.39: Deformation energy absorbed by the "Tandem" system in the cable deformation.

All this considered, it is spontaneous to introduce, in the end, an "Energy Efficiency" index. Its definition, intended as the ratio between the useful energy which effectively deforms the cable and the total hydraulic energy absorbed by the system, follows the formula below:

$$\eta_{en} = \frac{E_{def}}{E_{tot}}$$

(2.5)

and its graphical representation over time is depicted in Figure 2.40.
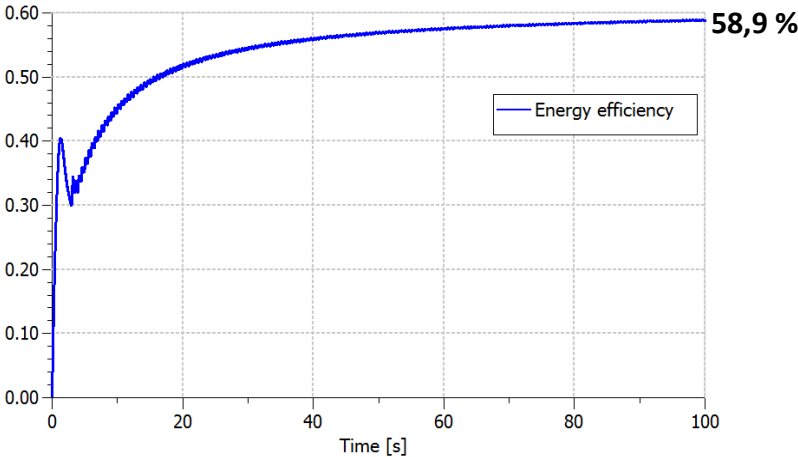
Figure 2.40: Energy efficiency of the "Tandem" system.

The function shows a first steep peak in correspondence of the starting of the system, when the cylinder is pulled only by the accumulator side: here in particular the efficiency is low because most of the fluid is used to fill the accumulator. After the peak there is a short fall in energy efficiency: this is due to the starting of the servo-valve which, for a very short period of time, works loadless with Valve 2 still bypassing the small cylinder. When Valve 2 gets closed, the servo-valve starts to really feed the system, and the energy efficiency grows until settling on a value of around 56%.

In the next section they will be presented the results of the simulations carried out for the other two systems presented in section 2.2. A comparison between the outcomes will demonstrate how much the "Tandem" system can allow a reduction in terms of energy consumption.

2.2 Simulation of the other configurations

In this second section the plant schemes of the other two configurations will be presented, such that their simulation results could be compared to those of the "Tandem" to exhibit which is the best, energetically speaking.

First the regulation of the single-stage hydraulic cylinder will be set up; specific components will be chosen in order to let the system guarantee the required specifications. Then the double-stage cylinder controlled by two servo-valves will be suitably sized and set up.

2.2.1 Simulation of the single-stage cylinder with one servo-valve

The hydraulic circuit of the above-mentioned system is shown below in Figure 2.41.
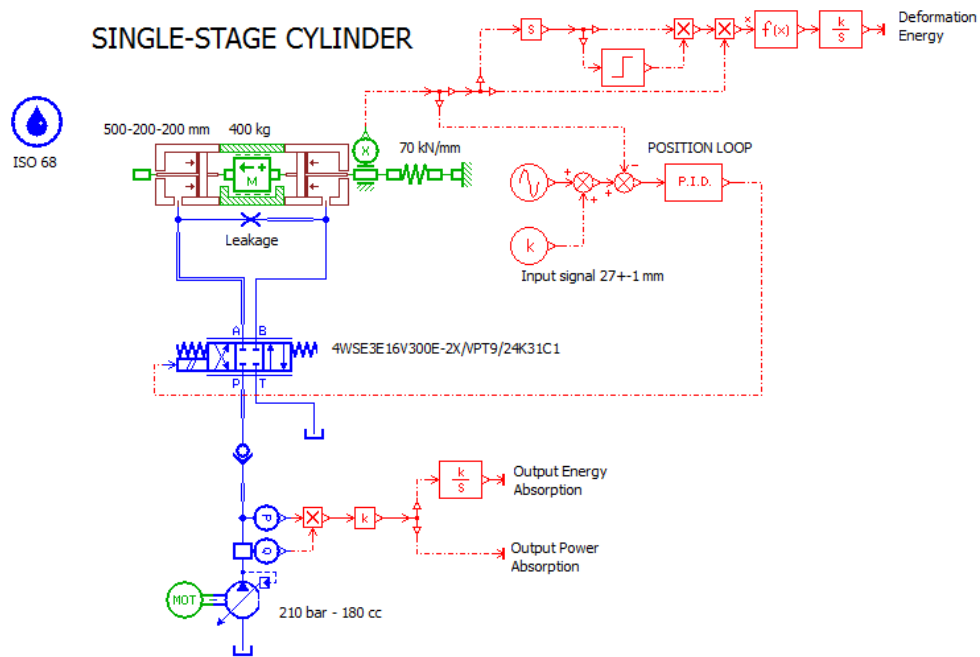
Figure 2.41: Final sketch of the circuit for the classical single-stage hydraulic actuator.

As far as it is possible to observe, the circuit is much easier than before. The system is composed of a big, single-stage, linear actuator, which pulls the cable according to a reference signal, whose tracking is guaranteed by the servo-valve.

The functioning of the machine is quite the same of before. The difference between this system and the "Tandem" is however intrinsic and consists of the fact that now the servo-valve needs to feed the cylinder for the whole load cycle, and not only for the alternate part.

This causes the system to absorb much larger quantities of fluid (and hence of energy). Therefore the system necessarily requires a completely different sizing of the circuit. If we used the servo-valve and the pump of the "Tandem", for sure the circuit would not have enough power to provide the cylinder with.

The pump, for example, is re-sized to generate a maximum flow rate of nearly 260 l/min (180 cc/rev with a nominal shaft speed of 1450 rev/min) at a pressure of 210 bar. Its characteristic curve is depicted hereinafter in Figure 2.42.
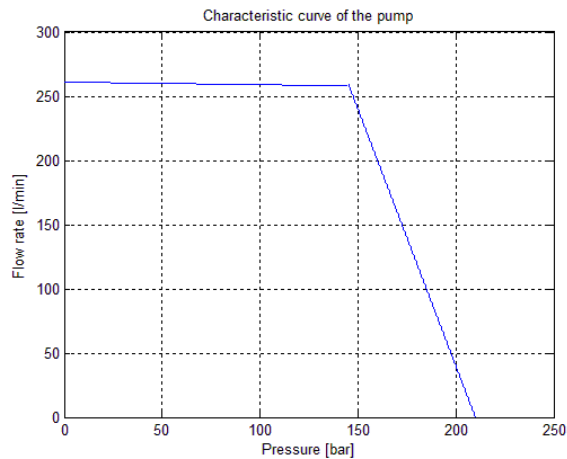
Figure 2.42: Characteristic curve of the pump for the single-stage hydraulic actuator.

This combination would be totally wasted if there was not a servo-valve with nominal flow rate large enough to ensure a good passage of fluid. In this case the choice is addressed towards a Bosch Rexroth 3-stage 3/4-way servo-valve as follows:

- 4WSE3E16V300E-2X/VPT9/24K31C1

which corresponds to an electrically operated valve, with nominal flow rate of 260 l/min at a pressure differential of 35 bar, and whose dynamic characteristics are represented below in Figure 2.43.
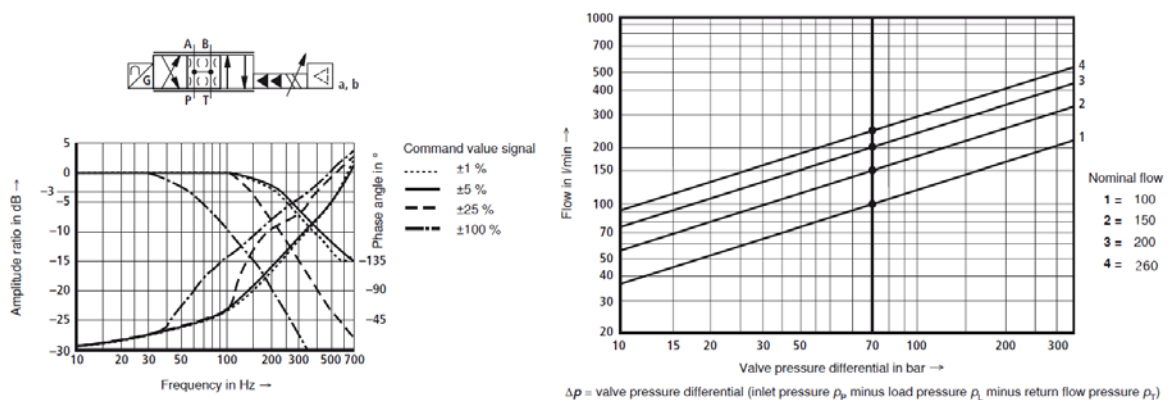
Figure 2.43: Servo-valve characteristics for the single-stage actuator, from Bosch Rexroth catalogue.

These feature defined, the system is now ready to be simulated and compared to the other solutions.

2.2.2 Simulation of the double-stage cylinder with two servo-valves

On the same guidelines used in the previous chapters, the double-stage cylinder regulated by two servo-valves will be now opportunely sized and got ready for the simulation.

The circuit scheme of this ending solution is hereinafter proposed in Figure 2.44.
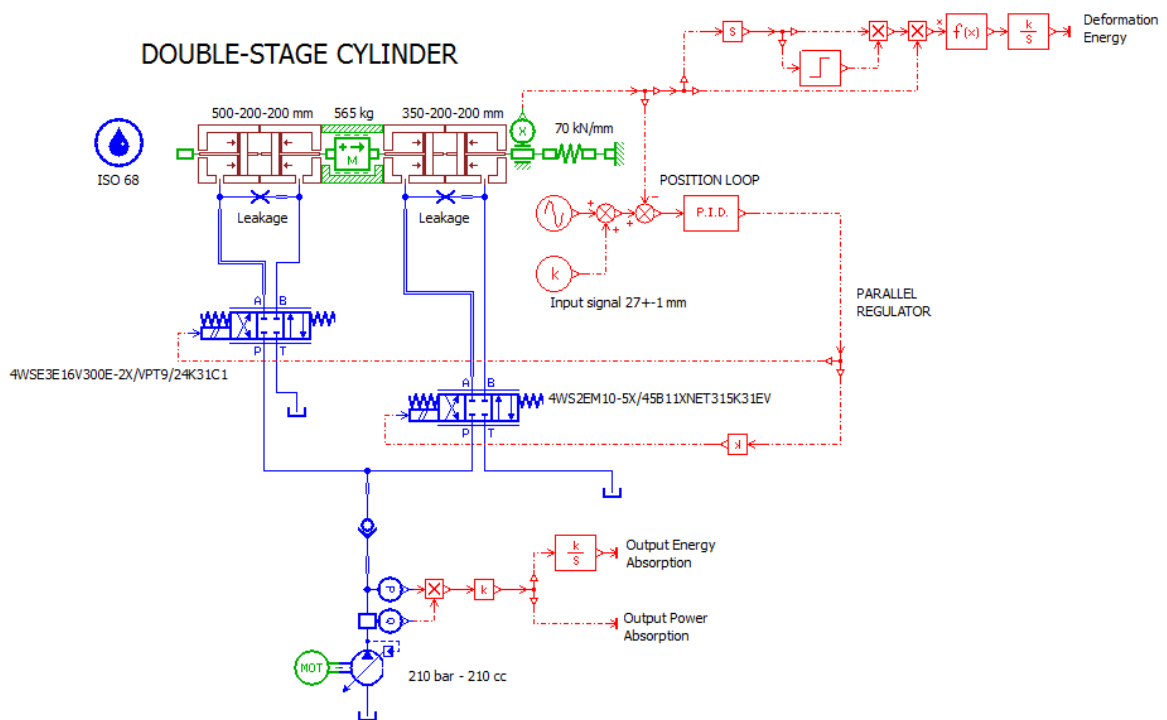
Figure 2.44: Final sketch of the circuit for the double-stage actuator driven by the two servo-valves.

In this last configuration the servo-valve of the single cylinder will be used to control the big-piston side of the circuit, the servo-valve of the "Tandem" system for the small one. The rest of the circuit is exactly the same as before, except for the pump, which in this case will still need more power than in the previous case. Its nominal displacement will be of 210 cc/rev which, at a nominal shaft speed of 1450 rev/min, corresponds to a max flow rate of about 305 l/min.

The characteristic curve of the pump is depicted in Figure 2.45.
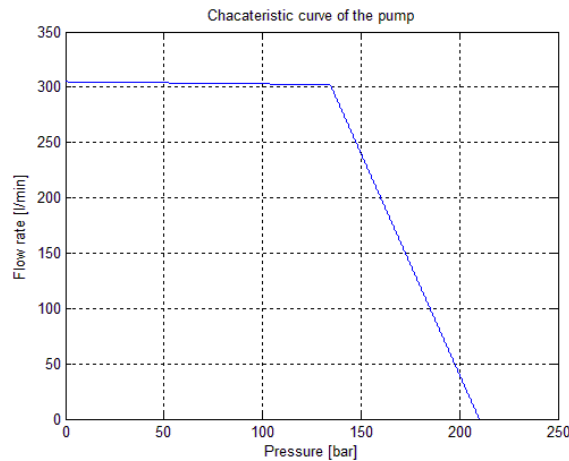
Figure 2.45: Characteristic curve of the pump for the double-stage hydraulic actuator driven by the two servo-valves.

The system is now ready to work correctly, and the simulation to be properly run.

2.3 Results comparison and analysis

The following section will be dedicated to the presentation of results and to their critical comparison, to show how each system effectively behaves in relation with the others. As already mentioned in the previous sections, we expect to see the "Tandem" showing a marked energy-saving conduct, without losing tracking power with respect to the single-cylinder actuator and the double-stage one controlled by the two servo-valves.

The first aspect to be screened is certainly the position reference tracking. As shown below in Figure 2.46, both the systems manage to perform the load cycle as required in the initial specifications (even because they are appositely designed to do that).
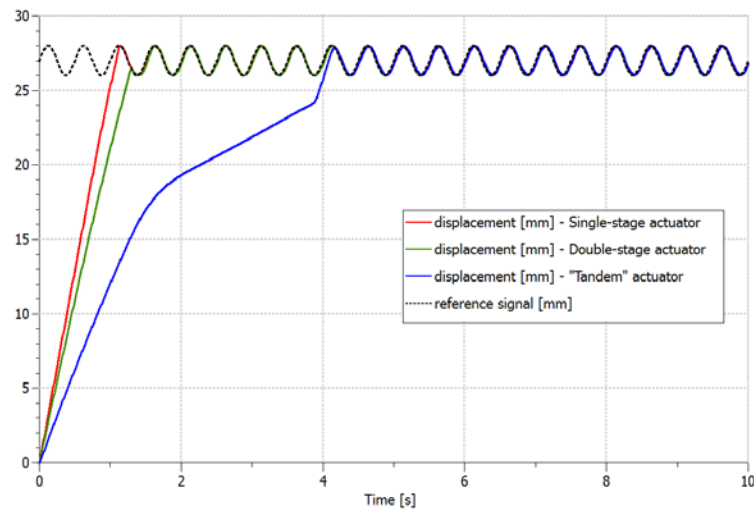
Figure 2.46: Comparison of the displacement of the three actuators.

A confirmation of the goodness of these behaviors is given from the error function, whose trend over time is represented in Figure 2.47: all the systems are, in fact, under the threshold of 1%.
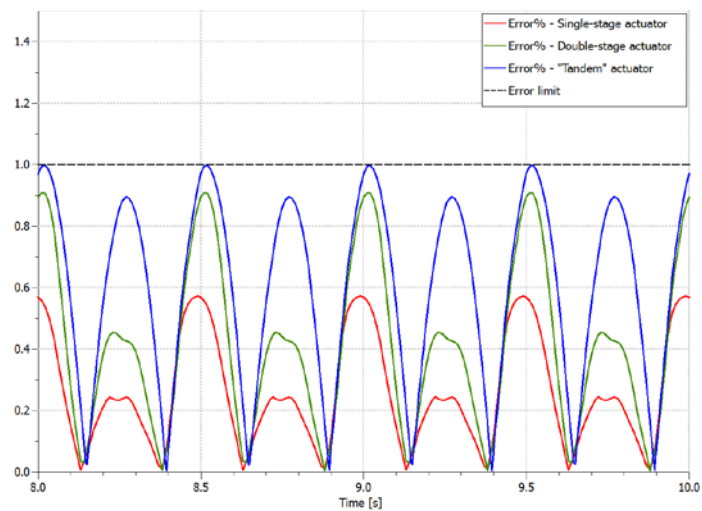
Figure 2.47: Tracking error for the three systems.

The present thesis is nevertheless centered on the development of a new-concept hydraulic linear actuator, the "Tandem", able to guarantee a strong spare in terms of energy. All along its design and configuration phases, the

biggest goal has been to do everything with a special care towards the flow rate absorption and the pressures at stake, trying to continuously reduce and restrain them. The following images will demonstrate that the goal has been brilliantly achieved.

Figure 2.48 in particular shows the cumulative energy consumption over the time span of 100 seconds.
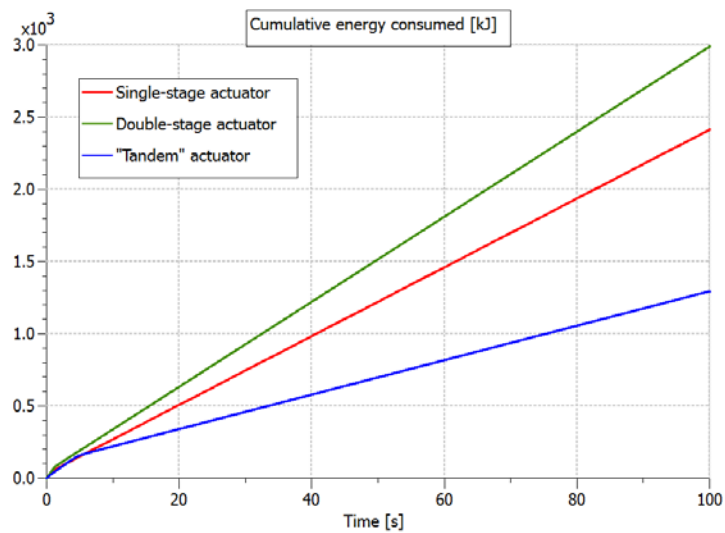
Figure 2.48: Cumulative energy in kJ absorbed by the three actuators.

The saving achieved by the "Tandem" actuator is impressive and, for sure, more than expected. It precisely consumes 1294 kJ (over 100 s) which is the 46% less than the single-stage cylinder (2412 kJ) and even about the 57% less than the double-stage actuator with two servo-valves (2988 kJ).

A final comparison is hence spontaneous between the energy efficiencies of the different systems. The graphical representation is shown below in Figure 2.49.
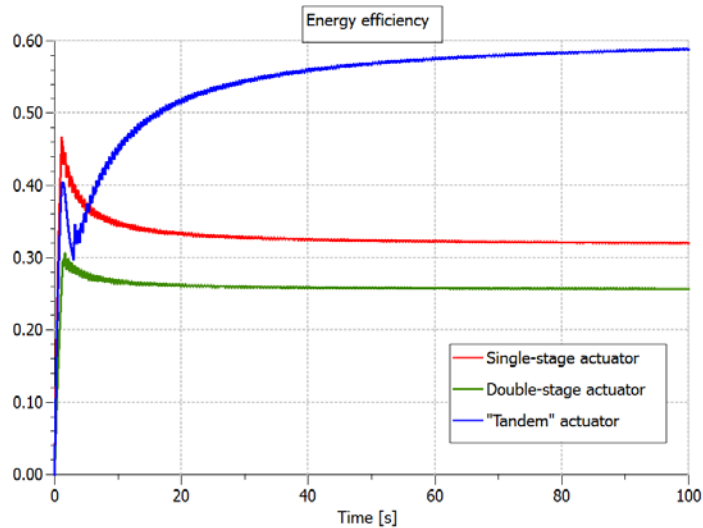
Figure 2.49: Comparison between the energy efficiencies of the three actuators.

It immediately stands out the difference in behavior between the three curves. The single-stage, and the simple double-stage actuator, not being endowed with an energy-saving system, show up for their initial peak (while the cylinder reaches the mean position, all the work done is "useful"), but after that they settle on an asymptotic value, which to be precise corresponds to a *32,0%* for the single-stage and a *25,7%* for the double-stage one. On the contrary the "Tandem" has a worse behavior at the beginning, when it pumps fluid into the system to get the accumulator filled; after that the energy efficiency curve can rise up, by reaching a value of *58,9%*.

Chapter 3

Frequency domain analysis

In the previous sections of this first half of thesis, the attention focused on the system response over time, in the case of chasing a variable position reference signal during a fatigue test. The results achieved showed the incontrovertible improvement in the energetic performances which the "Tandem" actuator carries with respect to the classical single-stage configuration.

The hydraulic architecture, which this new cylinder is characterized by, is moreover suitable for a possible improvement in terms of frequency response of the whole system. As already mentioned, the "Tandem" actuator keeps in fact the average stress of the load cycle almost "for free" (thanks to the accumulator). The remaining alternate load can be then exerted in a smaller cylinder endowed with a reduced piston area, which means a reduction in volume of oil, and which consequently let the reader think about a possible modification of the poles of the system, such that the bandwidth of the system is increased.

The prevision and the feeling about such an improvement is justified also by the fact that, in order to make all the systems reach the required performances in the time domain (chapter 2), the classical system and the double-stage actuator with two servo-valves required a much more powerful feeding system (pump and servo-valves included) with respect to the "Tandem" one. All the results shown in the time domain analysis descend in fact directly from an opportune sizing of the systems, which allowed all of them to achieve the required performances.

This section is instead meant to analyze the improvements in terms of frequency response of the "Tandem" cylinder with respect to the other configurations: the results we are interested in observing, should be purified

from the external factors of valve or pump properties: what we want to investigate is the advantage of simply one type of cylinder with respect to one other. That is why, in order to run this verification, all the systems have been endowed with the same valve, pump and other boundary conditions.

During this test, however, only the classical cylinder and the "Tandem" one have been tested: in fact the double-stage mid-span configuration has already been demonstrated significantly worse than the others. In this fashion, only the classical solution and the new one proposed have been compared.

Unfortunately the AMESim® software does not offer strong instruments for such a frequency analysis of the system. That is why a sort of *numerical sweep* test has been set up. The test under consideration has been executed just like in an experimental way. A reference signal with frequency linearly growing over time has been fed to the systems. The displacement of the two configurations have been then analyzed in the frequency domain (through *Fast Fourier Transform*) and then compared to the input in order to obtain the system transfer function.

3.1 Test execution

As already mentioned in the introductory part, the systems have been tested just like in an experimental way, by feeding the two cylinders with a reference signal with frequency linearly increasing over time:

$$x_{ref}(t) = 27 \pm \sin(2\pi f(t) \cdot t) \qquad\qquad (\,3.1\,)$$

Considering the system sizes, the forces exerted and the stiffness of the cable at stake, it is expected a very slow system, with limited bandwidth of the degree of order of few units of Hz. For this reason the frequency has been made vary very slowly from 0 Hz to a max frequency of 5 Hz, over a time horizon of 200 seconds.

In fact, according to measurements theory [7], the speed of variation cannot be too elevate, and it has to been selected depending on the damping of the system, in such a way to let the system responds to the input as if it was in stationary conditions.

In particular, firstly 15 seconds have been given to the systems in order to reach the average position; then 200 seconds more of simulation have been run in order to observe the system response.

According to all this preface, the defined frequency function is:

$$f(t) = \frac{t-15}{200}$$ (3.2)

for $t \geq 15\ s$. Results of this test are presented in Figure 3.1.
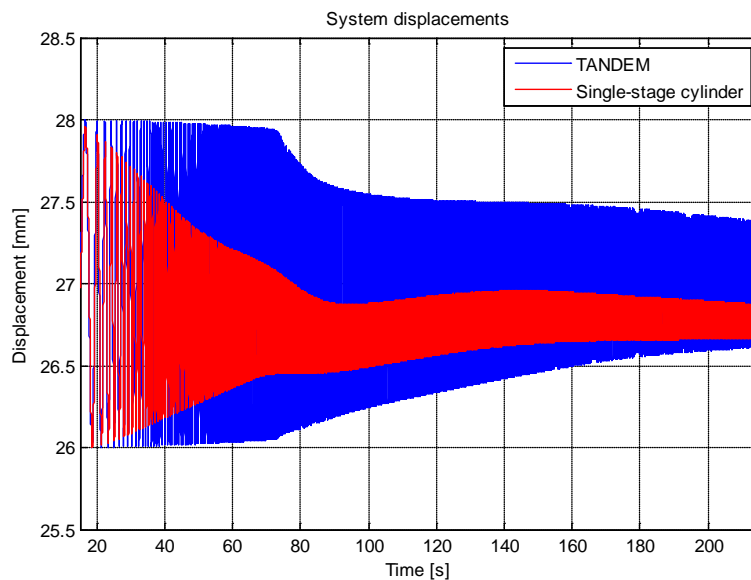
Figure 3.1: Zoom on the two systems responses between 15 s and 215 s.

In the figure above is in particular represented the zoom on the two systems responses over time, in the time window between 15 s and 215 s, the part of interest in which the sweep test has been executed. As far as it can be noticed, frequencies are initially low and they grow over time. Anyways a strange non linear behavior is found in the two systems, especially in "Tandem" cylinder.

This variation of signal average over time could be due to the system circuit properties: in particular, especially in the case of the "Tandem", this behavior could descend from the structure of the control strategy, according to which explained in the time analysis, Valve 1 is periodically re-opened and closed in order to feed the system pressure losses and leakages. This is not of interest in

our analysis, because what we want to observe is the decay of amplitude with increasing the frequencies, and then the bandwidth of the two systems.

That is why in the next section a suitable treatment has been applied on the data in order to cut out this part of the signal.

3.2 Data treatment

According to previous section, data have been elaborated to cut out that signal average variation over time, which was not of interest.

To do so, data have been converted a first time into the frequency domain with a Fast Fourier Transform. Results of this operation have been shown in Figure 3.2 by using a linear scale.
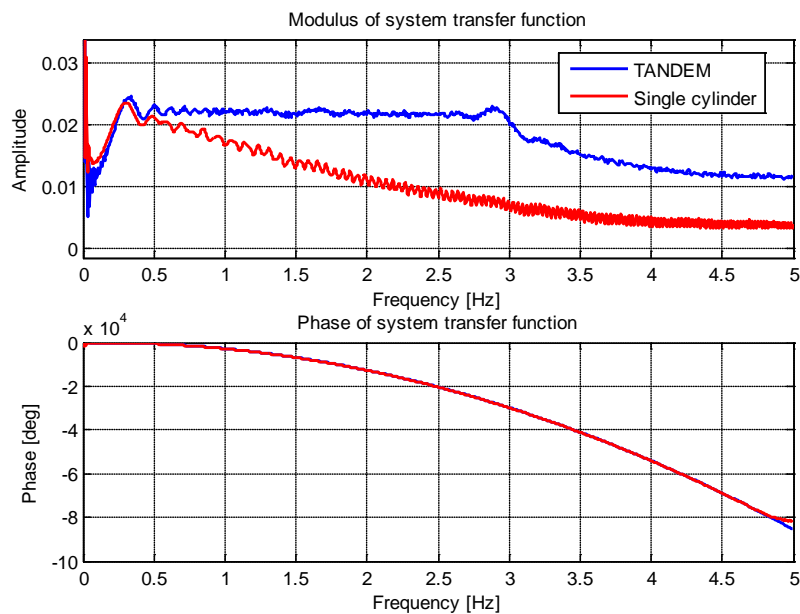
Figure 3.2: Zoom on the two systems responses between 15 s and 215 s.

The figure confirms what noticed in the time representation of the responses in Figure 3.1.

In order to purify this signal from this unwanted behavior, it is now possible to apply a *Low Pass Filter* on the spectrum of both the signals. The filter at stake is in particular a first order one which follows the transfer function:

$$F_{filter}(\omega) = \frac{1}{1 + \tau\omega}$$

<div align="right">(3.3)</div>

characterized by a cross-over frequency (- 3dB output) of:

$$\omega_0 = \frac{1}{\tau} \; rad/s$$

<div align="right">(3.4)</div>

In Figure 3.3 it is depicted a graphical representation of the LPF transfer function in use.
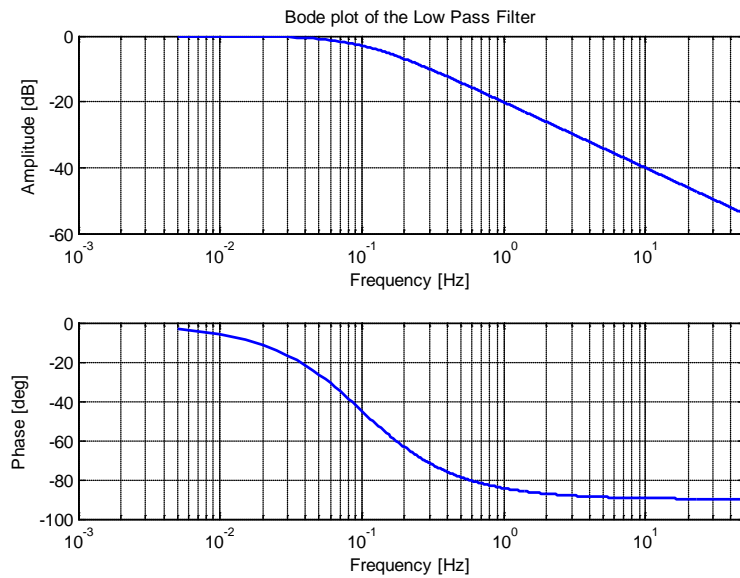
Figure 3.3: Low Pass Filter transfer function.

By choosing a time constant $\tau = 5/\pi \; sec$, it is possible to cut all the signal after a frequency of $f_0 = 0,1 \; Hz$, leaving then untouched all the frequency content we want to eliminate. The operation can be done by directly multiplying the amplitude of system's spectrum and filter's one, and by summing the phases.

The next step consists then in passing back to the time domain. Figure 3.4 shows perfectly the action of the filter: we managed to isolate the part of time signal we want to cut out by the total system response.
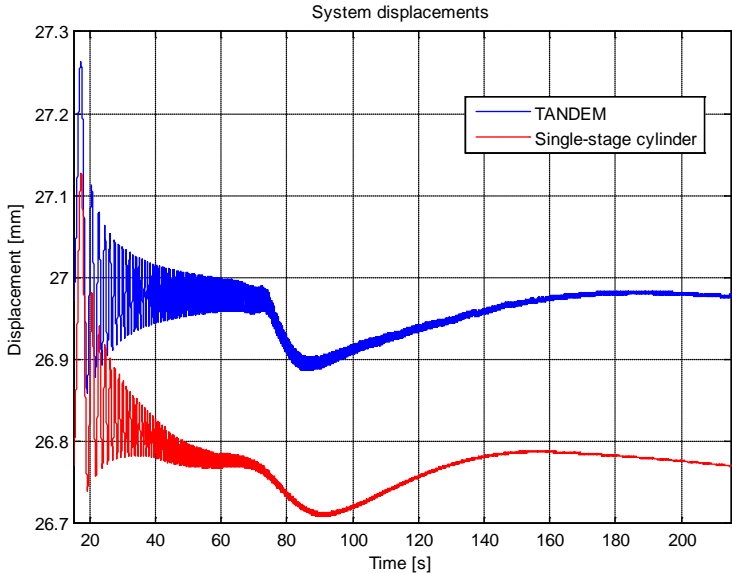
Figure 3.4: Results of the application of the filter in the time domain.
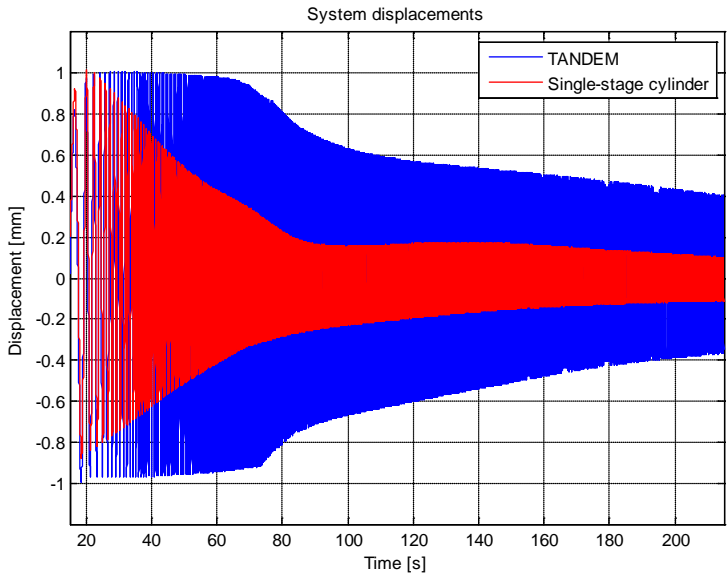
Figure 3.5: Purified time signal of the two cylinders.

By simply subtracting this time signal content to the initial one, we get then the "purified" signal (Figure 3.5), which is hence ready for the final analysis.

The final analysis consists then in taking these two time signals (for both the actuators) and the input one (which has been previously defined in equation (3.1)) and passing them back to the frequency domain through a second Fourier Transform.
In this way the final transfer functions are obtained as follows:

$$modulus_{TF}(\omega) = \frac{modulus_{CylinderOutput}(\omega)}{modulus_{input}(\omega)}$$

(3.5)

$$phase_{TF}(\omega) = phase_{CylinderOutput}(\omega) - phase_{input}(\omega)$$

(3.6)

3.3 Results analysis

Results of this operation, applied on both the cylinder signals, returns the transfer functions depicted in Figure 3.6.

We cannot be sure about the accuracy of the result obtained, because it clearly *depends entirely on* how *the software* models the system (and everything takes place inside it). Anyways, assuming its physical interpretation of the phenomena is correct, this sweep test has demonstrated that the bandwidth of the "Tandem" configuration is about 2,5 times bigger than the one of the classical actuator.
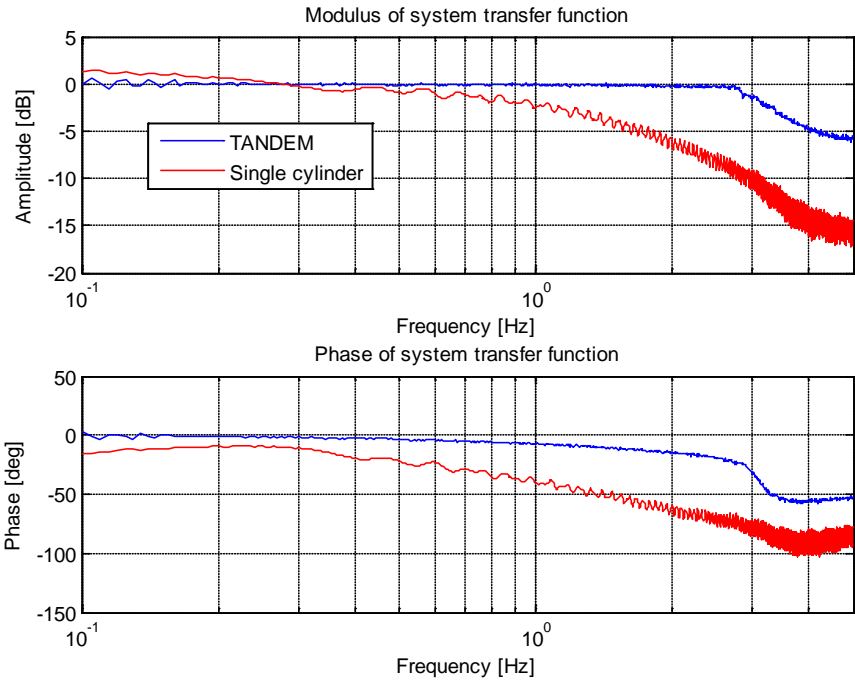
Figure 3.6: Bode plot of the system transfer functions

Part 2

Hydraulic actuator for vibration control

In the first part of the current thesis, the design of a special hydraulic actuator for fatigue tests has been successfully discussed and worked out. Its concept turned out to be particularly convenient for operations like fatigue tests because its structure allowed a huge spare in terms of energy, besides a significant increase in bandwidth. Reduction in dimensions of the cylinder, in nominal sizes of the valves and in volumes of oil at stake, revealed themselves fundamental in the achievement of such advantages.

The significance of the goodness of the results accomplished, forced a re-orientation of the design process towards the possibility of other applications for this actuator architecture.

Alongside of fatigue tests, one other industrial field in which hydraulic actuators still play a significant role is the control of vibrations. Let us take the example of concrete handling arms (Figure II.1): these ones are light and slender metallic structures, with hollowed section, thanks to which the concrete is pumped in suitable conducts towards the desired destination. In all the models of machinery, the handling is achieved by hydraulic actuators, connected to the arms by suitable kinematic motion. Because of their nature and their usage, they are unavoidably subject to deformation and vibration propagation.

Figure II.1: Example of mobile application of booms for concrete handling.

Vibrations can be caused from the most various and general reasons:

- Pumping the concrete: the concrete is admitted to the conduit within the arm thanks to a volumetric pump positioned at the base of the arm. Anyways, its motion within this sort of pipe faces some irregularities, which unavoidably translates in disturbance forces of unknown entities, and totally unpredictable.

- Operator inputs: according to the state of the art, in most cases these machines are totally controlled by human operators who, manually acting on a specific console, adjusts the opening of the valves, which consequently affect pressures and flow rates inside the chambers of the hydraulic actuator. The typology of valves used for these applications, and sometimes the lack of experience for the same operators in handling these devices, could result in sharp variations of pressure, which generate vibrations travelling along the structure.

- Environmental factors: further stimuli which can cause the birth of vibrations within the arms are the wind, weather conditions in general, or unforeseen bumps.

All these oscillations have as a natural consequence a heavy worsening of the pumping performances and, at the same time, an increase in mechanical stresses which affect the service lifetime of the machinery itself. That is why

the development of hydraulic actuator able to actuate the arms and, contemporaneously, to reject vibrations, turns out to be definitely necessary.

Literature is rich about this topic: most of the papers and patents [8, 9] found in libraries and on the web tell about light and slender structures which handle concrete, being actuated by hydraulic power cylinders. In some cases, attention was paid for the development of innovative robust motion control strategies [10], but in most of them they were applied on normal hydraulic structures, generally on single-rod hydraulic actuators (Figure II.2). Nobody actually focused and looked for an improvement in terms of performances of the cylinder itself which could positively affect the dynamics of the mechanical system.
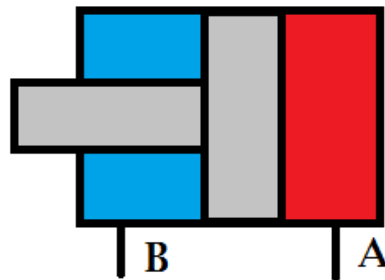
Figure II.2: Sketch of a single-rod hydraulic cylinder.

In the following sections a kinematic and dynamic analysis has been carried out, in order to come up with a clear comparison between the "Tandem" actuator and a normal symmetric single stage hydraulic cylinder, showing all the advantages of such application.

The "Tandem" cylinder in particular has been used as before in the fatigue testing application. At the beginning only the big stage of the cylinder has driven the arm in reaching the desired angle θ_0. Once achieved a stable equilibrium, the accumulator line has been closed by the 2-way valve, and the small piston (driven by the servo-valve) has started to compensate for the disturbances (Figure II.3).
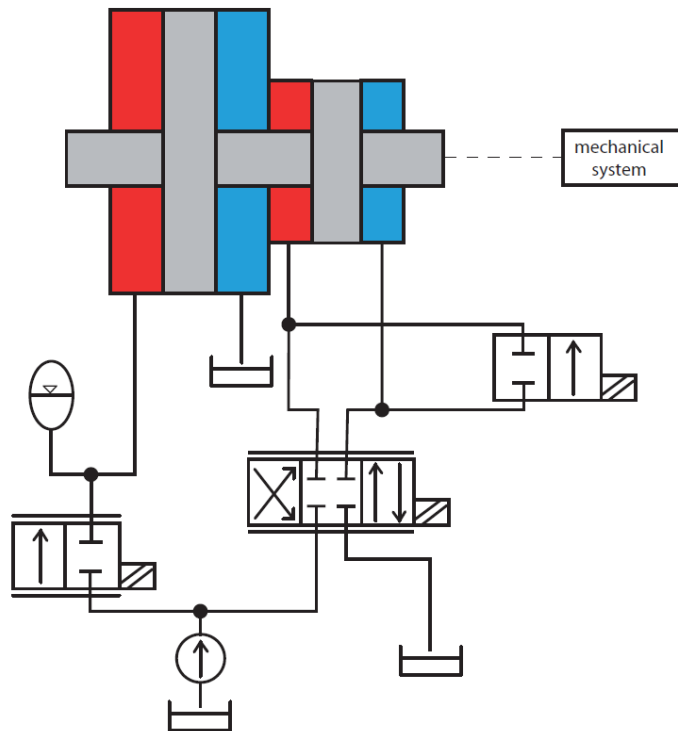
Figure II.3: Sketch of the hydraulic circuit of the "Tandem" cylinder.

Working in MATLAB® environment, a deep analysis for the two systems has been carried out, by comparing the different behaviors not only in time domain, but also in frequency domain.

Just like in the case of the fatigue test on the steel cable, we expect this treatment to show to the reader a series of positive outcomes which has, in the end, decreed the success of the proposed solution. Some of the advantages that will be analyzed further on the in text are:

- a better controllability of the whole system
- an amplification in bandwidth
- an improved external disturbance rejection
- a reduced power absorption.

Chapter 1

Description of the non-linear system

The application this chapter is going through concerns either the fixed or the mobile machinery devoted to concrete handling in civil construction sites.

Concrete delivery devices and all the similar heavy equipment, including a wide variety of carrier arms, are always actuated by hydraulic systems. Distributing concrete then is achieved thanks to a particular structure where the arms, provided with internal conduits and pipes, can be moved or swung each one with respect to the other.
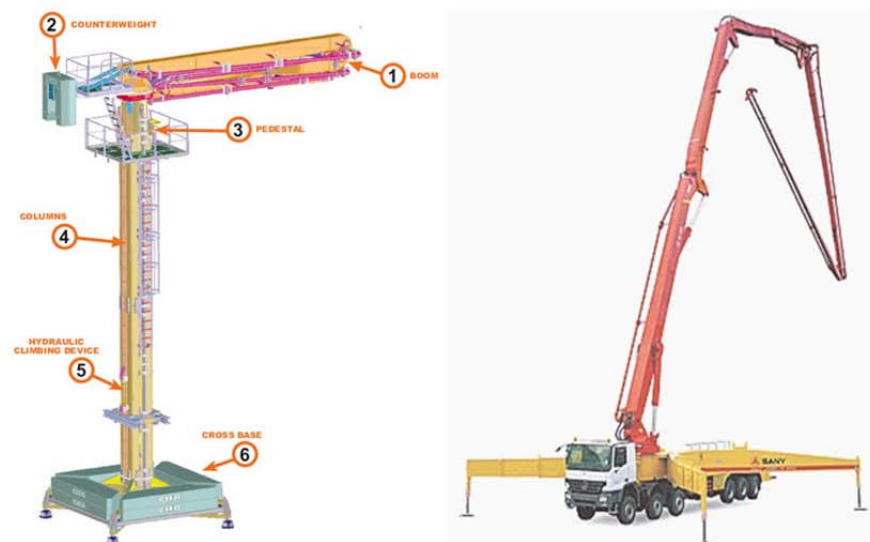
Figure 1.1: Examples of stationary (left) and mobile (right) applications of booms form concrete handling from Cifa.

As shown in Figure 1.1, both stationary and mobile applications can reach a high number of booms, each one with even several meters of length: this consequently implies significant problems in the growth (and hence in the control) of vibrations propagation along the structures.

1.1 Presentation of the mechanism

If the development of a control strategy for absorbing vibration had been the topic of the current part, a complex modeling would have certainly been requested. This is the case, for example, of validating precise control strategies to damp vibration propagation within a mechanical body: in this event, a technique for measuring the deformation of the body would have been necessary, in other words through a finite elements study of the system [11, 12].

Considering that the purpose of the present study is instead to investigate and demonstrate the advantages of implementing a new concept of hydraulic actuator, it is not necessary to get the system under investigation too complex. All this considered, the system the thesis goes through in the following passages is a 1 D.o.F. mechanism composed by a single boom pivoted to the ground, and pushed by a hydraulic cylinder (Figure 1.2).
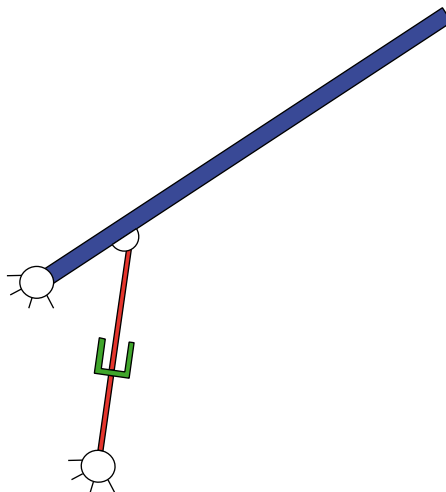
Figure 1.2: Sketch of the 1 D.o.F. system, representing the arm actuated by the hydraulic cylinder.

The arm to be actuated is, as already said, a light and slender metallic structure. In order to make simulations the most similar possible to reality, its section is inspired to a typical industrial steel boom for concrete handling, as shown below in Figure 1.3.
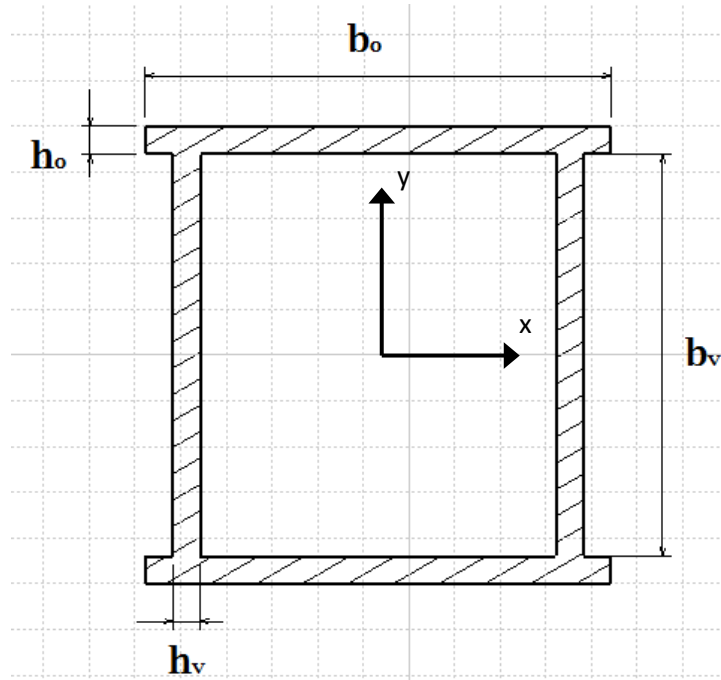
Figure 1.3: Section view of the boom under investigation.

As depicted here above, booms are hence obtained as box-type structures from the welding of different metallic layers. The actual dimensions of this solution are reported in Table 1.1.

Table 1.1: Dimensions of the section of the boom.

	b_v [mm]	h_v [mm]	b_o [mm]	h_o [mm]
Boom section dimensions	88	6	102	6

This sizing corresponds to a section area of 22,8 mm^2 which, considering a steel with density around 7800 kg/m^3, means a boom weight of nearly 17,18 kg per

meter of length. For simplicity, the boom is being assumed to have a constant section.

Before studying the non linear behavior of the selected kinematic motion, it is fundamental to finally size the whole system. The biggest difficulty faced while doing this has been to guarantee to the arm the possibility to reach different configurations, even because the total stroke of the actuators is, in this case, the real limit. In the following figure (Figure 1.4) it is presented a schematic view of the configuration that has been studied further on in the thesis.
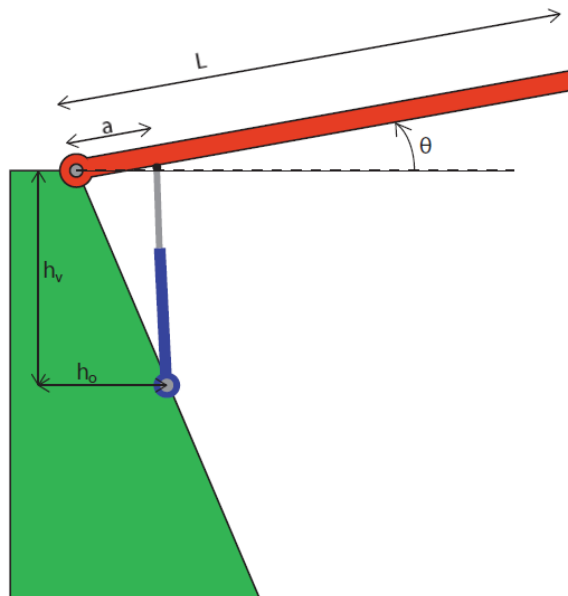
Figure 1.4: Sketch of the kinematism of the actuated arm.

The dimensions of the system above are presented in the following Table 1.2.

Table 1.2: Dimensions of the kinematism.

	L [mm]	a [mm]	h_v [mm]	h_o [mm]
Dimensions of the kinematics	4500	750	1299	750

The system is thus conceived in such a way that, in rest position ($\theta = 0$) the force transmission from the actuator to the arm is maximum (starting force non "dissipated" in constrain reaction forces).

1.2   Kinematics of the arm

As already stated in the previous pages, the system under investigation is characterized by a strongly non-linear kinematics. A schematic vectorial representation for the system is reported below in Figure 1.5.
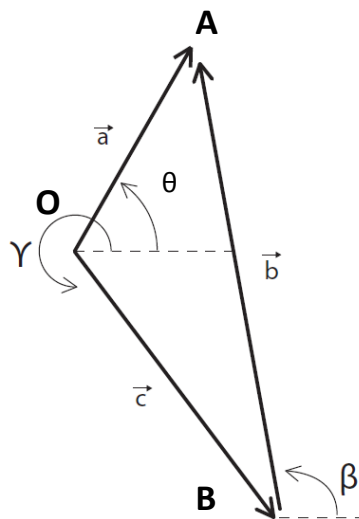
Figure 1.5: Vectorial representation of the kinematism.

In this sketch, vector $\vec{a}$ stands for the part of arm between the pivot and the connection with the actuator and θ for its inclination with respect to the horizon; $\vec{b}$ is itself the actuator, with variable length and variable inclination β; $\vec{c}$ represents in the end the structural chassis to which the arm and the actuator are pivoted, with fixed both length and inclination γ.

According to the previous sizing, it is possible to infer all the dimensions exposed below in Table 1.3:

Table 1.3: Dimensions and angles of the kinematism.

	Length [mm]		Angle [deg]
a	750	θ	variable
b	variable	β	variable
c	1500	γ	300°

We can now proceed to analyze more in detail the behavior of the system by writing down a vectorial equation like the following one:

$$(A - O) = (A - B) + (B - O)$$

(1.1)

which, more synthetically, can be rewritten as:

$$\vec{a} = \vec{b} + \vec{c}$$

(1.2)

Having a recourse to Euler's formula [13] for vectors in the complex plane, the previous equation takes the following form:

$$a \cdot e^{i\theta} = c \cdot e^{i\gamma} + b \cdot e^{i\beta}$$

(1.3)

Considering that the system at stake is a 1 D.o.F. one, it is possible to choose θ as the independent variable, used to describe the motion of the arm. In this way, by separating the real part from the imaginary one, it is obtained:

$$\begin{cases} a \cdot cos\theta = c \cdot cos\gamma + b \cdot cos\beta \\ a \cdot sin\theta = c \cdot sin\gamma + b \cdot sin\beta \end{cases}$$

(1.4)

which is a system in two equations and two unknown quantities, β and b.

By solving the system, it is possible to derive the two equations which express the behavior of β and b as functions of θ:

$$
\begin{cases}
b(\theta) = \dfrac{a \cdot sin\theta - c \cdot sin\gamma}{sin\beta} \\[2ex]
\beta(\theta) = atan\left(\dfrac{a \cdot sin\theta - c \cdot sin\gamma}{a \cdot cos\theta - c \cdot cos\gamma}\right)
\end{cases}
\tag{1.5}
$$

These relationships have been graphically depicted in the following Figure 1.6.
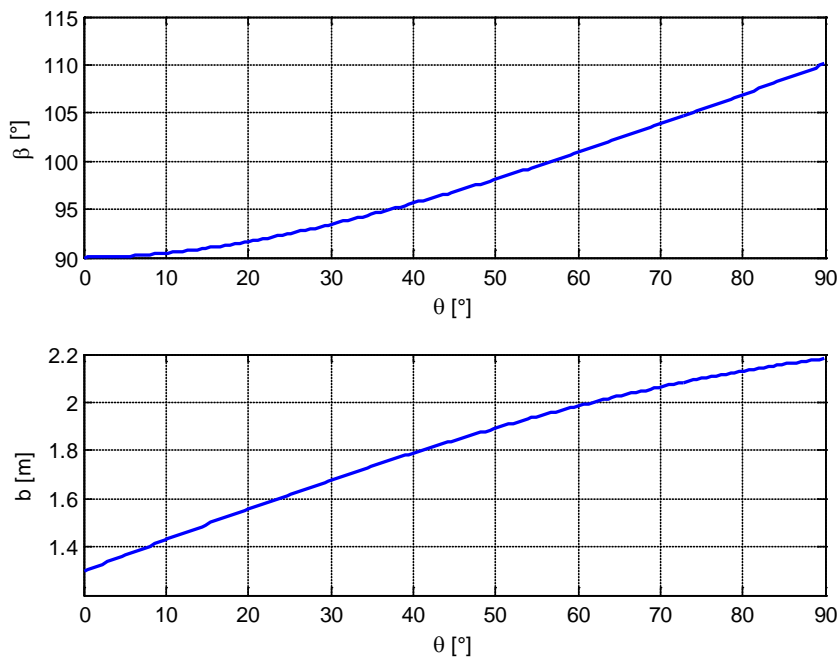
Figure 1.6: Graphical representation of b and β as functions of θ.

In this perspective, considering θ the real control parameter of the system for the motion of the arm (and then the handling of the concrete), we have defined the correspondence between displacement and inclination of the actuator (b and β respectively) with respect to the inclination of the boom.

Being θ a function of time t, further on in the chapters the dynamic description of what occurs within the system will also need to "know" the derivatives of b and θ in time. These relationships are presented in equations:

$$\begin{cases} \dot{b}(\theta) = \dfrac{db}{dt} = \dfrac{\partial b}{\partial \theta} \cdot \dfrac{d\theta(t)}{dt} = \dfrac{a \cdot c \cdot \sin(\theta - \gamma)}{\sqrt{a^2 + c^2 - 2 \cdot a \cdot c \cdot \cos(\theta - \gamma)}} \cdot \dot{\theta} \\[4mm] \dot{\beta}(\theta) = \dfrac{d\beta}{dt} = \dfrac{\partial \beta}{\partial \theta} \cdot \dfrac{d\theta(t)}{dt} = \dfrac{a^2 - a \cdot c \cdot \cos(\theta - \gamma)}{a^2 + c^2 - 2 \cdot a \cdot c \cdot \cos(\theta - \gamma)} \cdot \dot{\theta} \end{cases}$$

(1.6)

Chapter 2

Numerical model of the system

When analyzed to investigate deformations and vibrations in literature, arms for concrete-handling have generally been modelled with multi-body techniques, which allow to introduce and observe the flexibility of the structures.

As already stated in the previous paragraphs, however, the aim of the present thesis is not to validate a certain control logic or strategy for which it is needed to study how the whole arm behaves from this point of view.

The objective of this second part of the work is in fact to demonstrate that the new technology and architecture of the "Tandem" hydraulic actuator brings a series of improvements in the performances of the actuated systems. In order to do so, it is sufficient to study a one degree of freedom system, consisting in one rigid arm, actuated by the cylinder at stake. With this kind of representation we certainly expect to see much higher natural frequencies and lower system damping, but the evaluation of the actuator characteristics should not be affected.

So far, the introduction chapter with the kinematic study of the system have been worked out and written in general terms, which can be theoretically

applied on both the "Tandem" actuator or on a classical single-stage cylinder (Figure 2.1).
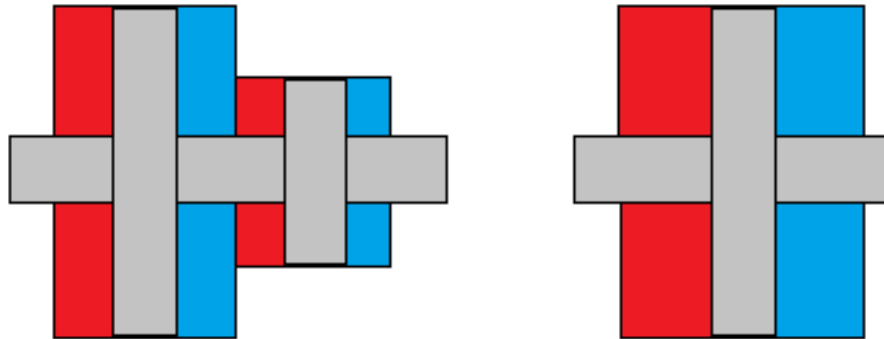
Figure 2.1: Sketches of the two cylinders under study, the "Tandem" (left) and the classical single-stage one (right).

From this moment on, the thesis will carry on a twofold analysis on the dynamic behaviour of both the systems in order to decree advantages and disadvantages, merits and flaws of each one.

Before doing this, is anyways necessary list all the *initial hypothesis* on which the whole analysis is based on:

- **Small oscillations:** the analysis consists of two principal phases, the former to study the non-linear big motion for the system to reach an interesting θ_0, the latter to investigate the response of the same systems to external disturbances. In the second part it is assumed that the system has to face only movements of reduced entity, which allows the linearization of the motion equations.

- **Motion in a plane:** it is assumed that the motion of the arm occurs only within a plane (x,y) and that all the other movements normal to this plane are neglected.

- **Small rotational speeds:** European normative EN12001:2003 [14] imposes that tip velocities of the arms have not to exceed respectively 0,75 m/s horizontally and 1,5 m/s vertically.

- **Homogeneous mass and elastic characteristics:** in this way density, elastic properties and sections remain constant along the different bodies.

2.1 Non-linear dynamics

The motion equations for the system under investigation can be obtained through the Lagrange formulation [15]:

$$\frac{d}{dt}\left(\frac{\partial E_c}{\partial \dot{q}}\right) - \frac{\partial E_c}{\partial q} + \frac{\partial V}{\partial q} + \frac{\partial \dot{D}}{\partial \dot{q}} = \frac{\delta^* L}{\delta q} \qquad (2.1)$$

where E_c is the kinetic energy, V is the potential one and D the dissipative one of the system, while $\delta^* L$ represents the virtual work of the external forces applied on the system itself.

As it can be easy noticed, this is a differential equation in partial derivatives, where all the energetic forms are function of the independent variable θ. As a matter of fact, the following paragraphs is dedicated to the analysis of each energetic form, both for the system with the "Tandem" and that one with the classical actuator, in order to eventually come up with the non-linear motion equations.

2.1.1 Kinetic energy
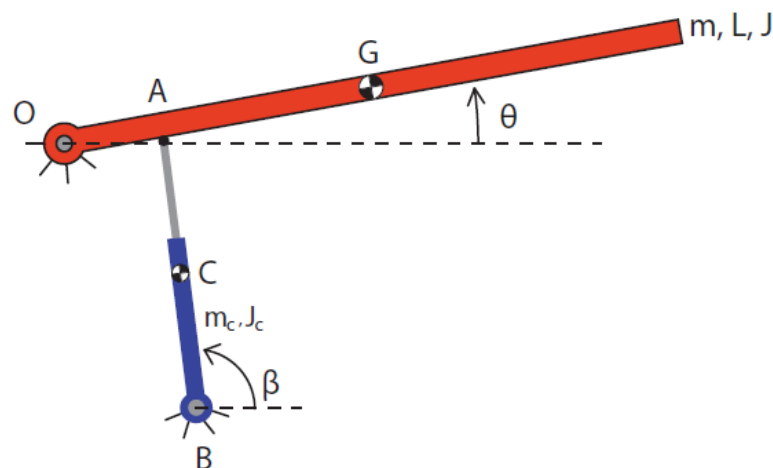
Figure 2.2: Dynamic scheme for the system under investigation, with evidence angles, dimensions, masses and momentums of inertia.

Referring to the scheme depicted in Figure 2.2, the kinetic energy owned by the system in a generic time (both for the "Tandem" and the classical configurations) is determined by the following equation:

$$E_c = \frac{1}{2} \cdot m \cdot v_G^2 + \frac{1}{2} \cdot J \cdot \dot{\theta}^2 + \frac{1}{2} \cdot m_c \cdot v_C^2 + \frac{1}{2} \cdot J_c \cdot \dot{\beta}^2 \qquad (2.2)$$

where v_G is the speed of the centre of mass of the arm, J is its momentum of inertia, v_C is the speed of the centre of mass of the actuator (for simplicity considered in the centre of the rod) and in the end J_c its momentum of inertia. J_c and m_c have been evaluated thanks to a CAD representation for both the "Tandem" cylinder and the classical one. They have been respectively evaluated as $J_c = 16{,}25 \ kg \cdot m^2$ and $m_c = 25{,}75 \ kg$ in the first case, and as $J_c = 18{,}37 \ kg \cdot m^2$ and $m_c = 23{,}26 \ kg$ in the second one. Moreover, the initial hypothesis of homogeneous materials, allows to express the momentum of inertia of the arm as follows:

$$J = \frac{m \cdot L^2}{12} \qquad (2.3)$$

Thanks to the relationships computed in section 1.2 about the kinematic motion of the system, we are able to express these quantities as functions of the independent variable θ. As follows:

$$\begin{cases} x_G = \frac{L}{2} \cdot cos\theta \\ y_G = \frac{L}{2} \cdot sin\theta \end{cases} \qquad (2.4)$$

By differentiating this in time, we get that:

$$v_G = \sqrt{\dot{x}_G^2 + \dot{y}_G^2} = \sqrt{\frac{L^2}{4} \cdot (cos\theta)^2 \cdot \dot{\theta}^2 + \frac{L^2}{4} \cdot (sin\theta)^2 \cdot \dot{\theta}^2} = \frac{L}{2} \cdot \dot{\theta} \qquad (2.5)$$

In the same way, we can compute:

$$\begin{cases} x_C = c \cdot \cos(\gamma) + \frac{b}{2} \cdot \cos\beta \\ y_C = c \cdot \sin(\gamma) + \frac{b}{2} \cdot \sin\beta \end{cases}$$

(2.6)

By substituting equations (1.5) into (2.6), we get:

$$v_C = \sqrt{\dot{x}_C^2 + \dot{y}_C^2} = \sqrt{\frac{a^2}{4} \cdot \dot{\theta}^2 \cdot ((\cos\theta)^2 + (\sin\theta)^2)} = \frac{a}{2} \cdot \dot{\theta} = \frac{L}{12} \cdot \dot{\theta}$$

(2.7)

Having already computed the derivative $\dot{\beta}$ in equation (1.6), we are now able to write the complete expression of the kinetic energy as follows:

$$E_c = \frac{1}{2}\left(\frac{mL^2}{4} + \frac{mL^2}{12} + \frac{m_c L^2}{144}\right) \cdot \dot{\theta}^2 + \frac{1}{2}J_c \left(\frac{\left(\frac{L^2}{36} - \frac{L}{6}c \cdot \cos(\theta - \gamma)\right)}{\frac{L^2}{36} + c^2 - \frac{L}{3}c \cdot \cos(\theta - \gamma)}\right)^2 \cdot \dot{\theta}^2$$

(2.8)

From this one it is now possible to obtain those derivatives necessary to derive the motion equation of the system. In particular we have:

$$\frac{d}{dt}\left(\frac{\partial E_c}{\partial \dot{\theta}}\right) = \left(\frac{mL^2}{3} + \frac{m_c L^2}{144} + J_c\left(\frac{\left(\frac{L^2}{36} - \frac{L}{6}c \cdot \cos(\theta - \gamma)\right)}{\frac{L^2}{36} + c^2 - \frac{L}{3}c \cdot \cos(\theta - \gamma)}\right)^2\right) \cdot \ddot{\theta} +$$

$$+ 2J_c \frac{\left(\left(\frac{L^2}{36} - \frac{L}{6}c \cdot \cos(\theta - \gamma)\right) \cdot \left(\frac{L}{6}c^3 - \frac{L^3}{216}c\right) \cdot \sin(\theta - \gamma)\right)}{\left(\frac{L^2}{36} + c^2 - \frac{L}{3}c \cdot \cos(\theta - \gamma)\right)^3} \cdot \dot{\theta}^2$$

(2.9)

Similarly, it is easy to compute:

$$\frac{\partial E_c}{\partial \theta} = J_c \frac{\left(\left(\frac{L^2}{36} - \frac{L}{6}c \cdot \cos(\theta - \gamma)\right) \cdot \left(\frac{L}{6}c^3 - \frac{L^3}{216}c\right) \cdot \sin(\theta - \gamma)\right)}{\left(\frac{L^2}{36} + c^2 - \frac{L}{3}c \cdot \cos(\theta - \gamma)\right)^3} \cdot \dot{\theta}^2$$

(2.10)

2.1.2 Potential energy

In this first non-linear configuration (Figure 2.2), there are no linear nor torsional springs, which means that only gravity introduces potential energy into the system, through the raising of masses.

According to this, V is expressed as a function of θ (and then of time) as follows:

$$V = \frac{mgL}{2} \cdot sin\theta + \frac{m_c gb}{2} \cdot sin\beta \qquad (2.11)$$

Having again a recourse to equations (1.5) the relationship above is transformed into:

$$V = \left(m + \frac{m_c}{6}\right)\frac{gL}{2} \cdot sin\theta - \frac{c}{2}m_c g \cdot sin\gamma \qquad (2.12)$$

Its derivative is easily obtained from:

$$\frac{\partial V}{\partial \theta} = \left(m + \frac{m_c}{6}\right)\frac{gL}{2} \cdot cos\theta \qquad (2.13)$$

2.1.3 Dissipative energy

In the system depicted in Figure 2.2, there is no form of concentrated dissipation like viscous dampers or vibration absorbers.

The only component which "wastes" useful energy into heat is the cylinder: inside a hydraulic actuator, in fact, several phenomena can cause the loss of energy. The model of study has taken into consideration the following ones:

- **Coulomb friction:** it is the dry resistance to lateral motion of two solid surfaces in contact. It is the case of the of the piston sliding inside the cylinder liner.

- **Viscous friction:** viscosity in fluids is the measure of the internal resistance to flow, namely to be deformed by either shear stress or tensile stress. The movement of the cylinder implies the relative motion

between layers of fluid which, sliding one on each other, absorb energy in the formation of heat.

Both of them proportionally depend on the velocity, in particular on the speed of the piston-rod sliding within the cylinder. That is why the dissipative energy can be written as follows:

$$D = \frac{1}{2} \cdot r_c \cdot \dot{b}^2 \tag{2.14}$$

Having $\dot{b}$ already been expressed as a function of θ in equation (1.6), the relationship is totally determined, except for r_c which is taken from the literature. Experimental verifications [16] demonstrated that, for a classical cylinder with characteristics similar to the one modeled, friction generates a resistance force proportional to piston velocity through constant value of around 5000 Ns/m; in the case instead of a cylinder with sizing and construction similar to the "Tandem" this value is around 7500 Ns/m.

The differentiation of equation (2.14) produces than the derivative necessary to fill Lagrange's equation in:

$$\frac{\partial D}{\partial \dot{\theta}} = r_c \cdot \frac{\frac{L^2}{36}c^2 \cdot (\sin(\theta-\gamma))^2}{\frac{L^2}{36}+c^2-\frac{L}{3}c \cdot \cos(\theta-\gamma)} \cdot \dot{\theta} \tag{2.15}$$

2.1.4 External forces work

The virtual work of the external forces is defined as the product between the force itself and the virtual displacement of the point on which the force is applied. This terms needs to be computed in order to include in Lagrange's equation (2.1) the effect of these active forces on the motion of the system.

Dealing with booms for concrete handling, external forces can be generated by different actors. In particular we talk about "active force" when referring to the "hydraulic" force generated by the pressure differential within the cylinder's chambers; disturbances are, on the other hand, all those unpredictable actions due to concrete pumping or external factors, which the actuator tries to damp.

In this first dynamic analysis, only the active pressure force has been taken into consideration. Disturbances have been introduced only at a later time under the form of a periodic torque whose effects needed to be eliminated.

According then to this formulation, the virtual work of the actuator force can be written as follows:

$$\delta^*L = F \cdot \delta x_A \qquad\qquad (\,2.16\,)$$

For the first time from the beginning of this second part of the thesis, it is now needed to make a differentiation between the behaviors of the two different actuators. In more detailed terms, the design process has lead to the choice of a "Tandem" actuator with big piston diameter of 140 mm, small piston diameter of 100 mm and a rod diameter of 50 mm. On the other hand, the classical actuator needs to perform all the job by means of one single piston: in order to reduce the risk of raising too much pressures, its piston diameter is chosen of 180 mm, while the rod is the same, with a diameter of 50 mm. These configurations correspond to a set of piston annulus areas summarized in Table 2.1:

Table 2.1: Dimensions of the piston areas of the two cylinders.

	Tandem		Single-stage
$A_{big\ T}$ [mm^2]	13433	$A_{big\ C}$ [mm^2]	23483
A_{small} [mm^2]	5890		

That being so, the force F has been differently defined according to the working conditions. The "Tandem" cylinder uses its bigger stage in the starting phase of the application in order to reach an equilibrium angle θ_0. Hence:

$$F_{Tandem} = (p_1 - p_2) \cdot A_{big_T} \qquad\qquad (\,2.17\,)$$

The small piston is instead actively used only for the linearized motion. For this, we defer to chapter 3.

For what concerns, instead, the classical single-stage actuator, its external force has exactly the same form expressed in equation (2.17), with the difference that surface interested by the pressures is A_{big_C}.

As easily understandable, the virtual displacement of the application point of this force, is represented by the following equation:

$$\delta^* x_A = \frac{L}{6} \delta\theta \tag{2.18}$$

The last remark is about the orientation of the two vectors. In fact, apart from the starting point ($\theta = 0$), the hydraulic force is never normal to the arm. This means that, in order to calculate the scalar product, a projection of the force on the normal direction is requested (Figure 2.3).
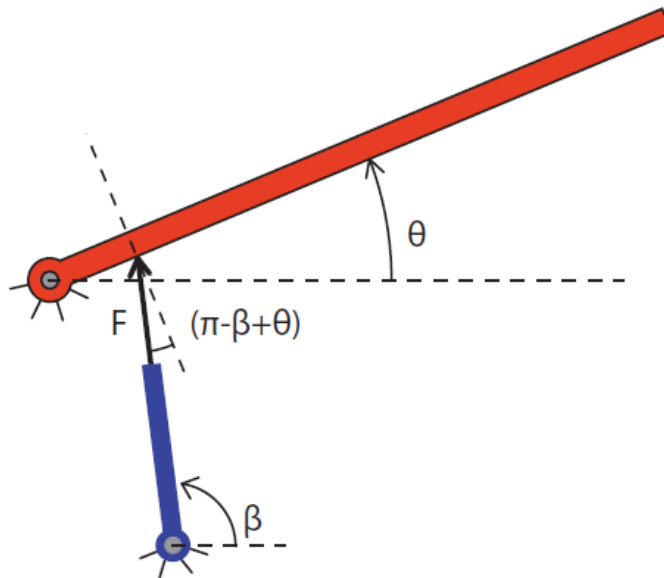
Figure 2.3: Scheme of the mechanism, with attention on external forces and their virtual work.

It is possible to conclude that:

$$Q = \frac{\delta^* L}{\delta\theta} = (p_1 - p_2) \cdot A_{big} \cdot \frac{L}{6} \cdot \cos(\pi - \beta + \theta) \tag{2.19}$$

The picture of the situation is now complete. All the energetic forms have been described and suitably differentiated. There is nothing left to do but putting all the pieces together and obtaining then the non-linear motion equations. For this we defer to the next paragraph.

2.1.5 Non-linear equations of motion

That being so, all the components of Lagrange's equation have been correctly computed. By putting together equations (2.9), (2.10), (2.13), (2.15) and (2.19), it is obtained:

$$f_1(\theta) \cdot \ddot{\theta} + f_2(\theta) \cdot \dot{\theta}^2 + f_3(\theta) \cdot \dot{\theta} + f_4(\theta) = f_5(\theta) \qquad (2.20)$$

where:

$$
\begin{cases}
f_1(\theta) = \left(\dfrac{mL^2}{3} + \dfrac{m_c L^2}{144} + J_c \left(\dfrac{\left(\frac{L^2}{36} - \frac{L}{6} c \cdot \cos(\theta - \gamma) \right)}{\frac{L^2}{36} + c^2 - \frac{L}{3} c \cdot \cos(\theta - \gamma)} \right)^2 \right) \\[6mm]
f_2(\theta) = J_c \left(\dfrac{\left(\left(\frac{L^2}{36} - \frac{L}{6} c \cdot \cos(\theta - \gamma) \right) \cdot \left(\frac{L}{6} c^3 - \frac{L^3}{216} c \right) \cdot \sin(\theta - \gamma) \right)}{\left(\frac{L^2}{36} + c^2 - \frac{L}{3} c \cdot \cos(\theta - \gamma) \right)^3} \right) \\[6mm]
f_3(\theta) = r_c \cdot \left(\dfrac{\frac{L^2}{36} c^2 \cdot (\sin(\theta - \gamma))^2}{\frac{L^2}{36} + c^2 - \frac{L}{3} c \cdot \cos(\theta - \gamma)} \right) \\[6mm]
f_4(\theta) = \left(m + \dfrac{m_c}{6} \right) \dfrac{gL}{2} \cdot \cos\theta \\[4mm]
f_5(\theta) = (p_1 - p_2) \cdot A_{big} \cdot \dfrac{L}{6} \cdot \cos(\pi - \beta + \theta)
\end{cases}
\qquad (2.21)
$$

This equation of motion stands exactly both for the "Tandem" system and for the classically actuated one (with the only difference of the values of some parameters like m_c or J_c or also A_{big}).

The description of the system is however still incomplete. This is due to the pressures p_1 and p_2 in the two chambers of the cylinder. Next sub-section clarifies how they can be expressed as functions of the state of the system.

2.1.6 Hydraulic equations

The system, in fact, still needs a further equation which describes the phenomena beyond the physical connection between the actuator and the mechanical system itself [17].
Referring in particular to the conservation of mass:

$$Q_{in} - Q_{out} = \frac{dV}{dt} + \frac{V}{\beta_c} \cdot \frac{dP}{dt}$$

(2.22)

where β_c is the compressibility of the fluid (for a standard ISO 68 industrial oil, it seizes around 17000 bar).
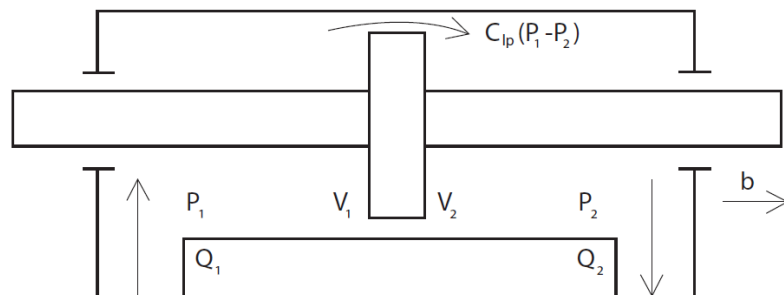
Figure 2.4: Sketch of a symmetric hydraulic cylinder.

This one, applied on a hydraulic cylinder (Figure 2.4), can be translated into two balance equations, for the two chambers of the same cylinder (external leakages neglected):

$$\begin{cases} Q_1 - C_i(p_1 - p_2) = \frac{dV_1}{dt} + \frac{V_1}{\beta_c} \cdot \frac{dp_1}{dt} \\ -Q_2 + C_i(p_1 - p_2) = \frac{dV_2}{dt} + \frac{V_2}{\beta_c} \cdot \frac{dp_2}{dt} \end{cases}$$

(2.23)

where $V_1 = V_0 + A \cdot \dot{b}$ and $V_2 = V_0 - A \cdot \dot{b}$. The system under investigation is strongly non-linear: this means that the derivatives of the volumes depend (non-linearly) on θ. Defining for simplicity $\dot{b}$ as follows:

$$\dot{b} = \frac{\frac{L}{6}c \cdot \sin(\theta-\gamma)}{\sqrt{\frac{L^2}{36}+c^2-\frac{L}{3}c \cdot \cos(\theta-\gamma)}} \cdot \dot{\theta} = \alpha^* \cdot \dot{\theta} \tag{2.24}$$

the equations of volumes become:

$$\begin{cases} \frac{dV_1}{dt} = \frac{d(V_0+A_{big}*b)}{dt} = A_{big} \cdot \dot{b} = A_{big} \cdot \alpha^* \cdot \dot{\theta} \\ \frac{dV_2}{dt} = \frac{d(V_0-A_{big}*b)}{dt} = -A_{big} \cdot \dot{b} = -A_{big} \cdot \alpha^* \cdot \dot{\theta} \end{cases} \tag{2.25}$$

Flow rates Q_1 and Q_2 are obtained from a second formulation depending on the valve characteristics, called "sharp-edge orifice equation" :

$$Q_{or}(x_d, \Delta p_{or}) = C_d \cdot w \cdot x_d \cdot \sqrt{\frac{2\Delta p_{or}}{\rho_{oil}}} \tag{2.26}$$

where C_d is the discharge coefficient, w a characteristic dimension of the valve, x_d the displacement of the spool, ρ_{oil} the density of the oil within the circuit (for a ISO 68 it is nearly 880 kg/m^3) and Δp_{or} the pressure differential between the two sides of the valve.

According to literature, and in particular to Jelali and Kroll [18], the discharge coefficient in turbulent conditions (which is the case of flow through valves) and short tube orifices, strongly depends on the geometry of the orifice. In particular Merritt (1967) [19] found a mathematical expression, whose graphical trend is summarized in :
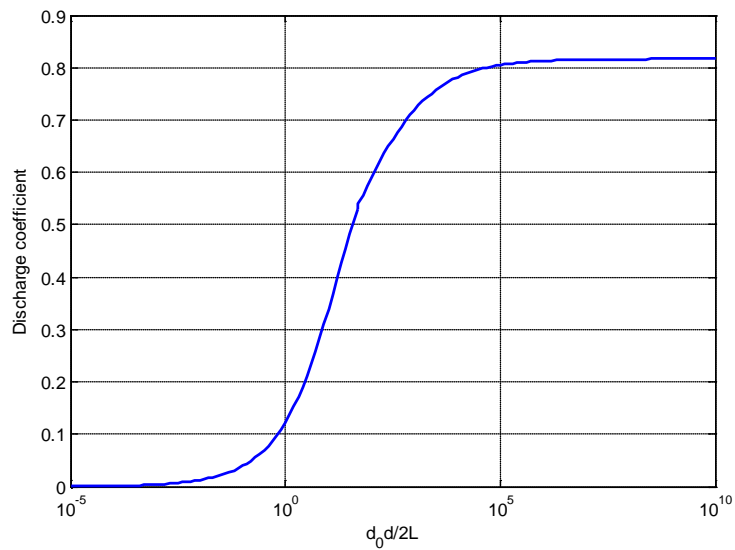
Figure 2.5: Graphical representation of the discharge coefficient as a function of the geometry.

Having a system with characteristics similar to that one under analysis, C_d can be estimated around a value of 0,69.

It is now necessary to differentiate between the two systems. As already claimed, the *classical cylinder* is actuated (both in the non-linear and in the linear motion) by the same servo-valve, that can be chosen from Bosch Rexroth S.p.A. catalogues. Selecting, for example, a 4WRAE6E-07-2X-G24-J-K4/A1-V, all the characteristics are determined (Appendix C).

In this case, hence we have two non-linear equations, each one for a chamber of the cylinder:

$$\begin{cases} Q_1 = C_d \cdot w \cdot x_d \cdot \sqrt{\dfrac{2(p_{pump} - p_1)}{\rho_{oil}}} = C_i \cdot (p_1 - p_2) + A_{big_C} \cdot \alpha^* \cdot \dot{\theta} + \dfrac{V_0}{\beta_c} \cdot \dot{p}_1 \\ \quad Q_2 = C_d \cdot w \cdot x_d \cdot \sqrt{\dfrac{2p_2}{\rho_{oil}}} = C_i \cdot (p_1 - p_2) - A_{big_C} \cdot \alpha^* \cdot \dot{\theta} - \dfrac{V_0}{\beta_c} \cdot \dot{p}_2 \end{cases} \quad (27)$$

The state of the system is thus determined by the two states p_1 and p_2.

On the contrary, the *"Tandem" actuator* is in this first phase controlled by a 2-2 proportional directional valve, feeding only the big cylinder.

Choosing valve KKDS-R-1-NB/H-C-G12-N0-K4-V from Bosch Rexroth S.p.A. catalogues (Appendix C), all the characteristics are determined.

Anyways, the "Tandem" cylinder has a particular set-up, according to which the second chamber of the big side is connected directly to the tank. This means the p_2 will approximately be 0 bar (only a small level of pressure to overcome losses is required) and hence only one flow equation will be written:

$$Q_1 = C_d \cdot w \cdot x_d \cdot \sqrt{\frac{2(p_{pump} - p_1)}{\rho_{oil}}} = C_i \cdot p_1 + A_{big_T} \cdot \alpha^* \cdot \dot{\theta} + \frac{V_0}{\beta_c} \cdot \dot{p}_1 \qquad (\,2.28\,)$$

This results in only p_1 being a state of the system.

Someone would wonder about what actually goes on in the small cylinder of the "Tandem" while the big one is actuated during the first positioning phase. Just like in the application of the fatigue test, when pulling the steel cable, in this second application the small cylinder is by-passed as well; the reader is advised to look at Figure II.3 for this.

If the 2-2 way valves are both opened, the big cylinder is actuated by the flow coming from the pump; on the contrary the small cylinder is completely by-passed from the working system, and let free to move either back or forth.

The motion of the rod imposed by the big stage, can anyhow cause a certain flow rate between the two small chambers (Figure 2.6). Since we know that in real fluids no flow would occur with zero gradient of pressure, the natural consequence of the motion is the birth of a small pressure differential.
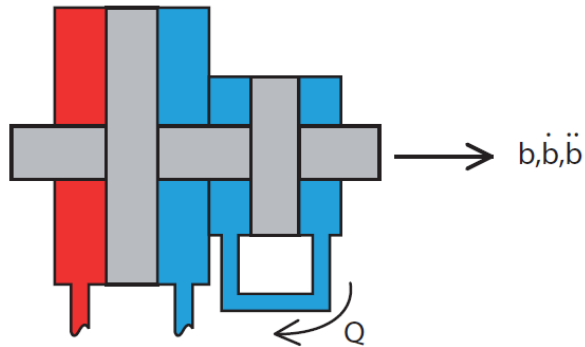
Figure 2.6: Sketch of the Tandem actuator during the non linear motion, with attention to the small cylinder, by-passed.

It is possible to compute numerically this phenomenon by the superposition of two different effect:

1. When *stationary*, the flow is linked to the pressure through the Bernoulli's equation:

$$z_2 + \frac{p_2}{\gamma} + \frac{v_2^2}{2g} = z_1 + \frac{p_1}{\gamma} + \frac{v_1^2}{2g} + \left(\frac{v_d^2}{2g} + \frac{1}{2}\frac{v_d^2}{2g} + 2 \cdot 0,6 \cdot \frac{v_d^2}{2g} \right) \qquad (\,2.29\,)$$

where the term between brackets refers to all the concentrated pressure losses (respectively outlet, inlet and 2 elbows). By making some simplifications, and assuming that in stationary conditions p_1 is the smallest possible ($p_1 = 0$), we get:

$$p_2 = 2,7 \cdot \gamma \cdot \frac{A_{small}^2}{2g \cdot \frac{\pi d^2}{4}} \cdot \dot{b}^2 = \delta \cdot \dot{b}^2 \qquad (\,2.30\,)$$

2. When non stationary, the flowing fluid undergoes accelerations and decelerations depending on its compressibility β_c. In fact, starting from the definition:

$$dp = \frac{dV}{V_0} \cdot \beta_c \qquad (\,2.31\,)$$

it is possible to infer that:

$$\dot{p} = \frac{\dot{V}}{V_0} \cdot \beta_c = \frac{A_{small} \cdot \dot{b}}{V_0} \cdot \beta_c \qquad (2.32)$$

Since the integration of motion has been performed through stepwise integration methods, the increment of pressure along one time-step *dt* will be defined by the following equation:

$$\Delta p = \frac{\beta_c}{(X_0 + b)} \cdot \dot{b} \cdot \Delta t \qquad (2.33)$$

where V_0 has been suitably substituted by $A_{small} \cdot (X_0 + b)$, in order to be updated step by step.

By composing these two terms, we get then:

$$\begin{cases} p_1 = \delta \cdot \dot{b}^2 + \frac{\beta_c}{(X_0 + b)} \cdot \dot{b} \cdot \Delta t \\ p_2 = -\frac{\beta_c}{(X_0 + b)} \cdot \dot{b} \cdot \Delta t \end{cases} \qquad (2.34)$$

The hydraulic part of the two systems has been now completely analyzed. In the next paragraph some aspects of the first control logic for this first non-linear study will be mentioned. Then the systems will be ready to be integrated.

2.1.7 Control logic for the non-linear motion

The device through which the servo-valve (but the valves in general) controls the flows and then the mechanical system connected to the actuator, is the spool and its displacement within its seating.
In the electrically operated valves the displacement of the spool is piloted by a solenoid which makes it move back and forth. To be precise, electromagnetic circuit and spool displacement are connected together by a transfer function: in

some application the dynamics of the electrical part (although much quicker) cannot be ignored, then:

$$\frac{x_d(s)}{i_c(s)} = \frac{k_s}{1 + 2\xi \cdot \frac{s}{\omega_n} + \frac{s^2}{\omega_n^2}}$$

(2.35)

where ξ and ω_n represent respectively the damping factor and the natural frequency of the dynamics of the spool of distribution [17].

In some other cases, either for simplicity, or for ω_n being much higher than the frequencies of interest within the system, this transfer function is assumed (with good approximation) constant, as follows:

$$x_d(s) = k_s \cdot i_c(s)$$

(2.36)

In particular, for the valves we have chosen (either for the non linear motion, either for the linearized one), input currents are assumed to be between 4 and 20 mA. Considering that the max spool displacement is of 6 mm, a typical value for k_s is computed as 0,3.

It is now necessary to introduce a suitable controller, that will drive the non-linear system to a desired configuration, assumed for example as angle θ_0.

This controller, being an electrical device, will produce an electrical signal to feed the solenoid, and then to drive the valve. Considering that generating and validating a complex and successful control strategy is not the target of the present thesis, we will use for this application a normal, classical proportional (P) controller. This will simplify the treatment, without losing the power to show the benefits of the "Tandem" actuator.

In this perspective, the control equation for the system at stake (both for the "Tandem" and for the classical cylinder) will become:

$$x_d(s) = k_s \cdot i_c(s) = k_s \cdot k_p \cdot \left(\theta_0 - \theta(t)\right)$$

(2.37)

By substituting this equation in equations (2.27) and (2.28) the system will be fully determined, and then ready for the integration.

2.1.8 Integration of non-linear motion equations

It has been demonstrated that, the application of the laws of dynamics to a generally constrained single or multi-body mechanical system, unavoidably leads to the formation of a group of precise differential algebraic equations (DAE).

Thanks to a proper differentiation of the kinematic constraint equations, by using specific independent coordinates, these equations can be transformed in 2nd order, ordinary differential equations (ODE).

In this fashion, a stable and accurate integration of both DAE and ODE is of great importance for the understanding and the solution of the equations of motion. For some few simple cases and configurations, analytical solutions can be found. Anyways, the number and the difficulty of equations grow quickly and significantly if the mechanical system is made more complex. Here it comes the importance of having to our disposal a series of numerical methods (time-marching schemes) to compute the approximate solution at discrete times $t1$, $t2$, ... tn. The integration time step Δt will be defined as the difference $(t_{n+1} - t_n)$ and, depending on the used method, it will be assumed constant or variable during the integration process [20].

Starting from the Taylor's expansion series, it exists a great variety of numerical methods in use, which differentiate between themselves depending on the hypothesis on the bond between acceleration at the actual step, and solutions of the previous steps [21].

In general, it is possible to distinguish between three fundamental categories of numerical methods:

1. Explicit methods
2. Implicit methods
3. Explicit-implicit methods

The first ones are used indifferently both for linear and non-linear problems. They are meant to compute directly the state at a generic step, starting from the knowledge of the previous steps, without any hypothesis on the actual

accelerations. Between them we mention Euler's method and Runge Kutta's one.

In implicit methods, instead, position and velocity of the states at a generic step depend on their acceleration at the same step. Requiring to compute all the terms of the state of the system at each time step, these methods are directly applicable only on linear systems, but they are generally more accurate and stable.

In the end, in explicit-implicit methods, positions and velocities depend on the accelerations of the considered step, but also of the previous ones.

Considered the strong non-linearity of our system, we necessarily will have recourse to an explicit method. Euler's method in particular is neither useful nor reliable because of its low accuracy. Higher order Taylor's series are, moreover, uncomfortable because of the trouble in obtaining the derivatives of the non-linear differential equations.

A solution to this problem is represented by the Runge Kutta methods [22], which actually match the accuracy of higher order Taylor's series, by sequentially computing the DAE function at several points within the time interval.

For the integration of the motion of our concrete-handling arm we will use in particular a *fourth order Runge Kutta method*, which in plain words requires four evaluation functions per time step:

$$y_{n+1} = y_n + \frac{\Delta t}{6} \cdot (k_1 + 2 \cdot k_2 + 2 \cdot k_3 + k_4) \qquad (\,2.38\,)$$

With:

$$\begin{cases} k_1 = f(t_n, y_n) \\ k_2 = f(t_n + \frac{\Delta t}{2}, y_n + \frac{\Delta t}{2} \cdot k_1) \\ k_3 = f(t_n + \frac{\Delta t}{2}, y_n + \frac{\Delta t}{2} \cdot k_2) \\ k_4 = f(t_n + \Delta t, y_n + \Delta t \cdot k_3) \end{cases} \qquad (\,2.39\,)$$

In particular, in the system under investigation, the vectorial non-linear differential equation to be integrated can be expressed in a general way as:

$$\dot{\underline{y}} = \underline{f}(t, \theta, \dot{\theta}) \tag{2.40}$$

where the vector $\underline{y}$ stands for:

$$\underline{y_T} = \begin{pmatrix} \dot{\theta} \\ \theta \\ p_1 \end{pmatrix} \quad and \quad \underline{y_C} = \begin{pmatrix} \dot{\theta} \\ \theta \\ p_1 \\ p_2 \end{pmatrix} \tag{2.41}$$

respectively for the "Tandem" and the classical cylinder configurations. This means that equation (2.40) becomes:

$$\underline{\dot{y}_T} = \begin{pmatrix} \dfrac{f_5(\theta) - f_2(\theta) \cdot \dot{\theta}^2 - f_3(\theta) \cdot \dot{\theta} - f_4(\theta)}{f_1(\theta)} \\[2em] \dot{\theta} \\[2em] \dfrac{\beta_c}{V_0} \cdot \left(C_d \cdot w \cdot k_s k_p (\theta_0 - \theta) \cdot \sqrt{\dfrac{2(p_{pump} - p_1)}{\rho_{oil}}} - C_i \cdot p_1 - A_{big_T} \cdot \alpha^* \cdot \dot{\theta} \right) \end{pmatrix} \tag{2.42}$$

for the "Tandem", and:

$$\underline{\dot{y}_C} = \begin{pmatrix} \dfrac{f_5(\theta) - f_2(\theta) \cdot \dot{\theta}^2 - f_3(\theta) \cdot \dot{\theta} - f_4(\theta)}{f_1(\theta)} \\[2em] \dot{\theta} \\[2em] \dfrac{\beta_c}{V_0} \cdot \left(C_d \cdot w \cdot k_s k_p (\theta_0 - \theta) \cdot \sqrt{\dfrac{2(p_{pump} - p_1)}{\rho_{oil}}} - C_i \cdot (p_1 - p_2) - A_{big_C} \cdot \alpha^* \cdot \dot{\theta} \right) \\[2em] \dfrac{\beta_c}{V_0} \cdot \left(-C_d \cdot w \cdot k_s k_p (\theta_0 - \theta) \cdot \sqrt{\dfrac{2 p_2}{\rho_{oil}}} + C_i \cdot (p_1 - p_2) + A_{big_C} \cdot \alpha^* \cdot \dot{\theta} \right) \end{pmatrix} \tag{2.43}$$

for the classical cylinder. For the expressions of $f_1(\theta) \ldots f_5(\theta)$ and for x_d we refer to the equations found in the previous sub-sections.
Results of the integration have been shown further on in chapter 3.

2.2 Linearized dynamics

Once the system has reached the desired angular position θ_0, a linearized analysis will be carried on. In fact, as explained before in chapter 1, the objective of this second study is to observe how the system reacts to small casual inputs entering the arm under the shape of disturbances.

According to the initial assumptions, in fact, the system is expected to respond to these inputs only with contained movements: the hypothesis of small oscillations will therefore stand.

Under this assumption, it is therefore possible to linearize (by means of Taylor's expansion series) all the energetic expressions such that the Lagrange approach will return a linear differential equation.

The general formulation for 1 D.o.F. mechanical systems, properly derived from Lagrange's equation, says that:

$$m^*(\theta_0) \cdot \ddot{\theta} + r_c \cdot \left(\frac{\partial \Delta l_d}{\partial \theta}\right)_{\theta_0}^2 \cdot \dot{\theta} + \left[k \cdot \left(\frac{\partial \Delta l_d}{\partial \theta}\right)_{\theta_0}^2 + k \cdot \Delta l_0 \cdot \frac{\partial^2 \Delta l_d}{\partial \theta^2}\bigg|_{\theta_0} + m^* g \frac{\partial^2 h}{\partial \theta^2}\bigg|_{\theta_0} - F(t) \cdot \right.$$
$$\left. \frac{\partial^2 x_F}{\partial \theta^2}\bigg|_{\theta_0} \right] \cdot (\theta - \theta_0) = \tilde{F}(t) \cdot \frac{\partial x_F}{\partial \theta}\bigg|_{\theta_0} \tag{2.44}$$

The objective of the next sub-sections is, indeed, to find all these "components". As a matter of fact, the structure of the following sub-chapter is exactly the same of before: firstly the four energetic expressions are analyzed, then a linear motion equation have been obtained by them, and in the end this will be eventually associated with a specific linear hydraulic equation. At this point everything will be ready for the final numerical integration.

2.2.1 Kinetic energy

The linearization of the kinetic energy is simple and immediate. Let us take equation (2.8) and rewrite it synthetically in the following form:

$$E_c = \frac{1}{2} \cdot m^*(\theta) \cdot \dot{\theta}^2 \qquad (2.45)$$

According to equation (2.44), the linear kinetic energy is given by:

$$E_c = \frac{1}{2} \cdot m^*(\theta_0) \cdot \dot{\theta}^2 = \frac{1}{2} \cdot \left(\frac{mL^2}{3} + \frac{m_c L^2}{144} + J_c \left(\frac{\left(\frac{L^2}{36} - \frac{L}{6} c \cdot \cos(\theta - \gamma) \right)}{\frac{L^2}{36} + c^2 - \frac{L}{3} c \cdot \cos(\theta - \gamma)} \right)^2 \right) \cdot \dot{\theta}^2$$

$$(2.46)$$

In this way, recurring to the definition of Lagrange's equation, we will have:

$$\begin{cases} \frac{d}{dt} \left(\frac{\partial E_c}{\partial \dot{\theta}} \right) = \left(\frac{mL^2}{3} + \frac{m_c L^2}{144} + J_c \left(\frac{\left(\frac{L^2}{36} - \frac{L}{6} c \cdot \cos(\theta - \gamma) \right)}{\frac{L^2}{36} + c^2 - \frac{L}{3} c \cdot \cos(\theta - \gamma)} \right)^2 \right) \cdot \ddot{\theta} = J_\theta \cdot \ddot{\theta} \\ \\ \frac{\partial E_c}{\partial \theta} = 0 \end{cases}$$

$$(2.47)$$

where J_θ stands for the equivalent inertia of the linearized system.

2.2.2 Potential energy

Potential energy requires certainly a greater attention during linearization. In particular, the two systems will need to be treated differently because of their inherent and intrinsic design differences.

As it is possible to remind from previous explanations, the *single-stage cylinder* configuration will not undergo substantial changes between the big non-linear motion, and the small linearized on. The cylinder (with always the same 2 chambers generating hydraulic power) will be controlled by the same servo-valve. Hence the potential energy will be given only by the gravitational components, just like in equation (2.11).

That being so, no elastic potential belongs to the system; according to equation (2.44), a hessian derivative of the heights is needed. This means that the linearized motion equation will have the following energetic contribute:

$$m^* g \frac{\partial^2 h}{\partial \theta^2}\bigg|_{\theta_0} = \frac{\partial \left(\left(m + \frac{m_c}{6} \right) \frac{gL}{2} \cdot \sin\theta - \frac{c}{2} m_c g \cdot \sin\gamma \right)}{\partial \theta}\bigg|_{\theta_0} = -\left(m + \frac{m_c}{6} \right) \frac{gL}{2} \cdot \sin\theta_0$$

(2.48)

It is possible to synthesize this value with the symbol k_θ, which in this first case is negative. In fact we are forcing a system to stay steady (and then linearized) around an unstable equilibrium θ_0. We will see further on that this will affect the stability and the controllability of the system, favouring implicitly the double-stage solution.

The treating of the system with the *"Tandem" actuator* is instead much more complex. The passage between the positioning phase (reaching θ_0) and the vibrations rejection implies a change in the control strategy of the whole system: in fact, as already explained in the previous paragraphs, when θ_0 is reached, the 2-2 way valve feeding the big cylinder will be closed, as well as the second 2-2 way valve which, on the other hand, will let the servo-valve feed and control the small side of the actuator.

This means that in this second phase, p_1 and p_2 of the small cylinder will become states of the system, while the big cylinder will be closed and not re-opened again (unless making the system change the value of θ_0, which will need to switch again to the non-linear control).
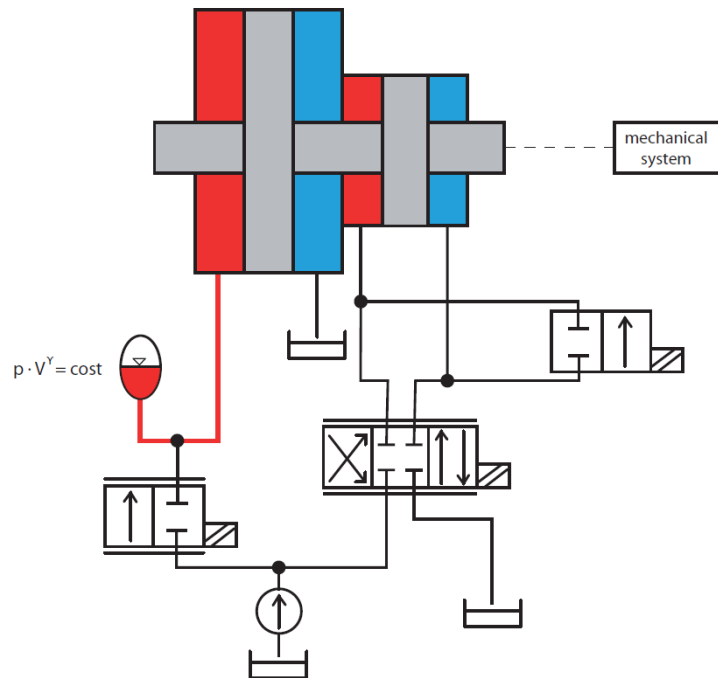
Figure 2.7: Sketch of the system when the angle set is reached. Focus on the changes of pressure into the accumulator.

According to Figure 2.7, the left side of the cylinder will be full of oil, and connected to the accumulator. While analyzing the first application for fatigue tests, we have already seen that in these conditions, the fluid inside the locked part of the circuit behaves like a very stiff spring: if there was not the accumulator the spring stiffness would coincide exactly with the compressibility of the fluid. Now, on the contrary, the system includes a hydraulic accumulator whose gas makes the whole fluid follow a polytrophic relationship between pressures and volumes.

$$p \cdot V^{\gamma} = cost \hspace{5cm} (2.49)$$

From another point of view, this structural change could be modelled exactly as a spring, which rotates with the actuator in the plane (look at Figure 2.8) and which unavoidably introduce elastic energy to the system.
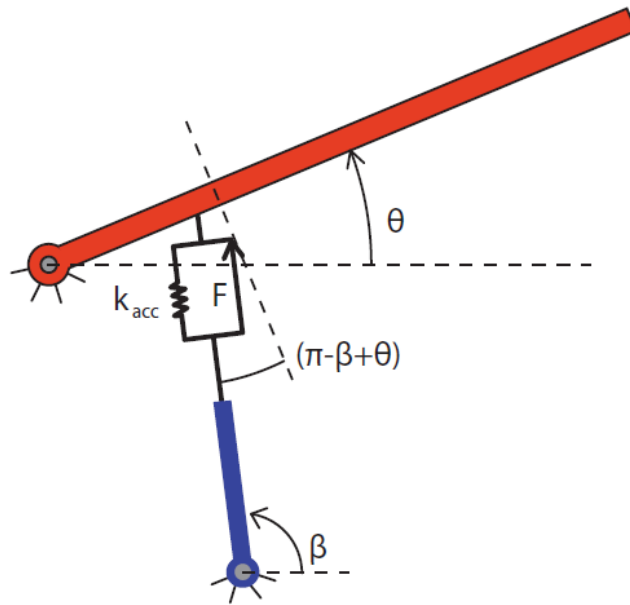
Figure 2.8: Sketch of the linearized mechanical system, with the modelled accumulator spring.

Of course this spring will have a non-linear characteristic (due to the polytrophic expression) but, considering that this configuration will only face small oscillations, we can try to linearize its behaviour around the equilibrium condition. In particular, by differentiating equation (2.49) over time, we get:

$$\frac{d(p \cdot V^{\gamma})}{dt} = V^{\gamma} \cdot \frac{dp}{dt} + \gamma \cdot V^{\gamma-1} \cdot p \cdot \frac{dV}{dt} = 0 \qquad (2.50)$$

By isolating the pressure derivative, it is possible to obtain:

$$\frac{dp}{dt} = -\frac{\gamma p}{V} \cdot \frac{dV}{dt} \qquad (2.51)$$

or better:

$$\frac{dp}{dV} = -\frac{\gamma \cdot p}{V} \qquad (2.52)$$

Let us now define the spring stiffness as the ratio between force and deformation; by substituting equation (2.52), we come up with:

$$k_{acc} = \frac{F}{\Delta x}\bigg|_{\theta_0} = \frac{dp \cdot A_{bigT}^2}{dV}\bigg|_{\theta_0} = \frac{\gamma \cdot p \cdot A_{bigT}^2}{V}\bigg|_{\theta_0} = \frac{\gamma \cdot p_{1_{\theta_0}} \cdot A_{bigT}}{X_{\theta_0}}$$

(2.53)

where $p_{1_{\theta_0}}$ and X_{θ_0} are respectively the pressure of oil and the displacement within the first chamber of the big cylinder, when the equilibrium configuration has been reached. It can be quickly computed that the stiffness of the accumulator spring is:

$$k_{acc} \cong 5117 \, N/m$$

Having this calculated, we can now proceed to study the linearization of the potential energy, which no will hence contain a twofold contribute, both gravitational V_g and elastic V_{el} ones. While however V_g coincides exactly with equation (2.11), V_{el} follows the formulation below:

$$V_{el} = \frac{1}{2} \cdot k_{acc} \cdot \Delta l^2$$

(2.54)

The spring stiffness has been linearized and then associated with a scalar number. Δl is still however a non-linear quantity, which behaves as follows:

$$\Delta l = b(\theta) - b(\theta_0) + \Delta l_0 =$$

$$= \sqrt{\frac{L^2}{36} + c^2 - \frac{L}{3} c \cdot \cos(\theta - \gamma)} - \sqrt{\frac{L^2}{36} + c^2 - \frac{L}{3} c \cdot \cos(\theta_0 - \gamma)} + \Delta l_0$$

(2.55)

where Δl_0 is the static pre-charge of the gas spring.

Therefore, the complete formulation of the potential energy will be given by:

$$V = \left(m + \frac{m_c}{6}\right) \cdot \frac{gL}{2} \cdot \sin(\theta) + \frac{1}{2} \cdot k_{acc} \cdot \Delta l^2 \qquad (2.56)$$

From this, we can calculate the algebraic expression for the static pre-charge of the spring: this, in fact, occurs when the system is in a condition of equilibrium, namely in correspondence of a stationary point of the potential energy:

$$\left.\frac{\partial V}{\partial \theta}\right|_{\theta_0} = 0 \qquad (2.57)$$

By means of few mathematical passages, we get the solution:

$$\Delta l_0 = -\left(m + \frac{m_c}{6}\right) \cdot \frac{gL}{2} \cdot \cos\theta_0 \cdot \frac{\sqrt{\frac{L^2}{36} + c^2 - \frac{L}{3}c \cdot \cos(\theta_0 - \gamma)}}{k_{acc} \cdot \frac{L}{6} \cdot c \cdot \sin(\theta_0 - \gamma)} \qquad (2.58)$$

As expected it is a negative quantity, which corresponds to the spring being compressed in the equilibrium condition.

The potential energetic description is then completed by the following derivatives:

$$\left.\frac{\partial \Delta l}{\partial \theta}\right|_{\theta_0} = \frac{\frac{L}{6} \cdot c \cdot \sin(\theta_0 - \gamma)}{\sqrt{\frac{L^2}{36} + c^2 - \frac{L}{3} c \cdot \cos(\theta_0 - \gamma)}} \qquad (2.59)$$

$$\left.\frac{\partial^2 \Delta l}{\partial \theta^2}\right|_{\theta_0} = \frac{\left(\left(\frac{L^3}{216}c - \frac{L}{6}c^3\right) \cdot \cos(\theta_0 - \gamma) - \frac{L^2}{36}c^2 \cdot (2\cos^2(\theta_0 - \gamma) + \sin^2(\theta_0 - \gamma))\right)}{\left(\frac{L^2}{36} + c^2 - \frac{L}{3}c \cdot \cos(\theta_0 - \gamma)\right)^{\frac{3}{2}}} \qquad (2.60)$$

For simplicity, we will define the following summarizing parameters:

$$\begin{cases} k_{\theta_T} = \left[k_{acc} \cdot \left(\dfrac{\partial \Delta l_d}{\partial \theta} \right)^2_{\theta_0} + k_{acc} \cdot \Delta l_0 \cdot \left. \dfrac{\partial^2 \Delta l_d}{\partial \theta^2} \right|_{\theta_0} + m^* g \left. \dfrac{\partial^2 h}{\partial \theta^2} \right|_{\theta_0} \right] \\ \\ \qquad k_{\theta_C} = m^* g \left. \dfrac{\partial^2 h}{\partial \theta^2} \right|_{\theta_0} \end{cases}$$

(2.61)

which respectively represent the equivalent stiffness of the arm with the "Tandem" and the arm with the classical actuator.

The linearized motion equations will be at a later time (in sub-section) filled in with them.

2.2.3 Dissipative energy

Oppositely to the potential energy, the dissipative energy remains the same as the non-linear case, but of course it will need to be linearized.

In fact the modification introduced by the accumulator in the "Tandem" system creates an effect which is purely elastic. Obviously the flow of the gas within its vessel will generate losses for viscous friction, but for simplicity we will assume the gas viscosity negligible. In this perspective, only viscous friction inside the cylinder will be considered.

Being that so, the dissipation term we will need to introduce in the linearized motion equation is:

$$r_c \cdot \left(\frac{\partial \Delta l}{\partial \theta} \right)^2_{\theta_0} = r_c \cdot \frac{\dfrac{L^2}{36} \cdot c^2 \cdot \sin^2(\theta_0 - \gamma)}{\dfrac{L^2}{36} + c^2 - \dfrac{L}{3} c \cdot \cos(\theta_0 - \gamma)} = r_\theta$$

(2.62)

where r_θ represents the equivalent damping of the linearized system.

2.2.4 External forces work

In this second phase of the motion, the already declared objective of the system is to reject a certain disturbance appeared on the arm (as a harmonic torque) because of the causes mentioned in the introductory paragraph. In particular we have stimulated the system with a torque of 2000 Nm of amplitude (which corresponds to approximately a mass of 50 kg on the tip of the arm.

This means that the systems, either the classical or the "Tandem" indifferently, assumes a new "force configuration" which is shown below in Figure 2.9. Differences between the first and the second are only given by the surfaces on which pressures is exerted.
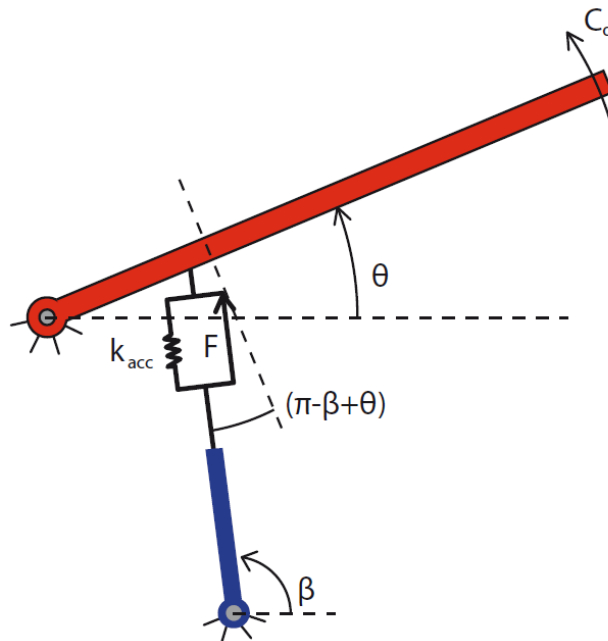
Figure 2.9: Sketch of the linearized force configuration of the system.

As a consequence of this, the linear work of the external forces for the *classical cylinder* configuration is:

$$Q = \frac{\delta^* L}{\delta \theta} = (p_1 - p_2) \cdot \frac{L}{6} \cdot A_{bigc} \cdot \cos(\pi - \beta(\theta_0) + \theta_0) + C_d(t) =$$
$$= (p_1 - p_2) \cdot \frac{L}{6} \cdot A_C^* + C_d(t)$$

(2.63)

In the configuration of the arm with the *"Tandem" actuator*, the lagrangian component is then:

$$Q = \frac{\delta^* L}{\delta \theta} = (p_1 - p_2) \cdot A_{small} \cdot \cos(\pi - \beta(\theta_0) + \theta_0) + C_d(t) =$$
$$= (p_1 - p_2) \cdot \frac{L}{6} \cdot A_T^* + C_d(t)$$

(2.64)

2.2.5 Linearized equations of motion

The description is now complete: there is nothing left to do but taking all the pieces computed in the previous paragraphs and assembling them together in two different motion equations.

The linear dynamics of the system composed by the arm, actuated by the classical single-stage hydraulic actuator, is described by the following expression:

$$J_\theta \cdot \ddot{\theta} + r_\theta \cdot \dot{\theta} + k_{\theta_C} \cdot (\theta - \theta_0) = (p_1 - p_2) \cdot \frac{L}{6} \cdot A_C^* + C_d(t) \qquad (2.65)$$

Similarly, the linear dynamics of the "Tandem" configuration follows the differential equation above:

$$J_\theta \cdot \ddot{\theta} + r_\theta \cdot \dot{\theta} + k_{\theta_T} \cdot (\theta - \theta_0) = (p_1 - p_2) \cdot \frac{L}{6} \cdot A_T^* + C_d(t) \qquad (2.66)$$

As it can be easily noticed, the difference between the two systems is merely contained in the different areas which the pressures act on, and in the equivalent stiffness from which the system are characterized. About this

second feature, in particular, we can make an observation: while k_{θ_T} is positive and then stable (thanks to the spring created by the accumulator), k_{θ_C} is negative (because defined by the sole gravitational contribute). This affects not only the stability but, consequently, also the controllability of the arm actuated by the classical cylinder.

We have seen further in the thesis on how this has disclosed during the analysis of the state space description of the system and in the frequency domain.

2.2.6 Hydraulic equations

Just like in sub-section 2.1.6, the chapter goes through the treatment of the hydraulic behaviour of the systems at stake.

In this second phase in particular, both the arm with the classical actuator, or that one actuated by the "Tandem", are controlled by means of a servo-valve. This results in both of them having a very similar hydraulic dynamics equation.

Holding the hypothesis of small oscillations, as a normal consequence of this, also flow rates vary "slowly" (as well as the spool displacement). It is hence allowed to linearize its equation. With reference to equation (2.26), it is possible to state that:

$$Q_{or}(x_d, \Delta p_{or}) \cong \left[\frac{\partial Q_{or}}{\partial x_d}\right]\Bigg|_{\Delta p_{or_0}} \cdot x_d + \left[\frac{\partial Q_{or}}{\partial \Delta p_{or}}\right]\Bigg|_{x_{d_0}} \cdot \Delta p_{or} = K_q \cdot x_d + K_c \cdot \Delta p_{or}$$

(2.67)

where K_q and K_c are respectively called *flow gain coefficient* and flow *pressure coefficient* [23]. In order to make a realistic simulation of the system, we need to compute these parameters. The first step towards this objective is obviously the choice of a servo-valve.

We remind to the reader that the aim of the actual analysis is to eventually show the advantages carried by a new type of architecture of hydraulic actuator. For this reason we choose the same servo-valve for both the systems, in order to evaluate, in the end, two systems different only in their actuator.

Being however the classical configuration endowed with one single servo-valve (used indifferently for the linear and non-linear motion), we should use that one already selected in sub-section 2.1.6.

According to the definitions, it is possible to compute the flow gain coefficient as follows:

$$K_q = \left[\frac{\partial Q_{or}}{\partial x_d}\right]\Bigg|_{\Delta p_{or_0}} = C_d \cdot w \cdot \sqrt{\frac{p_{pump} - p_L}{\rho_{oil}}}$$

(2.68)

where $p_L = p_1 - p_2$ is called *load pressure*. For the servo-valve in use, and the set-up of our system, K_q is evaluated to be $1{,}584 \cdot 10^{-2} \ m^2/s$.

In the same way, it is possible to evaluate the flow pressure coefficient as:

$$K_c = \left[\frac{\partial Q_{or}}{\partial \Delta p_{or}}\right]\Bigg|_{x_{d_0}} = -\frac{\partial Q_L}{\partial P_L} = \frac{C_d w}{2} \cdot \frac{x_d}{p_{pump} - p_L} \cdot \sqrt{\frac{p_{pump} - p_L}{\rho_{oil}}} = \frac{x_d}{2(p_{pump} - p_L)} \cdot K_q$$

(2.69)

Please note that the coefficient is given a negative sign because the differentiation of the mean flow rate Q_L results in a negative quantity (given that K_c is conventionally assumed positive). Applied on our servo-valve, the coefficient equals $1{,}023 \cdot 10^{-6} \ m^3/s/bar$.

Being that so, hydraulic equations are quickly computed by referring to the proceeding adopted in paragraph 3.1.6. For the system with the *classical cylinder*, we get:

$$\begin{cases} Q_1 = K_q \cdot x_d + K_c \cdot (p_{pump} - p_1) = C_i \cdot (p_1 - p_2) + A_{big_C} \cdot \alpha^* \cdot \dot{\theta} + \dfrac{V_0}{\beta_c} \cdot \dot{p}_1 \\[4mm] \qquad Q_2 = K_q \cdot x_d + K_c \cdot p_2 = C_i \cdot (p_1 - p_2) - A_{big_C} \cdot \alpha^* \cdot \dot{\theta} - \dfrac{V_0}{\beta_c} \cdot \dot{p}_2 \end{cases}$$

(2.70)

For the *"Tandem" actuator* it is instead obtained:

$$\begin{cases} Q_1 = K_q \cdot x_d + K_c \cdot (p_{pump} - p_1) = C_i \cdot (p_1 - p_2) + A_{small} \cdot \alpha^* \cdot \dot{\theta} + \dfrac{V_0}{\beta_c} \cdot \dot{p}_1 \\[4mm] \quad Q_2 = K_q \cdot x_d + K_c \cdot p_2 = C_i \cdot (p_1 - p_2) - A_{small} \cdot \alpha^* \cdot \dot{\theta} - \dfrac{V_0}{\beta_c} \cdot \dot{p}_2 \end{cases}$$

$$(2.71)$$

In this sense, both the configurations have two different states, one for each pressure inside the cylinder chambers. Moreover, again external leakages can be neglected thanks to the presence of seals with scraper rings.

2.2.7 Control logic for the non-linear motion

In the linearized motion, as well as in the non-linear one, the means by which flow rates and pressure within the cylinder are controlled is the spool and its displacement.

Following the same reasoning and the same proceeding shown in section 2.1.7, the controller can act on the current which enters the valve solenoid in order to maintain the system steady on its equilibrium configuration on θ_0, trying thus to reject the external disturbances.

The risk we encounter in these vibration control applications is to have a final system response too much rigid and nervous. In order to avoid this unwanted behavior this time the controller is chosen of a PD type (proportional-derivative), in which the derivative gain is meant to produce such an additional damping effect to "smooth" the system. In addition to this, the anticipation of phase, consequence of the derivative gain is expected to enhance the controllability of the system.

The expression of the control function (which obviously holds for both the cylinders studied) is then the following:

$$x_d(s) = k_s \cdot i_c(s) = k_s \cdot \left[k_p \cdot (\theta_0 - \theta(t)) + k_d \cdot \left(0 - \dot{\theta}(t) \right) \right] \qquad (2.72)$$

The system in now ready again to be integrated. Next paragraph specifies which kind of integration has been applied to study the linear response of the system under investigation.

2.2.8 Integration of linearized motion equations

Even if significantly simplified, the linear system still needs a numerical method to be integrated. For the reasons widely treated in paragraph 3.1.8, we still rely on a fourth order Runge Kutta method.

The comfort of a linear description is that now a matricial approach can be adopted. If we call z the state vector:

$$\underline{z} = \begin{bmatrix} \dot{\theta} & \theta & p_1 & p_2 \end{bmatrix}^T \qquad (\,2.73\,)$$

and u the vector containing the inputs of the system:

$$\underline{u} = \begin{bmatrix} C_d & \theta_0 & p_{pump} \end{bmatrix}^T \qquad (\,2.74\,)$$

the consequent state-space description for the two actuated systems can be written as:

$$\underline{\dot{z}} = [A]\underline{z} + [B]\underline{u} \qquad (\,2.75\,)$$

where, for *"Tandem" system*:

$$A = \begin{bmatrix} -\dfrac{r_\theta}{J_\theta} & -\dfrac{k_\theta}{J_\theta} & \dfrac{A_C^* \cdot L}{6 \cdot J_\theta} & -\dfrac{A_C^* \cdot L}{6 \cdot J_\theta} \\[2mm] 1 & 0 & 0 & 0 \\[2mm] -\dfrac{(A_{small}\alpha^* + K_q k_s k_d)\beta_c}{V_0} & -\dfrac{K_q k_s k_p \beta_c}{V_0} & -\dfrac{(K_c + C_i)\beta_c}{V_0} & -\dfrac{C_i \beta_c}{V_0} \\[2mm] +\dfrac{(A_{small}\alpha^* + K_q k_s k_d)\beta_c}{V_0} & +\dfrac{K_q k_s k_p \beta_c}{V_0} & +\dfrac{C_i \beta_c}{V_0} & +\dfrac{(K_c + C_i)\beta_c}{V_0} \end{bmatrix} \qquad (2.76)$$

$$B = \begin{bmatrix} \dfrac{1}{J_\theta} & \dfrac{k_\theta}{J_\theta} & 0 \\[2mm] 0 & 0 & 0 \\[2mm] 0 & \dfrac{K_q k_s k_p \beta_c}{V_0} & \dfrac{K_c \beta_c}{V_0} \\[2mm] 0 & -\dfrac{K_q k_s k_p \beta_c}{V_0} & 0 \end{bmatrix} \qquad (2.77)$$

while for the *classical system* we have exactly the same matrices, except for the state matrix A in which A_C^* and A_{small} are substituted by A_T^* and A_{big_C} respectively.

The dynamics of our concrete handling arm has been then totally described. Next chapter will be dedicated to a critical analysis of the results, which will eventually decree if the initial expectations of a better behavior for the "Tandem" actuator will be satisfied or not.

Chapter 3

Analysis of the results

Once completed the description of the two systems, in their structure, dimensions and dynamic behavior, they are now available all the instruments to conduct a detailed analysis which is expected to show the improvements the "Tandem" actuator can carry to the concrete handling arm.

The study starts from a comparison in the state-space description, by looking at poles and zeros of the two systems. From this first step, an analysis in the Laplace domain has been carried out. Then, the results of the integration of the equations of motion over time have been shown as a confirmation to what previously said. In the end a comparison on the power absorption of the two systems has been shown.

3.1 State-space analysis

The paragraph we are going trough will show the differences between the two *linearized systems* under investigation in the state-space description.

As already explained in the previous sections, in order to show advantages or disadvantages of the two hydraulic cylinders, with results depurated from any other external effect, the analysis has been conducted on both the systems based on the same boundary conditions. This means that the "Tandem" actuator and the single-stage cylinder both drive the same identical arm, being fed by the same servo-valve (linearized motion), with the *same controller* and the same pump pressure. This type of reasoning will help the reader in observing how the final performances differentiate between the two cylinders.

The analysis starts from the state-space description of both the non-controlled systems, which follows the matricial equation below:

$$\dot{\underline{z}} = A \cdot \underline{z} + B \cdot \underline{u} \tag{3.1}$$

$$\dot{\underline{z}} = \begin{pmatrix} -\dfrac{r_\theta}{J_\theta} & -\dfrac{k_\theta}{J_\theta} & \dfrac{A^*L}{6J_\theta} \\ 1 & 0 & 0 \\ -\dfrac{A\alpha^*}{V_0/2\beta_c} & 0 & -\dfrac{\left(C_i + \dfrac{K_c}{2}\right)}{V_0/2\beta_c} \end{pmatrix} \cdot \underline{z} + \begin{pmatrix} \dfrac{1}{J_\theta} & \dfrac{k_\theta}{J_\theta} & 0 & 0 \\ 0 & 0 & 0 & 0 \\ 0 & 0 & \dfrac{K_q}{V_0/2\beta_c} & \dfrac{k_c}{2} \end{pmatrix} \cdot \begin{pmatrix} C_d \\ \theta_0 \\ x_d \\ p_{pump} \end{pmatrix}$$

$$\tag{3.2}$$

where $\underline{z} = \begin{pmatrix} \dot{\theta} & \theta & \Delta p \end{pmatrix}^T$ is the state vector, A the state matrix, and $\underline{u}$ is the vector containing the inputs of the system.

The theory of control [24] teaches us that the poles of the system are not influenced by the inputs it receives from outside; in fact the poles of the non-controlled systems can be computed as the eigenvalues of the state matrix A. In this sense, according to the definition:

$$\det(\lambda I - A) = 0 \tag{3.3}$$

it can be computed that the two systems will have the poles listed in Table 3.1.

Table 3.1: Poles of the two non-controlled systems.

Tandem cylinder		ω_n [rad/s]	ξ
-4,61 ± 128,32 i	2 complex conj.	128,40	0,035
-9,01-4	1 real	3,58e-4	1,000
Single-stage cylinder		ω_n [rad/s]	ξ
-2,41 ± 242,04 i	2 complex conj.	242,06	0,010
1,97e-5	1 real	1,97e-5	-1,000

As expected, the system actuated by the classical single cylinder has an unstable pole. This is due to the linearization executed in a position ($\theta_0 = 30°$) which is not actually an equilibrium point for the system: it is the control action which manages to keep the arm stable in that position. In the case of the "Tandem", instead, because of the presence of an additional fictitious spring, which embodies the behavior of the accumulator, the system results inherently stable.

Moreover, in both cases the two complex conjugate poles are characterized by very *high imaginary parts.* This is clearly due to the type of analysis, which is not going in depth to see how the arm itself reacts to forces and vibrations: the arm is assumed to be a totally *rigid body*, which is certainly an approximation of what occurs in reality. If a FEM analysis had been conducted, natural frequencies would have certainly been lower. But however, this does not match with the objective of the thesis, which is instead focusing on the qualities of a new type of hydraulic actuator, and which does not need a so elaborate and complex study to come up with appreciable results. Referring to this, the "Tandem" solution shows lower natural frequencies because of its reduced piston area: considering that the ratio $A_{big}/A_{small} \cong 2,5$, and that the natural frequencies are proportional to the square root of the surfaces, it is justified an ω_0 of nearly 160 rad/s.

Being that so, and having the non controlled systems 3 poles, if the systems were controlled with a simple proportional (P) controller, they would be supposed to have a bode diagram with amplitude slope of -20 dB (after the first

pole) and of -60dB (after the two c.c.), and with phase descending first on -90° and then on -270° (look at the example in Figure 3.1).
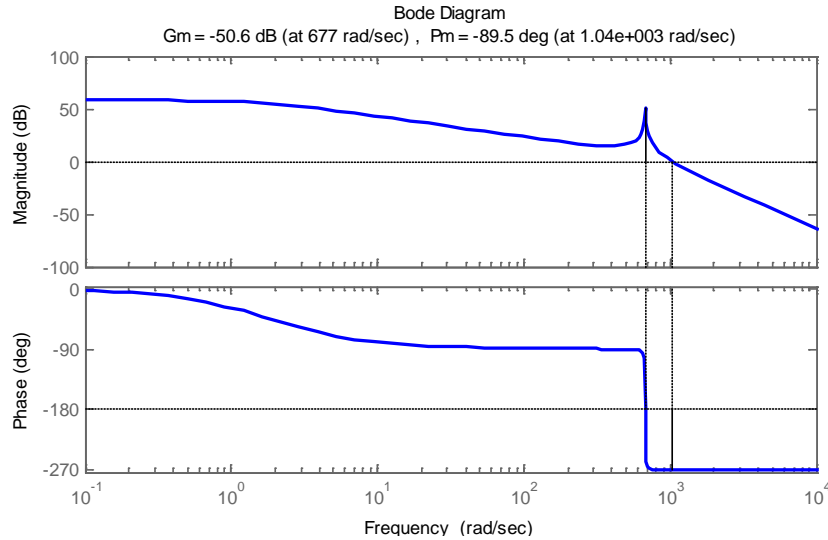
Figure 3.1: Example of bode diagram for transfer function with 3 poles and no zeros.

This configuration would certainly risk to be unstable and hardly controllable. That is why the controller is meant to be a proportional-derivative (PD) one, which introduces a zero in the system:

$$k_p + k_d s = 0 \quad \rightarrow s_{zero} = -\frac{1}{T_d} = -\frac{k_p}{k_d} \tag{3.4}$$

As a consequence of this, the general state-space description for the system in use is:

$$\underline{\dot{z}} = \begin{pmatrix} -\dfrac{r_\theta}{J_\theta} & -\dfrac{k_\theta}{J_\theta} & \dfrac{A^*L}{6J_\theta} \\ 1 & 0 & 0 \\ -\dfrac{(A\alpha^* + k_s K_q k_d)}{V_0/2\beta_c} & -\dfrac{k_s K_q k_p}{V_0/2\beta_c} & -\dfrac{\left(C_i + \dfrac{K_c}{2}\right)}{V_0/2\beta_c} \end{pmatrix} \cdot \underline{z} + \begin{pmatrix} \dfrac{1}{J_\theta} & \dfrac{k_\theta}{J_\theta} & 0 \\ 0 & 0 & 0 \\ 0 & \dfrac{k_s K_q k_p}{V_0/2\beta_c} & \dfrac{K_c}{V_0/2\beta_c} \end{pmatrix} \cdot \begin{pmatrix} C_d \\ \theta_0 \\ p_{pump} \end{pmatrix}$$

$$\tag{3.5}$$

The idea is to regulate the controller in order to place the zero between the real and the complex conjugate poles. This will help the amplitude to stay as long as possible horizontal (preserving then the bandwidth) and the phase in not going under the -180°. In this way the system will be stable and more controllable.

Starting from the "Tandem", two different positions for the zero have been tried out: $z = -10$ and $z = -8$. By keeping the zeros fixed, and by varying the values of k_p and k_d , two root locus have been computed (Figure 3.2).
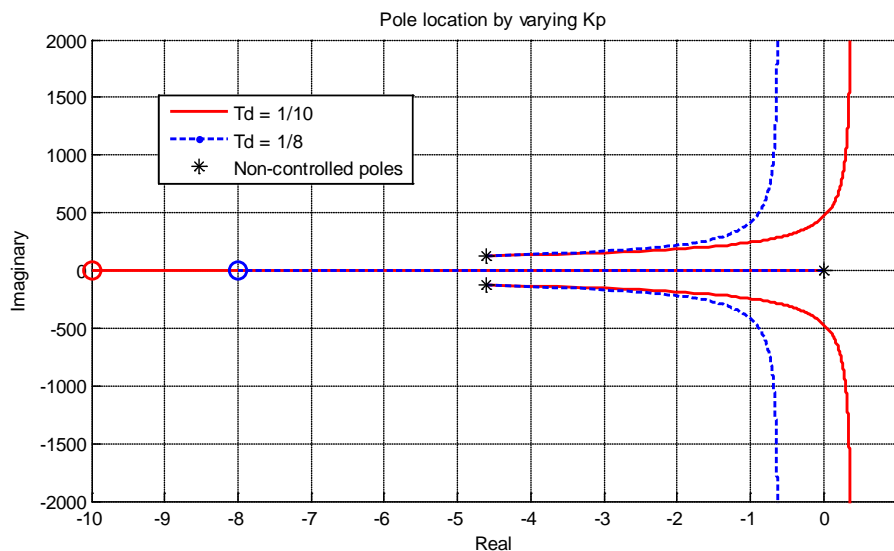
Figure 3.2: Root locus for the "Tandem" system, for three different positions of the zero.

It is easy to notice how the curve corresponding to $T_d = 1/10$ becomes rapidly unstable, because the two complex poles move into the right-half part of the complex plane (positive real part): this in particular happens for $k_p = 100$. It is a combination to be preferably avoided. The other configuration remains stable and, in addition to this, k_p can be reasonably increased without having the imaginary part blow off of the plot. The best solution is hence the second, having the zero in $s_{zero} = -8$. k_p will be taken equal to 120, k_d equal to 15. Aiming at using the same boundary conditions for both the systems, also for the classical cylinder the same controller (zero in $s_{zero} = -8$,) has been used.

For completeness in Figure 3.3 it is depicted the same analysis of before, carried out on the system with the single-stage actuator.
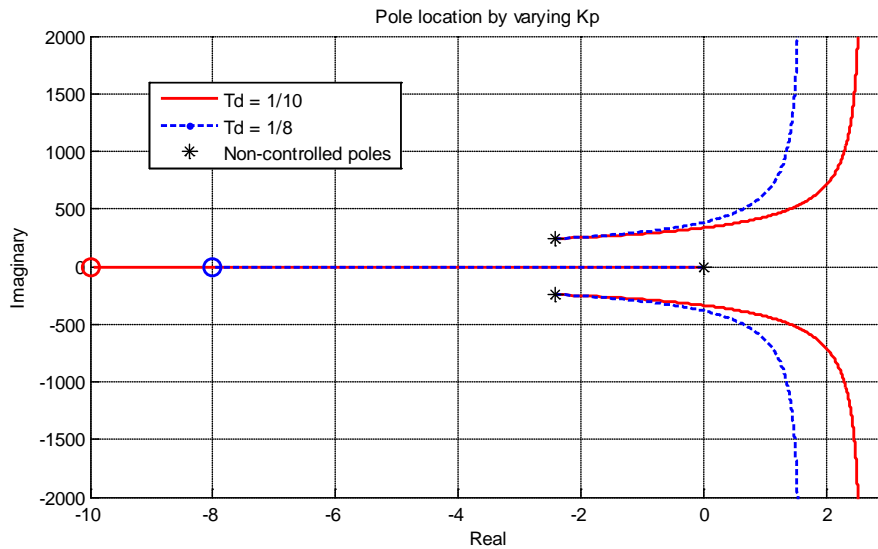
Figure 3.3: Root locus for the single-stage actuator system, for three different positions of the zero.

Showing how all the curves trespass in the right-half part of the complex plane, the figure implicitly demonstrates the *improved controllability* of the system actuated by the "Tandem".

In particular, for the chosen solution with the zero in $s_{zero} = -8$ (blue curve) the system becomes unstable when $k_p = 40.1$. We want however the system to be stable: therefore we take $k_p = 32$ and $k_d = 4$.

In Figure 3.4, in the end, a direct comparison between the two adopted solutions is depicted.
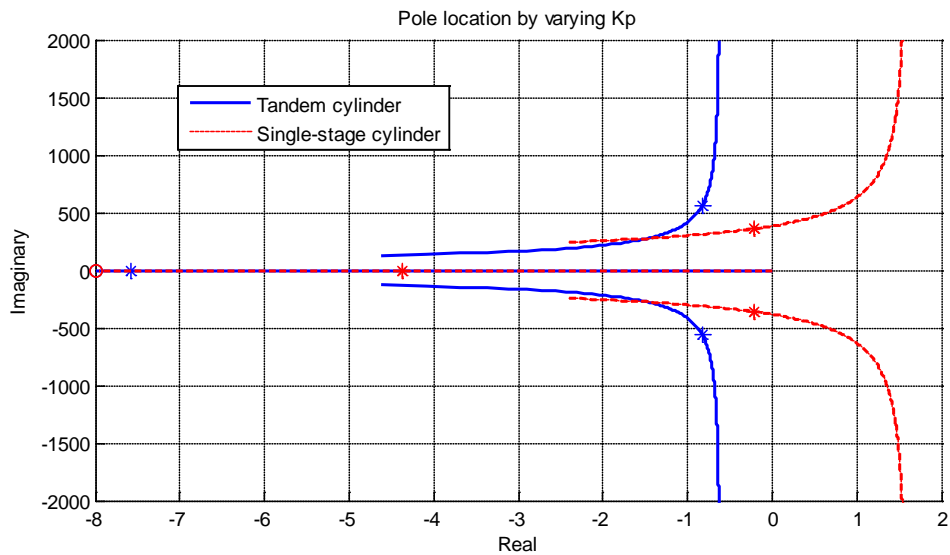
Figure 3.4: Comparison of the root locus for the two controlled systems.

3.2 Laplace domain analysis

In this second section, an analysis based on the Laplace domain has been carried out for the two systems.

It is well-known that the Laplace transform is an integral transform that allows to convert an equation (associated with a linear, time invariant system) from the time domain into the so-called "s-domain", even known as Laplace domain. In this domain, in fact, it is easy and immediate to study and observe some of those dynamic requirements which can decree the goodness of a system instead of one other: we are referring specifically to asymptotic stability, promptness and bandwidth [17]. This is of great interest for the two systems under observation, which are indeed linear and time invariant.

According to equations (2.75), (2.76) and (2.77), the application of the Laplace transform would result in the following block diagram (Figure 3.5):
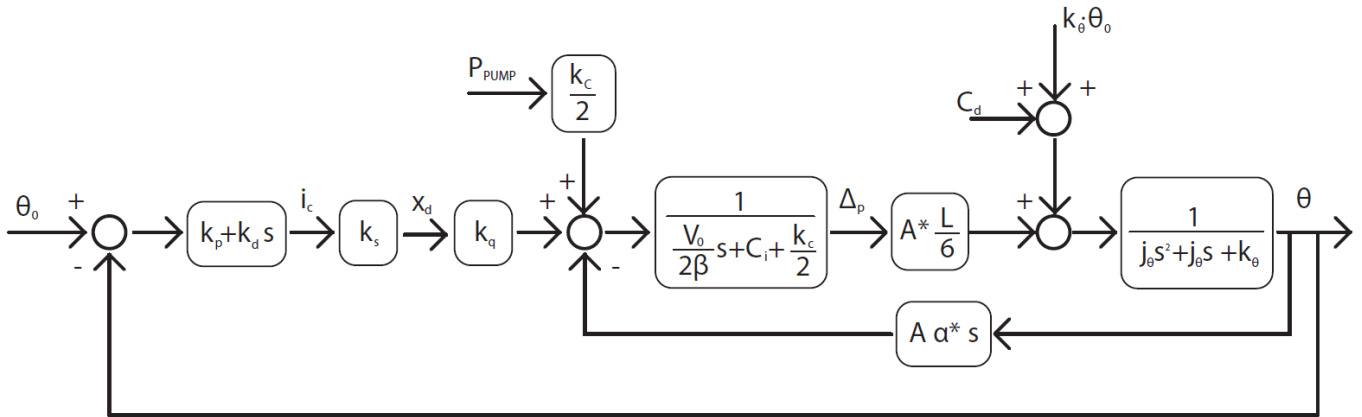
Figure 3.5: Block diagram for the system controlled in feedback.

In the diagram above all the inputs of the system have been represented: the disturbing torque C_d, the pump pressure p_{pump} (even if constant, it affects the transfer function by raising it of a constant gain) and the reference angle θ_0.

In the perspective of observing the *stability of the system* (which is controlled in position to keep the angle θ_0), it is necessary to define first of all the transfer function between the spool displacement x_d and the output θ:

$$L_{\theta \atop x_d}(s) = \frac{\dfrac{K_q A^* L}{6}}{\left(\dfrac{V_0}{2\beta_c}s + \left(C_i + \dfrac{K_c}{2}\right)\right) \cdot (J_\theta s^2 + r_\theta s + k_\theta) + \dfrac{A^* A \alpha^* L}{6}s}$$

(3.6)

This means that the loop transfer function is:

$$G_{loop}(s) = \frac{\dfrac{K_q k_s A^* L}{6} \cdot (k_p + k_d s)}{\left(\dfrac{V_0}{2\beta_c}s + \left(C_i + \dfrac{K_c}{2}\right)\right) \cdot (J_\theta s^2 + r_\theta s + k_\theta) + \dfrac{A^* A \alpha^* L}{6}s}$$

(3.7)

This formula gives us the possibility to study how the system behaviour changes depending on the controller parameters. In particular, the position of the zero has already been fixed in Section 4.1, but a corresponding variation of

k_p and k_d in the "Tandem" control function would results in what depicted in Figure 3.6:
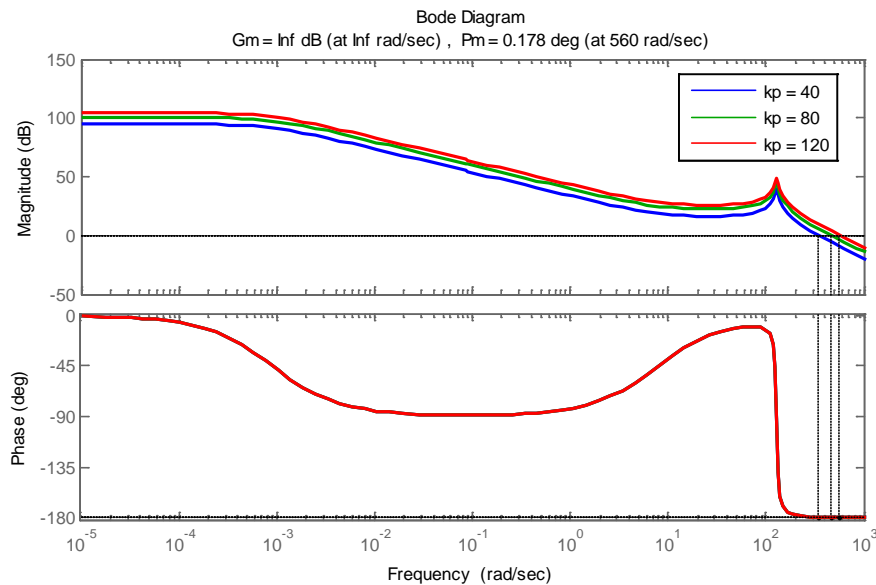
Figure 3.6: Bode plot of the loop transfer function for the system actuated by the "Tandem".

By looking at the figure, it can be inferred that, as expected from section 4.1, the system is endowed with a real pole, a couple of complex conjugate poles and a zero appositely placed between them. Moreover the plot clearly shows that, by increasing the proportional gain, nothing changes in the phase, while the amplitude plot is simply shifted upwards by the static gain. The functions are also *inherently stable*, considering that we have previously chosen the zero with this aim.

The same analysis can be conducted on the system actuated by the classical cylinder. Figure 3.7 shows again what seen in the state-space description: the phase diagram starts from -180° because of the negative stiffness k_θ, which makes the static gain change sign. This stiffness is also responsible for the real pole being unstable: that is why the phase raises of 90° firstly for the pole, then for the zero, before going down again to -180° in correspondence of the couple of complex conjugate poles. Exactly like in Figure 3.6: Bode plot of the loop transfer function for the system actuated by the "Tandem"., the phase is unaffected by changes in the control gains, while the amplitude is shifted upwards with increasing values of k_p.
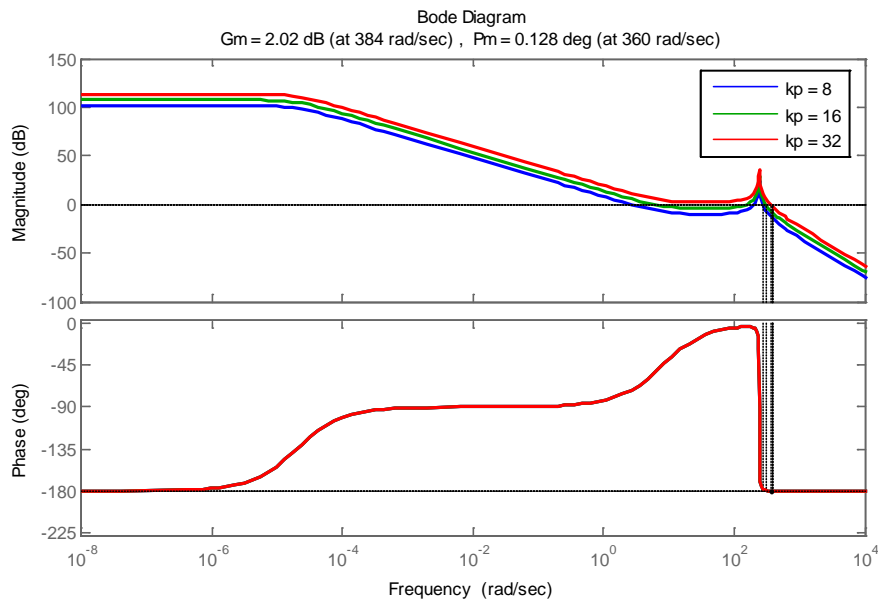
Figure 3.7: Bode plot of the loop transfer function for the system actuated by the classical cylinder.

An additional observation can be made about these bode plots, in particular about the very sharp resonances and changes of phase in correspondence of the complex conjugates poles. This is unfortunately the natural consequence of the analysis conducted so far, which did not take the deformation of the arm into consideration. As a consequence of this, not only the system becomes rigid (that means high natural frequencies) but also the damping is particularly low and associated only with the viscous friction within the cylinder.

The results we are interested in, are however unaffected by this phenomenon: Figure 3.8 shows indeed the comparison between the two loop transfer functions. The system has almost the same static gain, but the real difference is the absence of an unstable pole in the "Tandem" solution, which makes it much *more controllable* than the classical solution. A confirmation to this has already been given in the state-space description, by showing that for a zero place in $s = -8$, the "Tandem" can be hypothetically given any k_p, while for the single-stage cylinder it was limited to the value of 8.
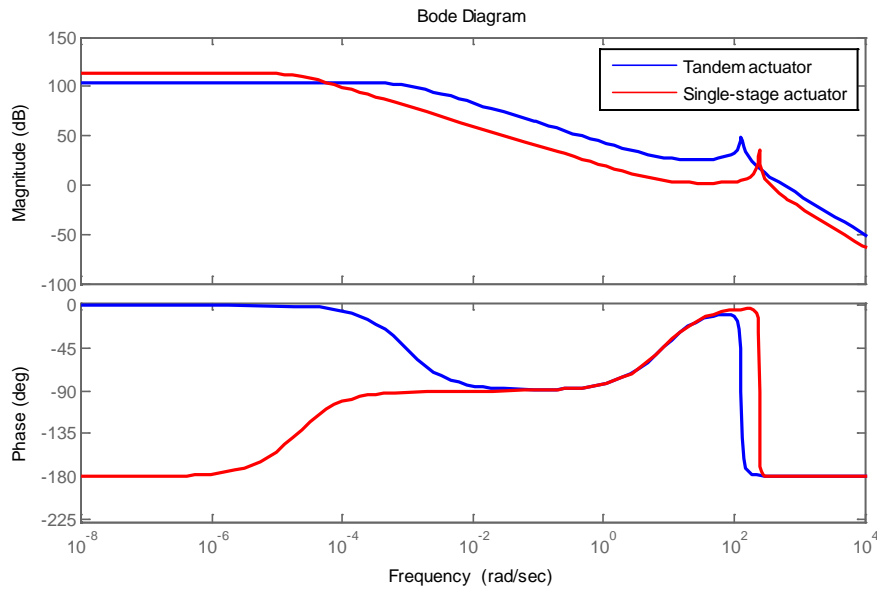
Figure 3.8: Comparison of the bode plots of the loop transfer functions for the two systems.

Furthermore, as mentioned in the introduction of this section, the Laplace domain is the suitable environment to study the bandwidth of the two systems. In particular, being them controlled in feedback on the angular position θ, we define the closed loop transfer function as follows:

$$L_{\frac{\theta}{\theta_0}}(s) = \frac{\frac{K_q k_s A^* L}{6} \cdot (k_p + k_d s)}{\left(\frac{V_0}{2\beta_c} s + \left(C_i + \frac{K_c}{2}\right)\right) \cdot (J_\theta s^2 + r_\theta s + k_\theta) + \frac{A^* A \alpha^* L}{6} s + \frac{K_q k_s A^* L}{6} \cdot (k_p + k_d s)}$$

(3.8)

Figure 3.9 shows for the "Tandem" system how the bode diagram of such transfer function varies for different values of proportional gain (keeping fixed the zero).
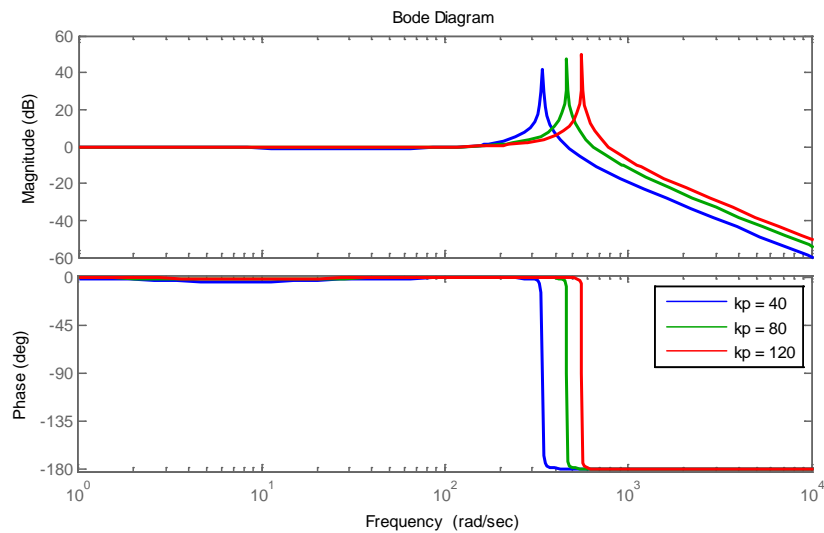
Figure 3.9: Bode plot of the closed loop transfer function for the system with the "Tandem" actuator.

The increase of k_p carries the disadvantage of reducing the damping ratio, which makes the resonance more sharp and the passage of phase from 0° to -180° almost immediate. We do not have an objective to respect on the damping of the system, even because what we observe is the consequence of the model applied, e not of the behavior of the cylinder.

What however is really interesting is the decisive increase in bandwidth, which definitely justifies the choice of taking a high value for k_p.

This happens for the classic cylinder as well: Figure 3.10 shows in fact exactly the same behavior, namely bandwidth growing by increasing k_p, and damping ratios decreasing in the meanwhile.
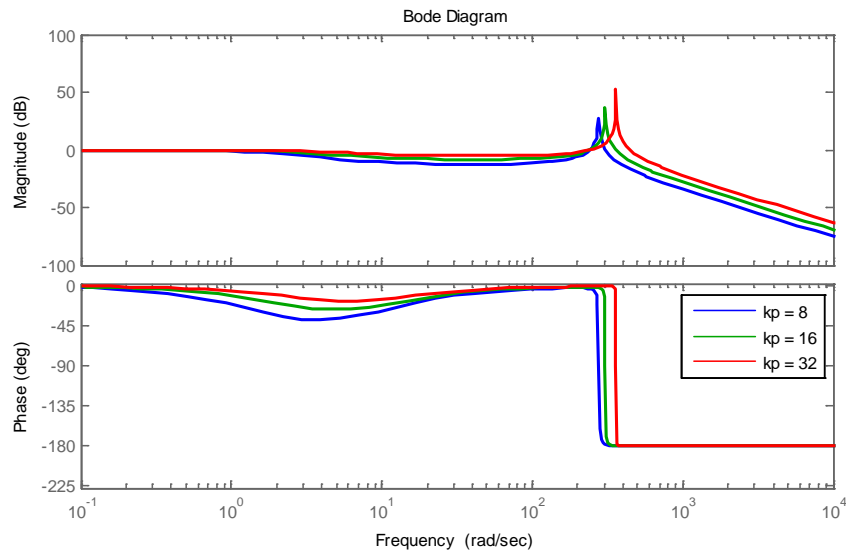
Figure 3.10: Bode plot of the closed loop transfer function for the system with the single-stage actuator.

The probably most important figure is however the direct comparison between the two solutions (Figure 3.11):
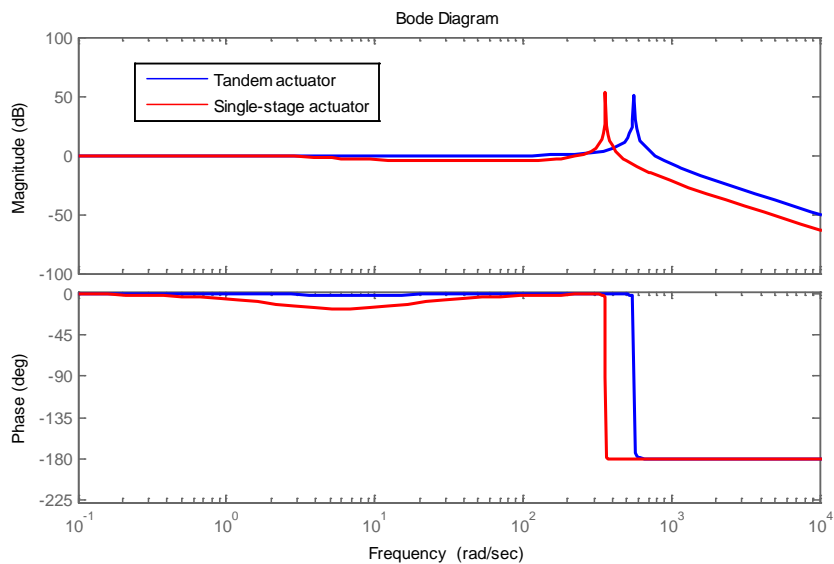
Figure 3.11: Comparison of the bode plots for the closed loop transfer functions of the two systems.

Just like it has been demonstrated in the first application on the fatigue test, the "Tandem" cylinder not only provides the system with a bandwidth almost doubled (at +3dB, about 156 rad/s for the classical cylinder, 285 rad/s for the "Tandem"), but also the phase difference results lower, and then better. This

plot demonstrates thus the great potentialities of this new concept of hydraulic actuator.

This second application of the thesis is moreover come to light to demonstrate the capability of such a cylinder to reject disturbances better than a classical one. In this case the system is a bit more complex than a classical one because its general answer descends directly from the combination and the superposition of the effects of three different input: C_d, θ_0 and p_{pump}.

The transfer function between θ_0 and θ has been already computed in equation (3.8). The transfer function between the pump pressure and the output of the system requires instead a more difficult treatment. If, in fact, there was not spool displacement, the transfer function of the system would be strongly similar to $L_{\frac{\theta}{x_d}}(s)$:

$$G_{\frac{\theta}{p_{pump}}}(s) = \frac{\dfrac{K_c}{2} \cdot \dfrac{A^*L}{6}}{\left(\dfrac{V_0}{2\beta_c}s + \left(C_i + \dfrac{K_c}{2}\right)\right) \cdot (J_\theta s^2 + r_\theta s + k_\theta) + \dfrac{A^*A\alpha^*L}{6}s}$$

(3.9)

However the system is controlled and in particular fed-back on the angular position. This makes the block diagram modified into (Figure 3.12):
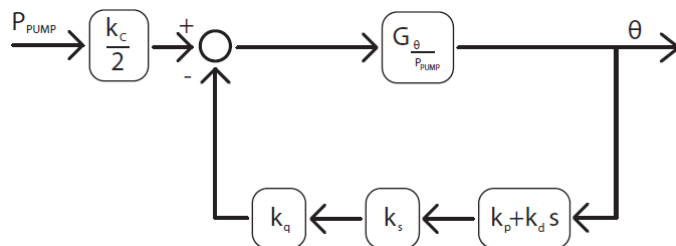
Figure 3.12: Block diagram for the closed loop transfer function between the pump pressure and the output angle θ

From this graphical representation, it descends that the closed loop transfer function between p_{pump} and θ is:

$$L_{\frac{\theta}{p_{pump}}}(s) = \cfrac{\cfrac{K_c}{2} \cdot \cfrac{A^*L}{6}}{\left(\cfrac{V_0}{2\beta_c}s + \left(C_i + \cfrac{K_c}{2}\right)\right) \cdot (J_\theta s^2 + r_\theta s + k_\theta) + \cfrac{A^*A\alpha^*L}{6}s + \cfrac{K_q k_s A^*L}{6} \cdot (k_p + k_d s)}$$

(3.10)

On the contrary, the other transfer functions can be computed according to Figure 3.13, which depicts a block diagram for the system when the input x_d is put to zero.
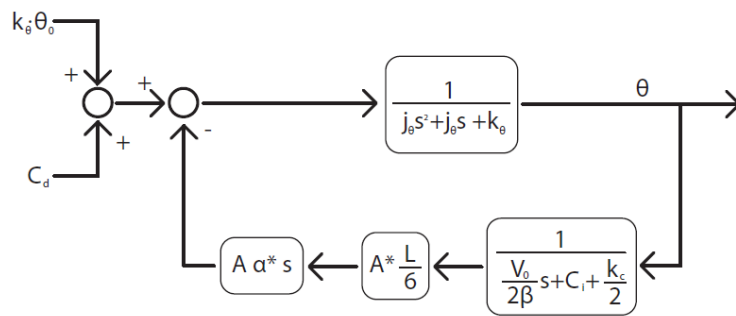
Figure 3.13: Block diagram for the system having only Cd and k$_\theta$ as inputs.

They can be computed:

$$G_{\frac{\theta}{C_d}}(s) = G_{\frac{\theta}{k_\theta \theta_0}}(s) = \cfrac{\left(\cfrac{V_0}{2\beta_c}s + \left(C_i + \cfrac{K_c}{2}\right)\right)}{\left(\cfrac{V_0}{2\beta_c}s + \left(C_i + \cfrac{K_c}{2}\right)\right) \cdot (J_\theta s^2 + r_\theta s + k_\theta) + \cfrac{AA^*\alpha^*L}{6}s}$$

(3.11)

They are the transfer functions in the case of the non-controlled system (with input x_d put to zero indeed). In the system under investigation, however, the angular position is fed-back to keep the arm inclined of θ_0. This means that the closed-loop transfer functions follow the block diagram depicted in Figure 3.14.
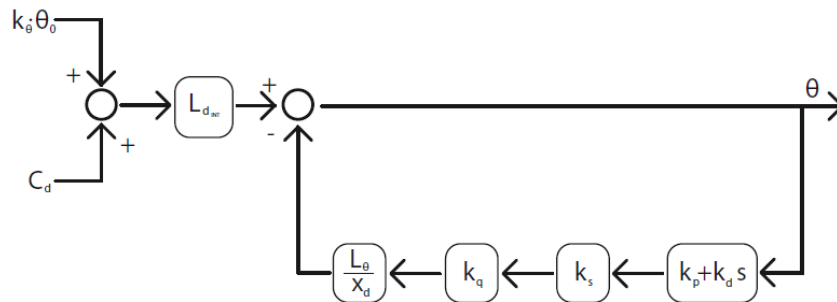
Figure 3.14: Block diagram for the closed loop transfer function between Cd and kθ, and θ.

And then they are:

$$L_{\frac{\theta}{C_d}}(s) = L_{\frac{\theta}{k_\theta \theta_0}}(s) =$$

$$= \frac{\left(\frac{V_0}{2\beta_c}s + \left(C_i + \frac{K_c}{2}\right)\right)}{\left(\frac{V_0}{2\beta_c}s + \left(C_i + \frac{K_c}{2}\right)\right) \cdot (J_\theta s^2 + r_\theta s + k_\theta) + \frac{A^* A\alpha^* L}{6}s + \frac{K_q k_s A^* L}{6} \cdot (k_p + k_d s)}$$

$$(3.12)$$

In this way the total (normalized) system transfer function will be given by the superposition of all these components, such that:

$$L_{\theta_{tot}}(s) = \frac{\theta_0 \cdot L_{\frac{\theta}{\theta_0}}(s) + (C_d + k_\theta \theta_0) \cdot L_{\frac{\theta}{C_d}}(s) + p_{pump} \cdot L_{\frac{\theta}{p_{pump}}}(s)}{\theta_0}$$

$$(3.13)$$

Actually, the contribute of C_d, p_{pump} and θ_0 is always multiplied by K_c and C_i, which are very small numbers. For this reason we expect this final transfer function to be not so different with respect to $L_{\frac{\theta}{\theta_0}}(s)$.

In fact, graphical results are presented in Figure 3.15. Once again the "Tandem" configuration behaves better than the classical one either in terms of amplitude and bandwidth, either in terms of phase.
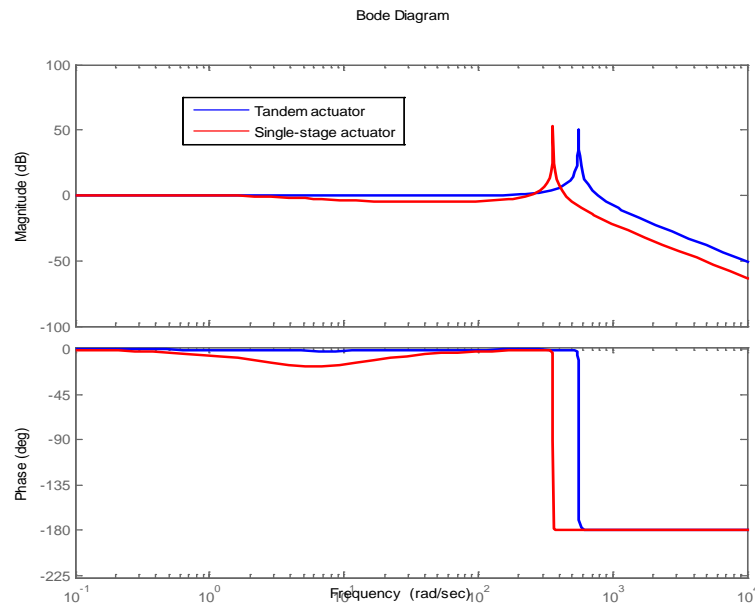
Figure 3.15: Bode plot for the total system transfer function.

3.3   Time domain analysis

In this final section the results of the integration of the non-linear and linear equations of motion have been presented. Some of the results shown hereinafter represent an additional confirmation of the observation and the conclusions achieved during the previous sections.

3.3.1   Non-linear motion

The non-linear behavior of the two systems over time shown in the following plots have been obtained from the numerical integration of equation (2.20). We remind that this first time span of integration was dedicated to the system to reach the desired angle of θ_0: the integration has been executed over a time horizon of 10 seconds.

In Figure 3.16 they are depicted for example the variation of θ and $\dot{\theta}$ over time for the system actuated respectively by the "Tandem" and by the classical cylinder.
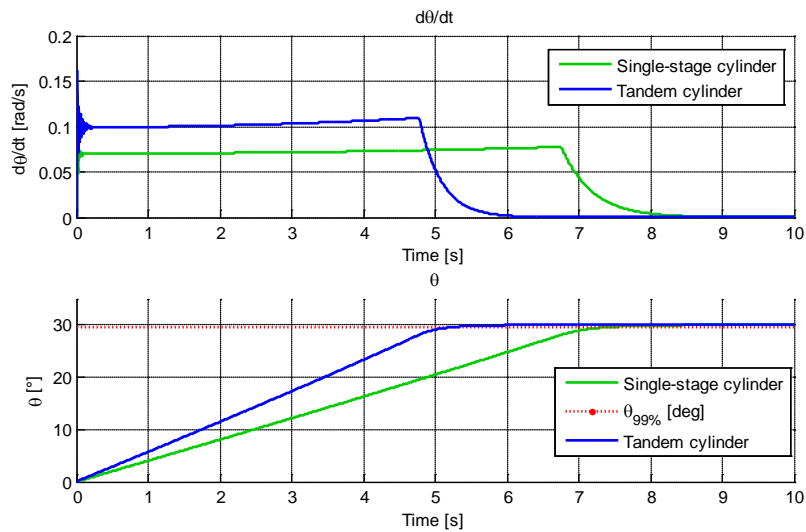
Figure 3.16: Angular displacement and speed during the non linear motion for both the "Tandem" system and the single-stage cylinder.

As it can be easily noticed, both the systems reach the angle set within the chosen integration time. In particular the Tandem is faster than the classical configuration because of its architecture, according to which in this first phase the big part of the cylinder is in use, and the second chamber of this is directly connected to the tank (Figure II.3). In this way, pressures in the first chambers can be optimized and better exploited.

On the other hand velocities are not excessive: in fact, according to the max speeds imposed in norm EN12001:2003 [14], the arm under investigation should not position in less than 1,4 seconds, which is certainly respected in both cases.

The plots of the angular position show also a small initial transient carrying a bit of noise: this kind of behavior is certainly associated with the high poles of the system, according to which sudden variations of boundary conditions can result in this kind of oscillations. While in the AMESim® results of the first part of the thesis this phenomenon was not observed (due to the too high time step of integration), these integrations in Matlab® allow us to observe it also in the pressures plots.
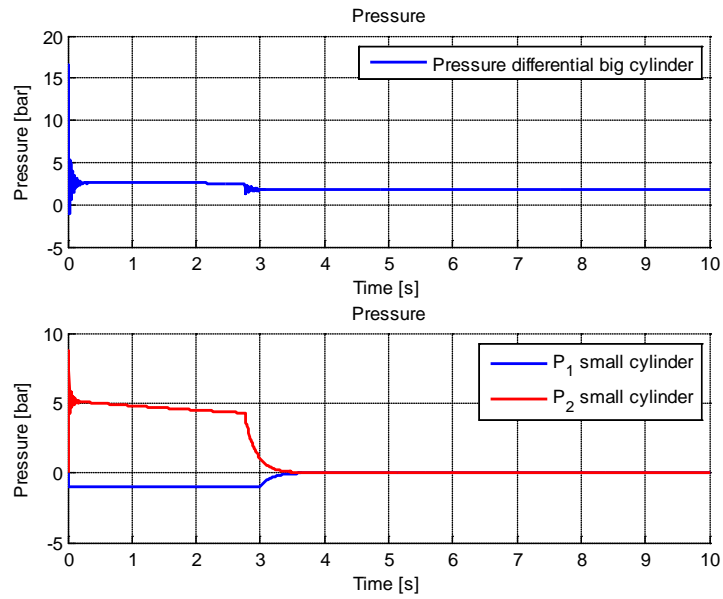
Figure 3.17: Pressure differential in the big cylinder chambers (up) and pressures in the chambers of the small cylinder (down).

Figure 3.17 shows the pressures inside the "Tandem" actuator, either in the active cylinder (big one), either in the passively driven one (small one, bypassed in this phase).
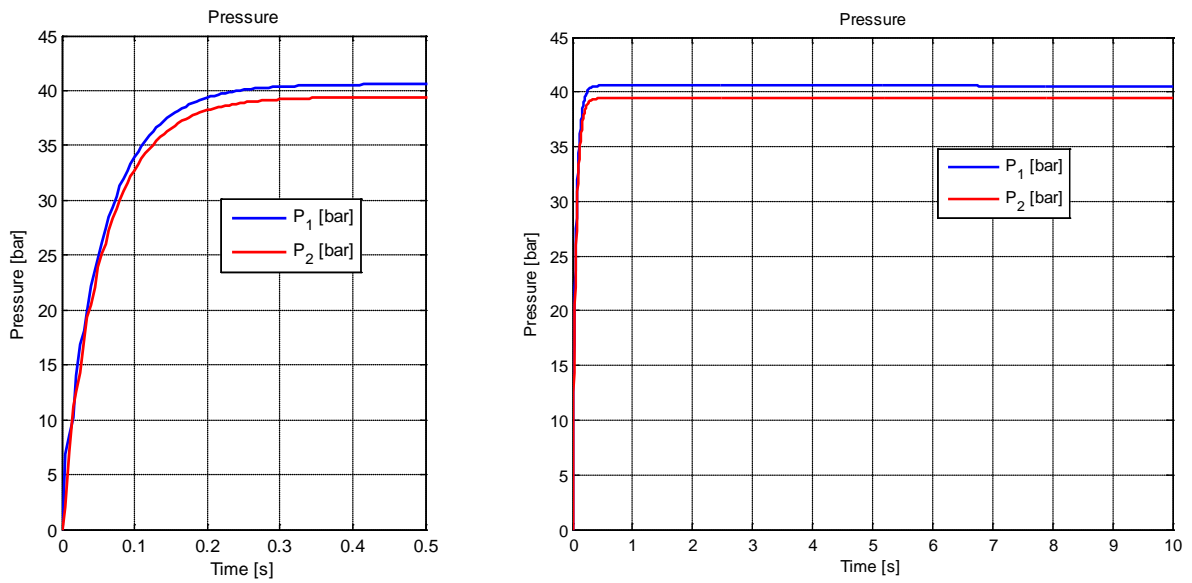
Figure 3.18: Pressures in the chambers of the single-stage cylinder with zoom (left) on the first 0.5 s.

Figure 3.18 shows instead the pressures inside the two chambers of the single-stage classical cylinder (with a zoomed window on the initial transient).

3.3.2 Linearized motion

In this second sub-section, the results of the integration over time of the equation (2.75) have been shown. Other 10 seconds of simulation have been produced: in this period of time it is possible to observe how the linearized systems react to the external input of the disturbance torque, trying to eliminate its effects.

As a consequence of this torque (function of time), pressures vary now according to the frequency of the disturbance. Figure 3.19 shows for example the behavior of the "Tandem" (please note that the linearized system response starts from 10 seconds, which corresponds with the end of the integration of the non-linear motion).
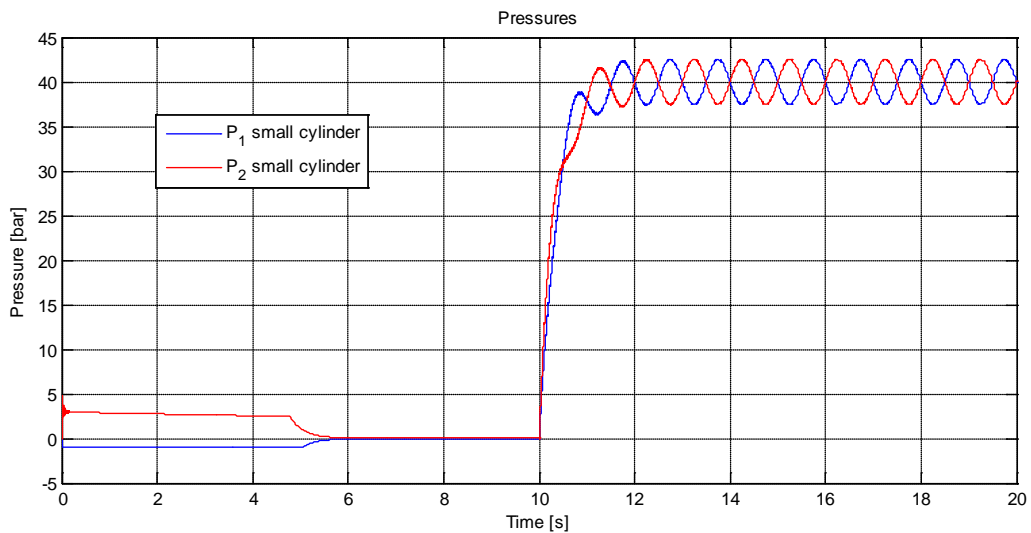
Figure 3.19: Pressure variation in the "Tandem" chambers in order to reject the external disturbance.

In Figure 3.20 is instead shown what happens in the chambers of the classical single-stage actuator.
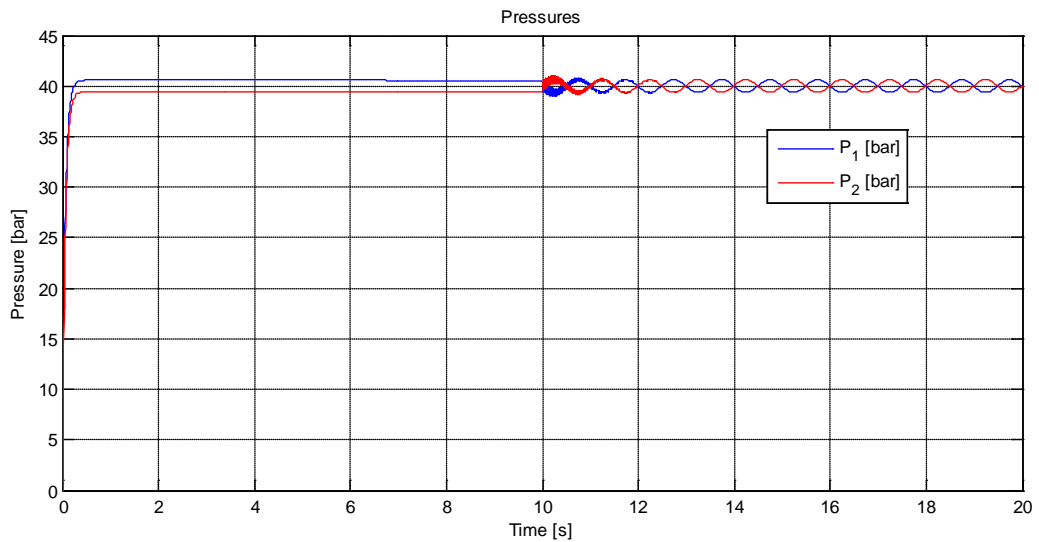
Figure 3.20: Pressure variation in the single-stage cylinder chambers in order to reject the disturbance.

This last plot about the behavior of the classical cylinder differs from the Tandem's one because the pressures in the chambers start already from a non-zero value (which is the average to keep the arm on θ_0), even if a brief *transient* (like a noise) can be noticed. In addition to this, pressures in the chambers result much lower than the case of the "Tandem" because of the piston area being bigger than the "Tandem" small piston area.

In the end a comparison between the tracking errors needs to be carried out.
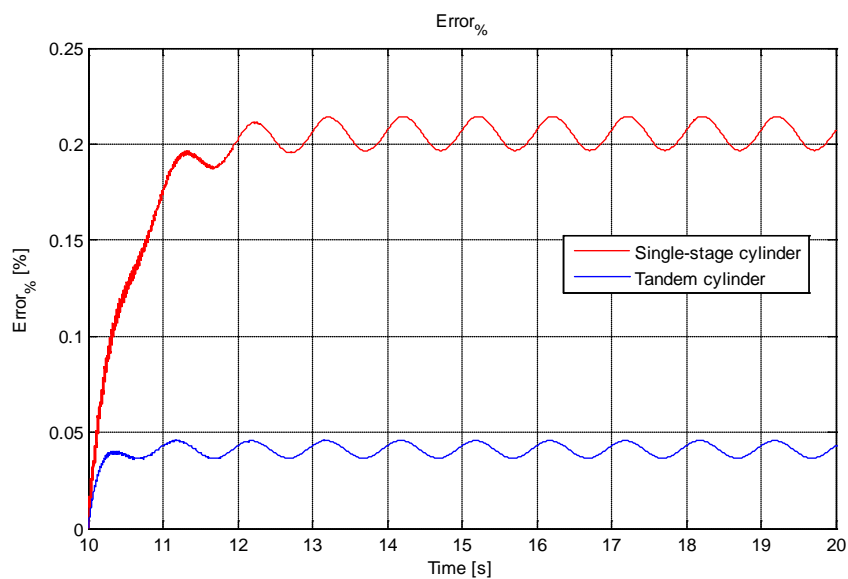
Figure 3.21: Comparison of the tracking error of the two actuated systems.

As it can be inferred from Figure 3.21, for a disturbance torque of 2000 Nm at 1Hz, the "Tandem" response is certainly more precise than the classical actuator. Considering the high stiffness of the system, the errors are both extremely low, but the graphical representation below gives us the confirmation of what expected, namely that in the "Tandem" the *error* becomes *five times smaller* than the error of the single-stage cylinder.

3.4 Power absorption

The integration of the equations of motion has moreover been exploited in order to compute the average power absorption of the two systems.

In particular, we want to observe what rate of power the two systems do absorb when they have reached a stationary condition (transients exhausted).

It is possible to define the hydraulic power absorbed by the system as follows:

$$P_{hydr} = Q(t) \cdot p_{pump} \qquad\qquad (3.14)$$

We hence need the time history of the flow rate. Having a recourse to the linearized hydraulic equations, we can compute it according to equation (2.70), where all the quantities are now known.

The results, depicted in Figure 3.22, show the trend of the power absorption over time: this is however an averaged plot that clearly depicts the benefit of using the "Tandem" cylinder not only during the transient, but also when the cycle is in "steady" conditions. This is fundamental if we consider that the use of such applications lasts generally for very long periods of time.

In particular, while the classical single-stage actuator is characterized by a mean steady state power absorption of nearly 27 W, the "Tandem" cylinder sucks only 15,6 W, with a spare of about the *42 %* of the total hydraulic energy.

We can conclude that even in this second application, the "Tandem" actuator keeps high its particularly advantageous energy-saving performance.
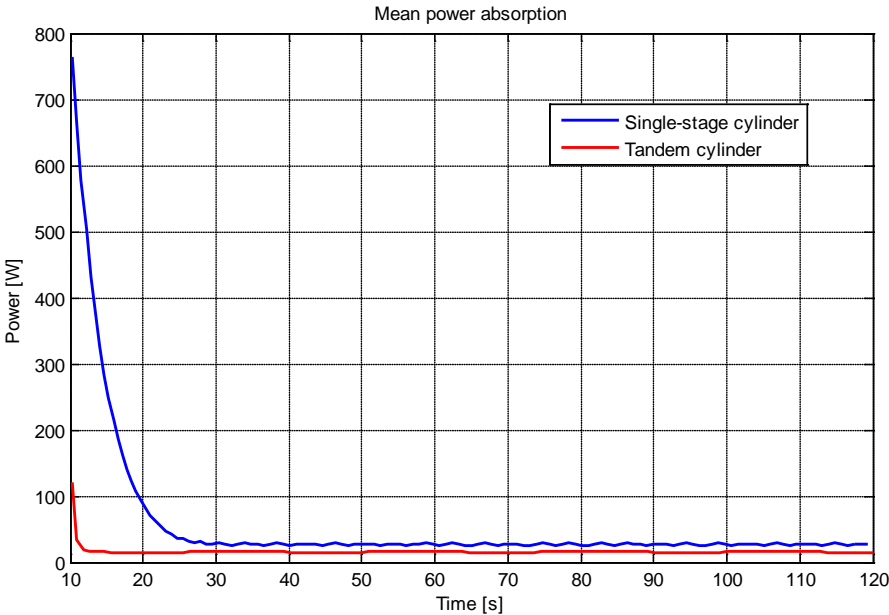
Figure 3.22: Averaged power consumption over time for the two cylinders.

Conclusions

The present work of thesis led to the numerical verification of the high performances of an innovative double-stage energy-saving hydraulic actuator, called "*Tandem*". The work, carried out in collaboration with Bosch Rexroth®, initially aimed at demonstrating numerically the energetic efficiency of such a system on linear applications for testing building materials.

In the first part, the actuator was in fact implemented in a circuit for fatigue tests on steel cables for bridges. The whole hydraulic circuit has been modelled in the AMESim® environment. Firstly an appropriate energy-saving control strategy has been successfully developed for the system, in order to let it achieve the test requirements; then the system was suitably sized. The analysis was conducted both in time and in the domain of frequencies.

A threefold comparison was drawn between the proposed solution, a classical configuration with a single-stage cylinder, and a mid-span design of double-stage actuator. Time results for the "*Tandem*" showed an impressive reduction in energy consumption, besides an almost doubled energetic efficiency with respect to the classical configuration.

The analysis in the frequency domain assigned instead to the "*Tandem*" a bandwidth nearly 2,5 times bigger than the single-stage cylinder's one.

The impressive results, exceeding the initial expectations, suggested the research of new fields where to apply this innovative cylinder. In particular, the second part of the thesis tried to exploit and analyze these advantages shown by the "*Tandem*" in a new application on a non-linear system for vibration control. In order to investigate these new performances, a numerical model was developed in the Matlab® environment. The system at stake was a rotating arm, representing in particular the case of a boom for concrete-handling, subject to external forces and disturbances. The model studied was just a simple one, but the objective of the thesis was not to develop a precise control

- 148 -

strategy, while rather to demonstrate the goodness of the actuator with respect to the old configurations. Firstly the non-linear equations of motion were computed; then the system was linearized around an equilibrium position, which the actuator was asked to maintain against the action of the external disturbances.

Also in this second case, the simulations clearly demonstrated for the "*Tandem*" a better controllability, besides an amplified bandwidth with respect to a classical single-stage configuration. In addition to this, the disturbance was rejected with greater efficacy, by reducing the error of five times. Power absorbed was in the end significantly decreased.

The thesis reached therefore his objective: the demonstration of the enhanced performances achievable with the hydraulic architecture of the "*Tandem*" cylinder.

Possible future developments for the present work could be oriented in researching new applications with further energy-saving features. We could mention, for example, the chance to implement a series of programmable valves, coordinated by a task-level controller, which sets up the circuit in the most appropriate way, depending on the "working mode". This kind of management is able not only to reduce pressures, but also to contain flow rate, by exploiting regenerative flows.

Appendix A

Nomenclature

They are reported, in alphabetic order all the symbols and notations used along the text. Symbols which start with Greek alphabet are reported after those in Arab alphabet. Being equal the initial letter, scalar numbers come first, followed by vectors and matrices.

a Length of the arm in the kinematic motion

A Nominal section area of the cable

A_{big_C} Piston area of the single-stage cylinder

A_{big_T} Piston area of the big-stage of the "Tandem" cylinder

A_{small} Piston area of the small-stage of the "Tandem" cylinder

A_C^* Equivalent piston area (classical) in non-linear force transmission

A_T^* Equivalent piston area ("Tandem") in nonlinear force transmission

$[A]$ State matrix

α^* Equivalent displacement for non-linear velocity (actuator)

- A2 -

b	Length of the actuator in the kinematic motion
b_o	Boom section dimensions
b_v	Boom section dimensions
$[B]$	Input matrix
β	Angle of the actuator in the kinematic motion
β_c	Compressibility of the fluid
c	Length of the chassis in the kinematic motion
C_d	Discharge coefficient, Disturbance torque
C_i	Coefficient of internal leakages
γ	Polytrophic exponent, Angle of the chassis in kinematic motion
dt	Infinitive time interval
D	Dissipative energy
δ	Summarizing factor for Bernoulli's equation
Δl	Variation of length of the spring
Δl_d	Dynamic variation of length of the spring
Δl_0	Static pre-charge of the spring
Δp_{or}	Pressure differential at the sides of the orifice
Δt	Time step for motion equations integration
ΔV	Variation of volume in the accumulator during cycles
E	Modulus of elasticity of the cable
E_c	Kinetic energy

E_{def} Deformation elastic energy (cable)

F_{filter} Transfer function of the first order filter

$f(t)$ Frequency of the reference signal, varying over time

g Acceleration of gravity

$G_{\frac{\theta}{k_\theta \theta_0}}$ Internal loop transfer function between $k_\theta \theta_0$ and θ

G_{loop} Loop transfer function between θ_{ref} and θ

$G_{\frac{\theta}{C_d}}$ Internal loop transfer function between C_d and θ

$G_{\frac{\theta}{p_{pump}}}$ Internal loop transfer function between p_{pump} and θ

h Gravitational height

h_o Boom section dimensions

h_v Boom section dimensions

i_c Current coming out of the controller

k_{acc} Equivalent spring generated by the accumulator

K_c Flow pressure coefficient

k_{cable} Cable stiffness

k_d Derivative gain

k_p Proportional gain

K_q Flow gain coefficient

k_s Electrical constant

k_θ Equivalent rotational stiffness in linearized motion equation

J	Momentum of inertia of the arm
J_c	Momentum of inertia of the actuator
J_θ	Equivalent momentum of inertia for the linearized system
L	Length of the cable, Length of the arm, Lagrangian work
$L_{\theta_{tot}}$	Total closed-loop transfer function for θ
$L_{\frac{\theta}{C_d}}$	Closed-loop transfer function between C_d and θ
$L_{\frac{\theta}{k_\theta \theta_0}}$	Closed-loop transfer function between $k_\theta \theta_0$ and θ
$L_{\frac{\theta}{p_{pump}}}$	Closed-loop transfer function between p_{pump} and θ
$L_{\frac{\theta}{\theta_0}}$	Closed-loop transfer function between θ_0 and θ
$L_{\frac{\theta}{x_d}}$	Closed-loop transfer function between x_d and θ
m	Mass of the arm
m_c	Mass of the actuator
m^*	Equivalent mass in linearized motion equation
η_{en}	Energy efficiency
p	Pressure
P_{hydr}	Hydraulic power consumed
p_{pump}	Pump pressure
p_0	Pre-charge pressure for accumulator
p_1	Pressure in the first chamber (both for "Tandem" or single-stage)

p_2 Pressure in the first chamber (both for "Tandem" or single-stage)

p_L Load pressure

q Independent variable

Q Lagrangian energy component of external forces

Q_{in} Flow rate entering the cylinder

Q_L Mean flow rate between cylinder's chambers

Q_{or} Flow rate through orifice

Q_{out} Flow rate coming out of the cylinder

r_c Viscous friction in the actuator

r_θ Equivalent rotational damping for the linearized system

ρ_{oil} Density of the oil

$\underline{u}$ Input vector

v Velocity of the centre of mass of the arm

V Potential energy

v_c Velocity of the centre of mass of the actuator

V Volume

V_{el} Elastic potential energy

V_g Gravitational potential energy

V_0 Initial nominal volume (accumulator, cylinder)

T_d Characteristic ratio between derivative and proportional gain

τ Characteristic time of the filter

- A6 -

θ Angle of the arm in the kinematic motion

θ_{ref} Reference angle for the arm

θ_0 Equilibrium angle for the arm

w Characteristic dimension of the valve intake port

x_A Position of the point of application of the external force

x_d Spool displacement

x_{ref} Reference position signal for the cable

X_0 Initial position of the piston within the cylinder

ξ Dimensionless damping

$\underline{y_C}$ Non-linear state vector for the single-stage cylinder

$\underline{y_T}$ Non-linear state vector for the "Tandem" cylinder

z Gravitational quote

$\underline{z}$ Linear state vector

ω_n Natural frequency

ω_0 Cross-over frequency of the filter

Appendix B

Hydraulic accumulators

Considering they are a fundamental element at the base of the main application the thesis is centered on, we thought it could have been of help to delve into the topic of hydraulic accumulators, to let the reader understand better their applications and their working principles.

B.1 State of the art

The accumulator is certainly the greatest peculiarity of the "Tandem" hydraulic system, which allows to achieve (demonstrations are provided in the text) a big saving in terms of energy consumption. In order to try to understand the job it does in our circuit, it is essential to clarify that hydraulic accumulators are appositely designed to play a simple but crucial role: taking a certain amount of fluid under pressure from the hydraulic system and storing it until it is required newly.

Accumulators were hence initially designed to be temporary stocks of fluid, even if in brief their applications spread to carry out the most various functions among hydraulic systems:

- They were first of all conceived as *energy storages*. The success they have had in this field is due to the fact that frequently, in industrial applications such as plastic injection machines, hydraulic presses, etc., the max power is only required in very short periods of time, while the average power absorption is definitely lower. This means that the pump should be designed powerful enough to feed the system at the max pressure, even being used for only few moments.

  The introduction of an accumulator allows the pump power to be decreased to the mean power required (thus minimizing the heat produced) such that the accumulator is charged during low-power operations, and in the end used to release the energy stored when necessary.

- A secondary (not less important) usage of the hydraulic accumulators is for *emergency operations*, such as fluid reserve, emergency braking systems, lubricating systems or for compensating oil leakages.

- Accumulators are widely used also for *cushioning shocks and vibrations*, when the state of the flow is forced to vary frequently, or suddenly, depending on the operation of the system. It is the case of spring-mass systems (just like the suspension of a car), switching on and off of distributors pumps, or industrial operations in which forces need to be balanced smoothly, in order to reduce the stresses applied on foundations and frames.

A clarification is thus necessary because, in our case, the accumulator has been added to the system in order to allow a particular energy-saving design. Accumulators, in fact, have a long tradition (demonstrated by a wide literature) in energy-saving applications or systems.

Let us take the example of *hydraulic elevators*. This kind of mechatronic systems, largely diffused in North America and Europe in the last decades, has been facing serious challenges because of its huge power installation and energy consumption, if compared to electrically driven elevators. The real problem of hydraulic elevators is the commonly diffused usage of the bypass-throttling system for the cabin speed control; this solution, efficient from a

control point of view, is anyways totally negative from an energetic one, because during the downwards movement, the entire potential energy of the cabin is wasted into heat by the throttling valve (Figure B.1). The speed of the cabin is, in fact, proportional to the oil flow rate driving the cylinder; when it is moving upwards, the check valve is opened and the flow control valve can control the oil speed according to curve 1. On the contrary, when the cabin is moving downwards the check valve gets closed, then fluid inside the cylinder is pushed back to tank by the weight of the cabin, following a flow rate imposed by the flow control valve, according to curve 2.
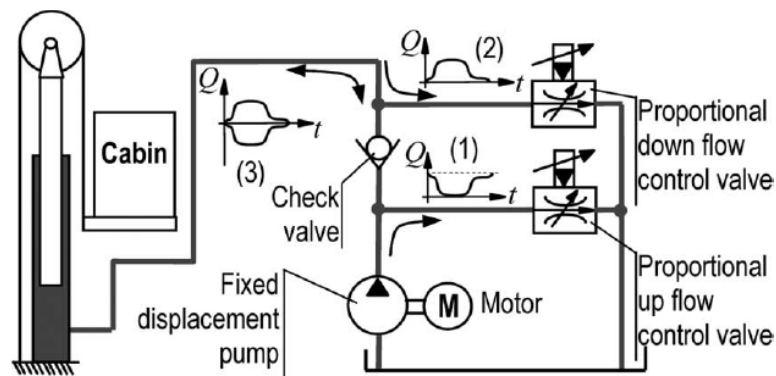
Figure B.1: System design of valve actuated hydraulic elevator [25].

Researchers from all over the world have proposed interesting solutions to this issue, involving the use of hydraulic accumulators.

Let us consider, for example, the "variable voltage variable frequency (VVVF) hydraulic elevator" proposed by X. Bing, Y. Jian and Y. Huayong [26]. Their innovative system, depicted in Figure B.2, consists of two principal parts, the first containing the pump/motor and the cylinder, the second containing the accumulator with its hydraulic pump/motor. While the cabin starts moving upwards, the controller sets the system such that the accumulator releases its energy to pump/motor 3, providing the additional power for motor 1 (which fosters the pump 2). On the other hand, when the elevator starts descending, pump/motor 2 is turned to work as a motor, which drives pump 3 to recover part of the potential energy of the cabin in form of fluid stored under pressure in the accumulator.

Figure B.2: Control system of the VVVF hydraulic elevator with the pressure accumulator [26].

This study was able to demonstrate an increase in energy efficiency from the original 37% (without accumulator system) to an impressive 60%.

A second, more complex, hydraulic energy-saving system for elevators was developed recently by H. Yang, W. Sun and B. Xu [25] (Figure B.3). They not only managed to reach high efficiencies and low energy consumptions, but they also achieved a good controllability of the plant thanks to some innovations listed below:

- Usage of an all-quadrant-running hydraulic motor technology.
- Hydraulic counter balance.
- Double acting cylinder, instead of the previous plunger type, in order to avoid buckling problems.

Figure B.3: Frequency-converter-controlled hydraulic elevator using double-acting cylinder and hydraulic accumulator counter balance in closed circuit with embedded controller [25].

Many other applications could be mentioned. Some Korean researchers, for instance, have developed a new concept of hydrostatic transmission with energy regeneration through to the use of a hydraulic accumulator, recovering energy during deceleration phases or while lowering of the load [27].

In the same way, another breakthrough in accumulator applications was represented by the study of braking energy-regeneration systems for buses [28]: it is well-known that, in fact, buses are often accelerated and braked and, without a system like this, the braked kinetic energy would be totally wasted into heat by the friction of the braker and by the tire friction with the road surface.

B.2   Accumulator typologies

Being the fluid kept under pressure, accumulators are designed to compensate for this energy amount by generally loading the same fluid in three different ways: by an external weight, by a spring or by a pressurized gas.

Weight and spring loaded accumulators are typically used only for very special industrial applications, hence hydro-pneumatic ones are the most diffused. These accumulators have in common their particular design involving a separating element placed to divide the gas from the fluid: the fluid compartment is directly connected to the hydraulic circuit. This means that

when pressure increases, the gas gets compressed and the fluid is pushed into the component.
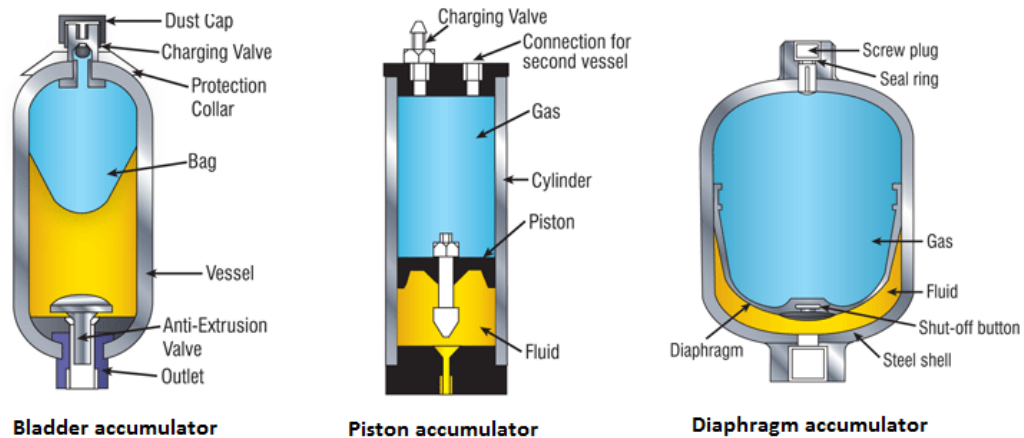
Figure B.4: Most common types of gas-pressurized accumulators.

The most common typologies of gas-pressurized accumulators with separating elements are (Figure B.4):

1. *Bladder accumulators*: the gas compartment and the fluid one are separated by a bladder. As already mentioned, the fluid part is connected to the circuit, hence the gas compresses or expands depending on the line pressure, always finding a balancing condition. They generally comprise a pressure vessel, a bladder and two valves for gas inlet and fluid inlet. In addition to this, because of their constructive features, they are used for medium effective volumes, but for very short cycle times (fast response).

2. *Diaphragm accumulators*: in these accumulators a pressure-resistant steel vessel contains the two compartments, which are typically separated by a diaphragm made of an elastic material (elastomer). Unlike bladder type, these accumulators are employed in very small volume applications, with the advantage of having an almost perfect sealing, and a very long service life.

3. *Piston accumulators*: in this third configuration, the two compartments are separated by a piston moving inside a cylinder barrel, which holds

the same function of the previous vessels. These last accumulators are instead used for large effective volumes, especially when the connection of an additional gas bottle is required.

B.3   Working parameters and principles

This section is dedicated to the explanation of the principles a hydraulic accumulator is based on. In both cases and typologies, at the beginning the gas compartments are pre-filled with gas (generally nitrogen) with the fluid valve being closed (obstructing the passage of fluid and then preventing a discharging). Then it is reached the p_0, namely the pre-charge pressure. The accumulator is then designed (and sized) in order to work between a minimum (p_1) and a maximum (p_2) operating pressure, whose transformation, in the hypothesis of an ideal gas, will be described by the expression:

$$p \cdot V^\gamma = cost \tag{ B.1 }$$

Actually, the type of transformation that occurs inside the accumulator always depends on the time needed for the charging and the discharging processes. As a rule of thumb if the process is slow enough (longer than 3 minutes) the hypothesis of isothermal change of state stands ($\gamma = 1$). This happens because the transformation is slow enough to allow the temperature to stay constant.
When, on the contrary, the operations are faster than 1 minute (which is more common in industrial applications of the gender of our "Tandem") the change of state can be associated with an adiabatic transformation ($\gamma = 1.4$). Actually, the exponent γ of the polytropic is not constant, because it strongly depends on the operation conditions: temperature and pressure, in fact, can deeply change their numerical value.

Assuming however an adiabatic change of state, we can now size the accumulator according to the max and min pressures, by following the formula:

$$V_0 = \frac{\Delta V}{\left(\frac{p_0}{p_1}\right)^{\frac{1}{\gamma}} + \left(\frac{p_0}{p_2}\right)^{\frac{1}{\gamma}}}$$

(B.2)

which, in few words, means that (ΔV fixed) an oversizing in V_0 would result in a decrease in p_1 and p_2 (and vice versa). We will see this reasoning in practice on a later time, by acting directly on the simulation results.

Appendix C

Components datasheets (Bosch Rexroth®)

Figure C.1: Accumulator datasheets (1).

Technical data (for applications outside these parameters, please consult us!)

General

Weight	kg	See table on page 11
Design		Bladder-type accumulator
Installation position		Preferably with fluid connection pointing downwards or horizontal
Type of mounting		With clamps and console
Ambient temperature range	°C	−15 to +65 [1)]
Pipe connection		Female thread

Hydraulic

Nominal capacity	V_{nom}	l	1	2.5	4	6	10	20	35	50
Effective gas volume	V_{eff}	l	1.0	2.4	3.7	5.9	9.2	18.1	33.4	48.7
Permissible max. flow	q_{max}	l/min	240	600	600	600	900	900	900	900
Permissible max. operating pressure	P_{max}	bar	350	350	350	350	330	330	330	330
Permissible max. pressure fluctuation width	Δp_{dyn}	bar	200	200	200	200	200	200	200	200
Operating pressures and useful volume		See Calculation on pages 5 to 10								
Hydraulic fluid		Hydraulic oil to DIN 51524; other fluids on request!								
Hydraulic fluid temperature range Others on request	°C	−15 to +80 (NBR) −35 to +80 (ECO)								

Pneumatic

Charge gas			nitrogen, purity degree 4.0, $N_2 = 99{,}99$ Vol.-%
Gas charge pressure	p_0	bar	2

Figure C.2: Accumulator datasheets (2).
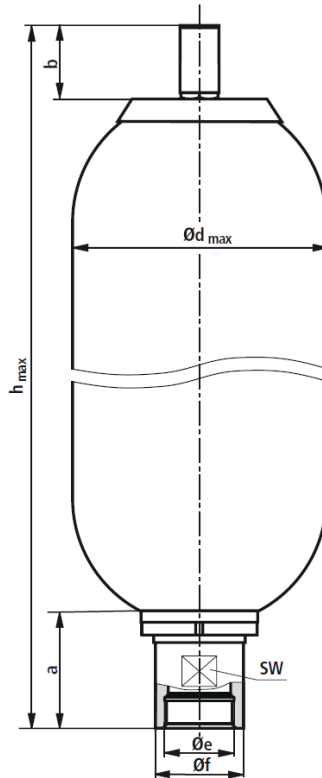
Nominal capacity in liters	Ordering code / type	Material no.	h max	Ød max	a	b	Øe	Øf	A/F	Weight kg
1	HAB1-350-4X/2G05G-2N111-BA	R901195131	333,5	115,5	56	70	G3/4"	36	32	5
	HAB1-350-4X/2G05G-2E111-BA	R901195132								
2,5	HAB2,5-350-4X/2G07G-2N111-CE	R901195133	554	115,5	69	70	G1 1/4"	53	50	10
	HAB2,5-350-4X/2G07G-2E111-CE	R901195134								
4	HAB4-350-4X/2G07G-2N111-CE	R901195135	438,5	170	67	70	G1 1/4"	53	50	16
	HAB4-350-4X/2G07G-2E111-CE	R901195136								
6	HAB6-350-4X/2G07G-2N111-CE	R901195137	564,5	170	67	70	G1 1/4"	53	50	20
	HAB6-350-4X/2G07G-2E111-CE	R901195138								
10	HAB10-330-4X/2G09G-2N111-CE	R901195139	590,5	225,5	104	70	G2"	76	70	32
	HAB10-330-4X/2G09G-2E111-CE	R901195140								
20	HAB20-330-4X/2G09G-2N111-CE	R901195141	900,5	225,5	104	70	G2"	76	70	53
	HAB20-330-4X/2G09G-2E111-CE	R901195142								
35	HAB35-330-4X/2G09G-2N111-CE	R901195143	1424	225,5	104	70	G2"	76	70	85
	HAB35-330-4X/2G09G-2E111-CE	R901195144								
50	HAB50-330-4X/2G09G-2N111-CE	R901195145	1940	225,5	104	70	G2"	76	70	123
	HAB50-330-4X/2G09G-2E111-CE	R901195146								

Figure C.3: Accumulator datasheet (3).

The ordering code configuration:

4WRA | | | **–2X** / **G24** | | / | **V** | *

Without integrated electronics (OBE) = No code
With integrated electronics (OBE) = E
Nominal size 6 = 6
Nominal size 10 = 10

Spool symbols

= E
E1–

= W
W1–

= EA

= WA

With spool symbols E1– and W1–:
$P \rightarrow A$: $q_{V\,max}$ $B \rightarrow T$: $q_V/2$
$P \rightarrow B$: $q_V/2$ $A \rightarrow T$: $q_{V\,max}$

Note:
With spools W and WA, in the neutral position, there is a connection from A to T and B to T with approx. 3 % of the relevant nominal cross-section.

Further details in clear text

Seal material
V = FKM seals, suitable for mineral oil (HL, HLP) to DIN 51524

Electronic interfaces A1 or F1 for 4WRAE
A1 = Command value input ± 10 V
F1 = Command value input 4 to 20 mA
No code = For 4WRA

Electrical connections
for 4WRA:
K4 [2] = Without plug-in connector, with component plug to DIN EN 175301-803 plug-in connector – separate order, see page 7
for 4WRAE:
K31 [2] = Without plug-in connector, with component plug to DIN EN 175201-804 plug-in connector – separate order, see page 7

Special protection
No code = Without special protection
J [1] = Sea water resistant (only for NS6)
For details regarding the sea water resistant versions see RE 29055-M

G24 = Supply voltage 24 VDC

2X = Component series 20 to 29
(20 to 29: unchanged installation and connection dimensions)

Nominal flow at a valve pressure differential $\Delta p = 10$ bar
NS6
07 = 7 l/min
15 = 15 l/min
30 = 26 l/min
NS10
30 = 30 l/min
60 = 60 l/min

[1] Other types of electrical protection on request
[2] Only for NS6: for version "J" = sea water resistant only state "K31"!

Figure C.4: Servo-valve datasheet (1).

Technical data (for applications outside these parameters, please consult us!)

Electical

Nominal size		NS	6	10
Voltage type			DC	
Command value signal	Voltage input „A1"	V	±10	
with type WRAE	Current input „F1"	mA	4 to 20	
Max. current per solenoid		A	2.5	
Solenoid coil	Cold value at 20 °C	Ω	2	
resistance	Max. warm value	Ω	3	
Duty		%	100	
Max. coil temperature [1]		°C	150	
Electrical connections	4WRA		with component plug to DIN EN 175301-803 or ISO 4400	
see page 7			plug-in connector to DIN EN 175301-803 or ISO 4400 [2]	
	4WRAE		with component plug to DIN EN 175201-804	
			plug-in connector DIN EN 175201-804 [2]	
Valve protection to EN 60529			IP65 with mounted and fixed plug-in connector	

Control electronics

For 4WRA	Digital amplifier in Eurocard format [2]		VT-VSPD-1-2X (to RE 30523 - middle of 2006)	
	Analogue amplifier in Eurocard format [2]		VT-VSPA2-1-2X/… to RE 30110	
	Analogue module amplifier [2]		VT-MSPA2-1-1X to RE 30228	
For 4WRAE			integrated into the valves, see page 8	
	Analogue command value module		VT- SWMA-1-1X/... to RE 29902	
	Analogue command value module		VT-SWMKA-1-1X/... to RE 29903	
	Digital command value card		VT-HACD-1-1X/… to RE 30143	
	Analogue command value card		VT-SWKA-1-1X/... to RE 30255	
Supply voltage	Nominal voltage	VDC	24	
4WRAE, 4WRA [3]	Lower limiting value	V	21 / 22 (4WRA); 19 (4WRAE)	
	Upper limiting value	V	35	
Amplifier current	I_{max}	A	1.8	
consumption	Max. impulse current	A	3	

[1] Due to the occurring surface temperature of the solenoid coils, the European Standards DIN EN 563 and DIN EN 982 must be taken into account!

[2] Separate order

[3] With Bosch Rexroth AG control electronics

☞ **Note:** For details regarding the **environmental simulation test** covering EMC (electromagnetic compatibility), climate and mechanical loading see RE 29055-U (declaration regarding environmental compatibility).

Figure C.5: Servo-valve datasheet (2).

7 l/min nominal flow at 10 bar valve pressure differential

P ⊠ A / B ⊠ T
or
P ⊠ B / A ⊠ T

1 Δp = 10 bar constant
2 Δp = 20 bar constant
3 Δp = 30 bar constant
4 Δp = 50 bar constant
5 Δp = 100 bar contant

Performance limit, nominal flow 7 l/min

P ⊠ A / B ⊠ T
or
P ⊠ B / A ⊠ T

1 Com. value = 40 %
2 Com. value = 50 %
3 Com. value = 60 %
4 Com. value = 70 %
5 Com. value = 80 %
6 Com. value = 90 %
7 Com. value = 100 %

Types 4WRA and 4WRAE

Signal change in %

0 – 100
0 – 75
0 – 50
0 – 25

Figure C.6: Servo-valve datasheet (3).
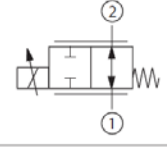
KKDS	R	1		B/H	C				V	*

Direct operated
proportional directional valve

Maximum operating pressure 350 bar = R

Component size = 1

2 main ports

Symbols			
② ①	Normally closed	= N
② ①	Normally open	= P

1) Cable sockets (separate order), see RE 08006

2) See page 8

Further details in clear text

Seal material
V = FKM seals
⚠ Caution!
Observe compatibility of seals with hydraulic fluid used!

Electrical connection 1)
K4 = Component plug 03-pin (2+PE) K4, DIN EN 175301-803
C4 = Cable plug 02-pin C4/Z30 type: Junior-Timer

N0 = Without manual override
N9 = With concealed manual override

Supply voltage
G24 = Control electronics 24 V DC
G12 = Control electronics 12 V DC

C = Proportional solenoid, wet pin

H = High-Performance and mounting cavity R/T-13A 2)

B = Component series

Direction of flow 1 → 2
Symbol "N"

Direction of flow 2 → 1
Symbol "N"

1 Command value = 40 %
2 Command value = 50 %
3 Command value = 60 %
4 Command value = 70 %
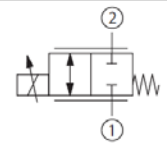5 Command value = 80 %
6 Command value = 90 %
7 Command value = 100 %

Direction of flow 1 → 2
Symbol "N"

Direction of flow 2 → 1
Symbol "N"

1 Command value = 40 %
2 Command value = 50 %
3 Command value = 60 %
4 Command value = 70 %
5 Command value = 80 %
6 Command value = 90 %
7 Command value = 100 %

Figure C.7: Proportional valve (Valve 1) datasheet (1).

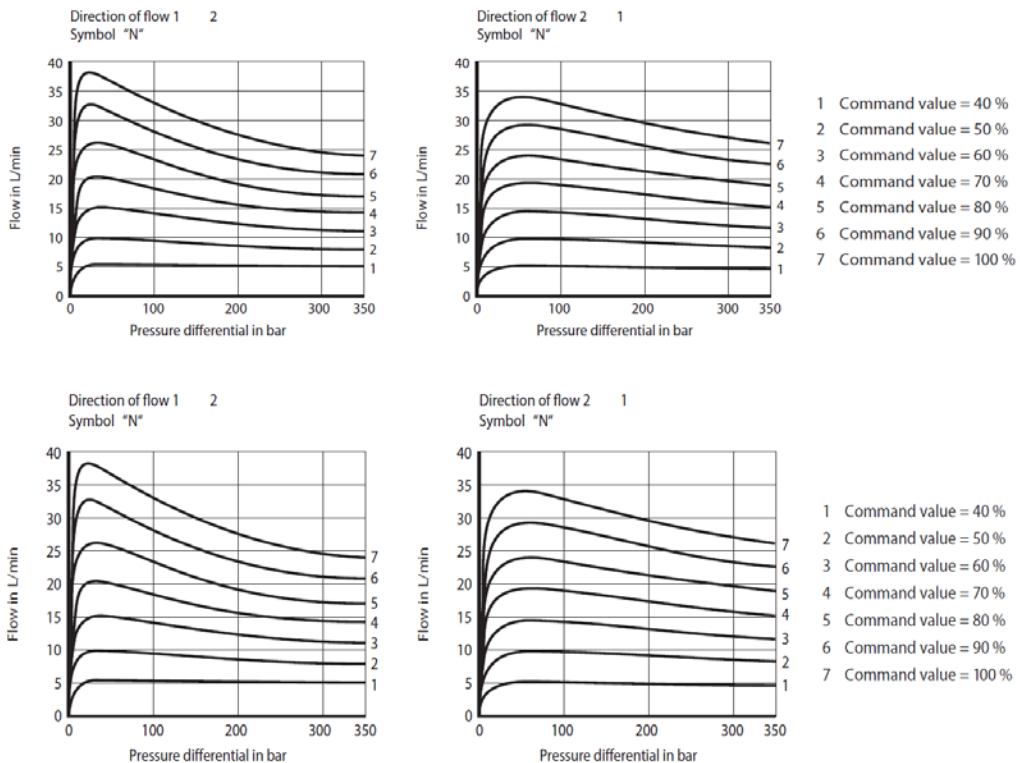**Technical data** (for applications outside these parameters, please consult us!)

General

Weight	kg	0.66
Installation orientation		Optional, if it can be ensured that no air can collect upstream of the valve. Otherwise, we recommended that the valve be mounted in a suspended position.
Ambient temperature range	°C	−20 to +70
Storage temperature range	°C	−20 to +80

Hydraulic

Maximum operating pressure		bar	350
Maximum flow	– Symbol "N"	L/min	38 (1 → 2), 34 (2 → 1) others flow on enquiry!
	– Symbol "P"	L/min	32 (1 → 2), 45 (2 → 1)
Step response	0 to 100 %; 100 to 0 %	ms	< 65 (at $p_S = 10$ bar)
Hydraulic fluid			Mineral oil (HL, HLP) to DIN 51524; fast bio-degradable hydraulic fluids to VDMA 24568 (see also RE 90221); HETG (rape-seed oil); HEPG (polyglycols); HEES (synthetic esters); other hydraulic fluids on enquiry
Hydraulic fluid temperature range		°C	−20 to +80 (preferably +40 to +50)
Viscosity range		mm^2/s	20 to 380 (preferably 30 to 46)
Max. permissible degree of contamination of the hydraulic fluid - cleanliness class to ISO 4406 (c)			Class 20/18/15 [2]
Hysteresis [1]		%	≤ 5
Range of inversion [1]		%	≤ 2
Response sensitivity [1]		%	≤ 1

Electrical

Type of voltage			DC	
Supply voltage		V	12 DC	24 DC
Maximum solenoid current		A	1.8	1.2
Coil resistance	– Cold value at 20 °C	Ω	3.3	7.2
	– Max. hot value	Ω	5.0	10.8
Duty cycle		%	100	
Maximum coil temperature [3]		°C	150	
Type of protection to VDE 0470-1 (DIN EN 60529) DIN 40050-9	– Version "K4"		IP 65 (with cable socket mounted and locked)	
	– Version "C4"		IP 66 (with cable socket mounted and locked)	
			IP 69K (with Rexroth cable socket, material no. R901022127)	
Control electronics [4]			Modular amplifier VT-MSPA1-100, see RE 30225 Plug-in amplifier VT-SSPA1-1 .., see RE 30116	
Rating according to VDE 0580				

[1] Measured with modular amplifier VT-MSPA1-100/V0/0-24 to RE 30225

[2] The cleanliness classes specified for components must be adhered to in hydraulic systems. Effective filtration prevents malfunction and, at the same time, increases the service life of components.
For the selection of filters, see data sheets RE 50070, RE 50076, RE 50081, RE 50086 and RE 50088.

[3] Due to the surface temperatures occurring on solenoid coils, the European standards EN 563 and EN 982 must be observed!

[4] Separate order

> **For electrical connection "K4", the PE conductor (⏚) must be connected in accordance with regulations.**

Figure C.8: Proportional valve (Valve 1) datasheet (2).

Bibliography

[1]   G. Marquis, J. Solin, *Fatigue Design and Reliability*, ELSEVIER SCIENCE Ltd. Oxford, 1999.

[2]   Davoli, Bernasconi, Filippini, Foletti, *Comportamento Meccanico dei Materiali*, McGraw-Hill, Milano, 2003.

[3]   Yang, S.-Y., Kwon, S.-K., Jin, S.-M., Hydraulic simulation and remote control system of field robot. *10th International Conference on Control, Automation, Robotics and Vision*, Dec 2008, 2303-2308. Ieee. doi: 0.1109/ICARCV.2008.4795892.

[4]   Bonchis, a, Corke, P. I., Rye, D. C. A pressure-based, velocity independent, friction model for asymmetric hydraulic cylinders. *Proceedings 1999 IEEE International Conference on Robotics and Automation (Cat. No.99CH36288C)*, (May 1999), 1746-1751. Ieee. doi: 10.1109/ROBOT.1999.770361.

[5]   Townsend, W., Salisbury Jr, J. (1987). The effect of coulomb friction and stiction on force control. *1987 IEEE International Conference on Robotics and Automation* (Vol. 4, p. 883-889). Institute of Electrical and Electronics Engineers.

[6]   Livi, Lanzetti, *Regolazione Oleodinamica*, Bosch Rexroth Education, Milano, 2005.

[7]   Doebelin, E. (2003). *Measurement Systems* (p. 1078). McGraw-Hill.

[8]   Heinz Mertens, Hamm, F. R. O. G. (1986). Mobile Concrete Hanlding Apparatus. United States Patents, Pat. n° 4,625,760.

[9]   Cheng Yi. (1994). *IEEE Transactions on Control Systems Technology*, *2*(3), 183-197. doi: 10.1109/87.317976.

[10]   Yao, B., Bu, F., Reedy, J., Chiu, G. T. C. (2000). *IEEEASME Transactions on Mechatronics*, *5*(1), 79-91. IEEE, Piscataway, NJ, USA.

[11]   Cazzulani, G., Ferrari, M., Resta, F., Ripamonti, F. (2009). *paginas.fe.up.pt*, (July). Active Control of a Flexible Boom for the Concrete Placing: Numerical and Experimental Analysis.

[12]   Resta, F., Ripamonti, F., Cazzulani, G., Ferrari, M. (2010). Independet modal control for nonlinear flexible structures: An experimental test rig. *Journal of Sound and Vibration*, *329*(8), 961-972. Elsevier. doi: 10.1016/j.jsv.2009.10.021.

[13]   Bachschmid, N., Bruni, S., Collina, A., Pizzigoni, B., Resta, F. (2003). *Fondamenti di meccanica teorica e applicata* (1st ed.). Milano: McGraw-Hill.

[14]   European Standards, EN12001:2003, *Conveying, spraying and placing machines for concrete and mortar. Safety requirements*, 2004.

[15]   Diana, G., Cheli, F. (2009). *Dinamica dei sistemi meccanici*. Milano. Polipress.

[16]   Di Fonzo, A., Resta, F., Ghielmetti, C. (2008). *Modellazione di un sistema per il pompaggio del calcestruzzo: modello numerico ed analisi sperimantale*. Master of Science Thesis. Politecnico di Milano, Dipartimento di Ing. Meccanica.

[17]   Diana, G., Resta, F. (2007). *Controllo dei sistemi meccanici*. Milano. Polipress.

[18]   Jelali, M., Kroll, A. (2003). *Hydraulic Servo-Systems. Modelling, Identification and Control.* London. Springer-Verlag.

[19]   Merritt, H. E. (1967). *Hydraulic Control Systems*. United States of America. John Wiley & Sons, Inc.

[20]   de Jalòn, J. G., Bayo, E. *Kinematic and Dynamic Simulation of Multibody Systems.* Springer Verlag 1990.

[21]   Butcher, J. C. *Numerical Methods for Ordinary Differential Equations (2nd Edition)*. Auckland. John Wiley & Sons, Inc.

[22]   Carnahan, B., Luther, H. A., Wilkes, J. O. (1969). *Applied Numerical Methods*. John Wiley & Sons, Inc.

[23]   Akers, A., Gassman, M., Smith, R. (2006). *Hydraulic Power System Analysis*. Suite. Taylor & Francis Group.

[24]   Åström, K. J., Murray, R. M. (2009). *Feedback Systems*. Oxford. Princeton University Press.

[25]   Yang, H., Sun, W., Xu, B. (2007). New Investigation in Energy Regeneration of Hydraulic Elevators. *Mechatronics, IEEE/ASME Transactions on*, *12*(5), 519–526. IEEE.

[26]   Xu, B., Yang, J., Yang, H. (2005). Comparison of energy-saving on the speed control of the VVVF hydraulic elevator with and without the pressure accumulator. *Mechatronics*, *15*(10), 1159-1174. doi: 10.1016/j.mechatronics.2005.06.009.

[27]   Ho, T. H., Ahn, K. K. (2010). Modeling and simulation of hydrostatic transmission system with energy regeneration using hydraulic accumulator. *Journal of Mechanical Science*

and Technology, *24*(5), 1163-1175. doi: 10.1007/s12206-010-0313-8.

[28] Qu, J., Ren, C., Yang, Z., Zhang, X. (2009). Parameters Optimization Method for Variable Displacement Pump/Motor and Transmission of Hydraulic Braking Energy Regeneration System. *2009 International Forum on Computer Science-Technology and Applications*, 19-22. Ieee. doi: 10.1109/IFCSTA.2009.242.